University of Genoa
Ph.D. in Clinical and Experimental Immunology

CYCLE XXXVIII

Industrial Track – in collaboration with ImmunoScape Pte Ltd.

Overcoming Barriers in Cancer Immunotherapy: Technical and Experimental Approaches for Preclinical Discovery, Characterization, and Optimization of Antigen-Specific TCR-T Cells

Candidate:

Hannah Fields

MATRICOLA N. 5415643

Tutors:

Prof. Gilberto Filaci

Dr. Daniel T. MacLeod

Abstract

Background: The T cell receptor (TCR) is central to adaptive immunity, enabling cytotoxic T lymphocytes to recognize and eliminate disease. This specificity underpins TCR-engineered adoptive cell therapy (TCR-T), which redirects T cells against malignancy. However, major translational barriers limit broader clinical application of TCR-T therapy. First, current methodologies for identifying antigen-specific TCR candidates that are both safe and therapeutically potent remain limited. Second, even when suitable candidates are advanced into development, transferred TCR-T cells frequently demonstrate insufficient persistence and suboptimal functionality within the immunosuppressive tumor microenvironment.

Methods: To address these challenges, we implemented a three-part technical and experimental strategy encompassing: (i) high-throughput TCR discovery, (ii) streamlined preclinical evaluation, and (iii) functional optimization of TCR-T cell therapies. First, an agnostic high-throughput screening and validation pipeline combining multiplexed mass cytometry and TCR-transduced Jurkat reporter assays was developed to identify HLA class I-restricted TCRs targeting viral and tumor antigens. Next, a prioritized candidate—an HLA A*11:01–restricted TCR recognizing a novel mesothelin (MSLN) epitope—was advanced for detailed preclinical evaluation. Functional efficacy assays assessed antigen-specific activation and tumor cell cytolysis. Integrated safety testing included alloreactivity screening, alanine scanning mutagenesis, and structure-based peptide–MHC–TCR modeling to evaluate epitope specificity and off-target risk. Finally, to enhance therapeutic durability, functional augmentation strategies were explored, including co-stimulatory receptor engineering and characterization of a putatively immunosuppressive $CD8^+$ regulatory T cell subset.

Results: High-throughput screening identified more than 100 unique physiologically derived HLA class I-restricted TCRs targeting viral and tumor antigens, establishing a broad repertoire of therapeutically relevant candidates. The prioritized HLA A*11:01–restricted TCR recognizing a novel MSLN epitope demonstrated antigen-specific activation and tumor cell cytolysis. MSLN, a tumor-associated antigen overexpressed across several solid tumors, has not previously been targeted by an HLA A*11:01–restricted therapeutic TCR. Integrated predicted *in silico* and *in vitro* and safety assessment of the same TCR identified a cross-reactive antigen not readily identified in traditional screening methods, mitigating off-target risk. Among functional optimization strategies, co-expression of the co-stimulatory molecule CD27 most consistently enhanced cytokine release and sustained cytolytic activity, suggesting improved persistence and long-term efficacy potential.

Conclusions: These studies address key translational challenges in TCR-T therapy by advancing high-throughput discovery, improving preclinical safety evaluation, and enhancing functional durability. Collectively, this work informs the rational design of next-generation antigen-specific cellular immunotherapies with improved safety, specificity, and therapeutic persistence.

Index

---

1. Introduction

$CD8^+$ cytotoxic T lymphocytes (CTLs) are central effectors of adaptive immunity, responsible for the recognition and elimination of infected or malignant cells through engagement of antigenic peptides presented by major histocompatibility complex class I (MHC-I) molecules. The antigen specificity of $CD8^+$ T cells is mediated by the TCR, which recognizes peptide–MHC (pMHC) complexes with high sensitivity. This specificity underpins both immune surveillance and the therapeutic potential of TCR-T, an emerging form of adoptive cell therapy (ACT) designed to redirect T cells toward defined targets in cancer and infectious disease (1).

Despite compelling clinical outcomes in hematologic malignancies, the success of ACT in solid tumors has been limited. Within the solid tumor microenvironment (TME), cytotoxic T cells encounter multiple barriers to effective function—including chronic antigen exposure, inhibitory signaling, and the presence of immunosuppressive cell subsets. These conditions drive T cell dysfunction, characterized by reduced proliferation, cytotoxicity, and cytokine production (2,3). Consequently, understanding and overcoming these mechanisms of dysfunction remain central challenges in developing durable, antigen-specific T cell therapies.

1.1. Naturally occurring antigen-specific TCRs as a source of therapeutic candidates

TCRs recognize short peptide antigens—also called epitopes—when they are presented on the cell surface bound to major histocompatibility complex (MHC) molecules, which in humans are referred to as human leukocyte antigens (HLA). TCRs can recognize both extracellular and intracellular epitopes presented by HLA molecules on the cell surface, enabling them to target a broad spectrum of antigens. The polymorphic nature of HLA genes allows the presentation of diverse peptide–MHC complexes on the cell surface, enabling T cells to survey a wide repertoire of potential antigens, including viral and tumor antigens (4).

Given the vast diversity of TCR specificities, naturally occurring antigen-specific TCRs represent a rich and clinically relevant resource for therapeutic development. The human TCR repertoire is estimated to encompass 10^7–10^8 distinct clonotypes in an individual, and potentially up to 10^{15} possible specificities at the population level (5,6). This TCR diversity is generated through somatic recombination of V(D)J gene segments, random nucleotide additions and deletions at junctions, and pairing of independent α and β chains. In addition, naturally occurring TCRs pass through thymic positive and negative selection, which filters out TCRs with high affinity for self-peptides while preserving those with sufficient affinity for foreign peptides presented by self-MHC (7). Because of this selection history, such TCRs often display a balance of functional potency and reduced baseline self-reactivity, making them attractive and potentially safer starting points for therapeutic use.

Naturally occurring antigen-specific TCRs can be isolated from circulating T cells in healthy donors or patients following infection or tumor exposure. However, the frequency of tumor-specific T cells in peripheral blood is often exceedingly low, necessitating sensitive and multiplexed detection strategies (8–11). Beyond experimental approaches, computational and machine learning–based models that predict TCR antigen specificity from structural motifs or sequence features have emerged as complementary tools (12,13). As such, integrating these models with experimental discovery can accelerate the identification of therapeutically relevant TCRs, particularly for rare or underrepresented tumor antigens for which circulating T cells are scarce.

1.2. TCR-T therapy: opportunities and limitations

ACT using TCR-T has emerged as a promising immunotherapeutic platform capable of redirecting T cell specificity toward defined tumor or pathogen-derived antigens. By transferring tumor-reactive TCR α/β chains into primary human T cells, this approach enables recognition of peptide–HLA (pHLA) complexes derived from both extracellular and intracellular antigens, including oncoproteins that are inaccessible to antibody- or CAR-based therapies (14).

Historically, ACT therapy has shown its greatest promise in hematologic malignancies, where target accessibility, tumor homogeneity, and immune microenvironmental factors are comparatively favorable (15). However, recent advances in TCR-T clinical development, highlighted by the FDA approval of MAGE-A4-targeting Tecelra®(afami-cel) for synovial sarcoma and the progression of PRAME-targeting ACTengine® (anzu-cel) into a phase 3 trial for melanoma, offer critical validation of TCR T therapy in solid tumors and support its expanding therapeutic potential across multiple antigens and disease settings (16,17). This success also highlights the potential of TCR-T therapy to overcome barriers inherent to solid tumor immunotherapy, including antigen heterogeneity, limited immune infiltration, and an immunosuppressive tumor microenvironment.

Despite these advances, the translation of TCR-T therapy to solid tumors continues to face major technical and biological challenges. Among these are the restricted HLA and epitope diversity of existing clinical candidates, which limits patient accessibility; the complexity of preclinical safety assessment required to mitigate off-target and alloreactive toxicities; and the functional persistence of engineered T cells in suppressive or metabolically hostile tumor niches. While hematologic malignancies often permit durable engagement between engineered T cells and target cells, solid tumors impose spatial, stromal, and cytokine-mediated barriers that attenuate T cell infiltration and effector activity (18,19).

Collectively, these challenges emphasize that the optimization of TCR-T therapy for solid tumors will require not only expansion of the antigenic and HLA landscape, but also improvements in receptor affinity tuning, cellular fitness, and safety profiling. The next section focuses on one of these critical

aspects—the limited HLA and epitope coverage in current TCR-T pipelines—which represents a central bottleneck for extending clinical benefit to diverse patient populations.

1.3. Limited HLA and epitope landscape in current TCR-T therapies

Although TCR-T therapy has demonstrated durable efficacy in selected malignancies, its clinical reach remains constrained by a limited repertoire of validated HLA–epitope pairs. To date, most investigational or approved TCR-T products have been designed to target a narrow subset of shared tumor-associated antigens (TAAs)—such as NY-ESO-1, MAGE-A4, PRAME, and MART-1—almost exclusively presented in the context of the HLA-A*02:01 allele (20,21). This intense focus on A*02:01–restricted epitopes has been largely driven by the availability of peptide–MHC binding data, the prevalence of A*02:01 in Caucasian populations, and the abundance of reagents and validation tools for A*02:01. However, this paradigm inherently restricts global patient eligibility, as the frequency of A*02:01 varies significantly among populations, dropping below 20% in many Asian, African, and Oceanian groups (22,23).

Beyond HLA restriction, the breadth of therapeutic epitopes recognized by current TCR-T candidates is also narrow in molecular and functional scope. Most target peptides are derived from a limited set of canonical tumor antigens—including differentiation antigens (e.g., MSLN, gp100), cancer-testis antigens (e.g., NY-ESO-1, MAGE family), and viral oncoproteins (e.g., HPV E6/E7). While these targets have demonstrated immunogenicity and safety in preclinical or clinical studies, they represent only a fraction of the potentially targetable intracellular tumor antigen landscape revealed by modern immunopeptidomics. Many tumor types, especially epithelial solid tumors, express mutated neoantigens, splice variants, and post-translationally modified peptides that remain underexplored in current TCR discovery pipelines.

The result is an imbalanced therapeutic map, densely populated around a handful of well-characterized epitopes but sparse across the broader space of antigenic diversity. This imbalance limits the capacity of TCR-T therapy to address tumor heterogeneity, a hallmark of solid malignancies, where multiple subclonal neoantigens may drive disease progression and immune escape.

Mesothelin (MSLN) exemplifies both the opportunity and the current limitations of this landscape. MSLN is a cell-surface tumor differentiation antigen with minimal expression in healthy mesothelium but marked overexpression in numerous solid tumors, including mesothelioma, pancreatic, ovarian, and lung cancers (24). Cumulative evidence indicates that MSLN is overexpressed in nearly one-third of all human malignancies, reinforcing its relevance as a therapeutic target (25–27). However, most MSLN-specific TCRs characterized to date are restricted to HLA-A*02:01, leaving other allelic contexts unexplored. The development of MSLN-directed, HLA-A*11:01–restricted TCRs would significantly expand therapeutic accessibility, particularly among patient populations with ancestry tracing to East and Southeast Asia and Oceania, where A*11:01 prevalence exceeds that of A*02:01.

Addressing these limitations requires systematic broadening of both the antigenic and allelic spectrum underpinning TCR-T development. Recent advances in mass spectrometry–based immunopeptidomics**,** machine learning models for pHLA binding prediction, and high-throughput TCR–pHLA pairing platforms are now enabling the identification of novel epitopes across underrepresented HLA alleles. Expanding this landscape is essential not only for global patient inclusivity, but also for enhancing therapeutic durability and tumor coverage, particularly within the immunologically complex environment of solid tumors.

1.4. Technical barriers to comprehensive TCR-T off-target evaluation

A critical consideration in TCR-T development is safety. Naturally occurring TCRs are subject to thymic selection, which reduces the likelihood of self-reactivity. Nonetheless, the preclinical safety analysis of TCRs is an essential stage of the development pipeline to ensure safe clinical application of TCR-T therapy (28). TCR promiscuity is now a well-established phenomenon in which a single TCR can recognize multiple different pMHC that share certain structural or chemical similarities (29,30). Such promiscuity permits the immune system to respond to a broad array of pathogens but also introduces the potential for unintended off-target interactions, presenting challenges in the context of TCR-T immunotherapy (31). To date, severe off-target clinical toxicities have been reported only with affinity-enhanced TCRs against self-antigens (31–33), for which the TCRs were engineered to enhance binding beyond what was achieved through normal thymic selection. While naturally occurring TCRs may have an improved safety profile over their affinity enhanced counterparts, TCR cross-reactivity has been established as an intrinsic property of the T cell receptor, and TCR-T involves giving a large dose of cells with a single specificity that likely exceeds natural T cell responses to a particular antigen. It is therefore essential to implement rational cross-reactive epitope interrogation of any TCR-T candidate of therapeutic interest for potential off-target activity, including cross-reactivity and alloreactivity, which may pose the risk of adverse events and toxicities in downstream clinical applications (28).

Off-target reactivity refers to the unintended activation of immune cells, such as T-cells, against non-target tissues or antigens that share structural similarities with the intended target, potentially leading to damage to healthy cells; this can occur due to shared epitopes between self and non-self antigens such as in autoimmunity (34). Established experimental approaches to evaluate off-target reactivity include peptide mutagenesis screening such as alanine-scan (A-scan) or X-scan. In an A-scan, each amino acid within the cognate epitope is individually replaced with alanine to identify residues that are essential for TCR recognition and binding. Alanine is commonly used for this type of mutational analysis because it is a small, non-polar amino acid whose minimal side chain effectively mimics the removal of larger side-chain functionalities without disrupting the peptide backbone. An X-scan expands this principle by substituting each amino acid with all 19 other naturally occurring amino acids, providing a more comprehensive map of the peptide positions that contribute to TCR specificity. In contrast to a comprehensive but unwieldy X-scan, a motif-based approach such as A/G-scan can aid in reducing the

space of potential cross-reactive peptides to be tested. However, even motif-based strategies carry the risk of missing rare or unanticipated cross-reactive peptides, which can result in costly failures at later stages of TCR-T development. As pointed out by Karapetyan (35), the A-Scan/peptide mutagenesis approach has limitations that can restrict its ability to detect cross-reactive peptides.

Currently, there are no *in vivo* models to effectively assess the toxicity of TCRs driven by alloreactivity or peptide-specific cross-reactivity. Immunodeficient xenogeneic murine models are commonly used to evaluate the efficacy of TCR-engineered human T cells, however, their utility for toxicity assessment is limited by the lack of HLA molecules in the host (36). While HLA-transgenic mice can mitigate this challenge, differences in the HLA-presented peptides between mice and humans still present a significant hurdle in evaluating TCR toxicity (37). Therefore, *in vitro* and *in silico* platforms remain the most valuable tools in identifying putative cross-reactive epitopes to compile a TCR safety profile prior to advancing to clinical trials.

1.5. Co-receptor engineering to enhance TCR-T function

Although adoptive cell therapy can elicit potent tumor specific responses, its efficacy in solid tumors remains limited by poor T cell persistence and the immunosuppressive tumor microenvironment, highlighting the need for strategies that more effectively bolster T cell responses. One promising avenue involves the incorporation of auxiliary engineering elements into the cell therapy product itself. In particular, the introduction of co-stimulatory receptors— "co-receptors"—into engineered T cells is an approach of increasing interest. Co-receptor engineering may help counterbalance the suppressive signals delivered through inhibitory receptors in the tumor microenvironment, thereby promoting more sustained T cell activation and function. Moreover, the ligands for several co-stimulatory receptors under investigation are expressed across a variety of solid tumor types, making them attractive targets for broad application. Importantly, this strategy is supported by existing precedents in CAR-T and other ACT modalities, where co-stimulatory domains have been shown to improve persistence and anti-tumor activity (38–40).

In this study, we focused on members of the tumor necrosis factor receptor superfamily (TNFRSF) as candidate co-receptors to enhance TCR-T function in the solid tumor setting. Specifically, we selected CD27 (TNFRSF7) and 4-1BB (CD137; TNFRSF9) for phenotypic and functional evaluation based on their expression profiles and biological relevance. CD27 is constitutively expressed on the majority of both $CD4^+$ and $CD8^+$ T cells, including tumor-infiltrating lymphocytes (TILs), and its ligand, CD70 (TNFSF7), is aberrantly expressed in various malignancies such as renal cell carcinoma, leukemia, non-small cell lung cancer, melanoma, and glioblastoma (41,42). In contrast, 4-1BB is transiently expressed on T cells following TCR engagement and plays a key role in promoting T cell survival and effector function (43). Its ligand, 4-1BBL (CD137L; TNFSF9), is expressed by multiple immune cell types—including T cells, B cells, dendritic cells, and macrophages—and has also been detected on tumor cells of diverse origin, including

carcinomas and colon cancers (44,45). These characteristics make both CD27 and 4-1BB attractive candidates for co-receptor engineering to potentiate TCR-T cell activity and persistence in the immunosuppressive tumor microenvironment.

1.6. $CD8^+$ regulatory T cell precursors and immunoregulatory dynamics

In addition to the challenges described above for TCR-T—such as limited persistence, inhibitory signaling within the tumor microenvironment, and the need for auxiliary strategies to sustain effector function—T cell dysfunction may also arise through intrinsic immunoregulatory mechanisms. In particular, the induction or expansion of regulatory T-cell (Treg) subsets during TCR-T manufacturing or after infusion has the potential to diminish therapeutic potency and affect clinical outcomes.

Tregs are essential for maintaining peripheral self-tolerance and preventing autoimmunity; however, they can also contribute to tumor progression by suppressing antitumor immunity. While the function and molecular regulation of classical $CD4^+Foxp3^+$ Tregs are well established, the biology of $CD8^+$ Tregs remains far less understood. There is currently no consensus regarding their defining phenotype or mechanisms of suppression, making the characterization of $CD8^+$ regulatory subsets—and assessment of whether they may arise or expand within TCR-T products—an important area for advancing more effective immunotherapies.

The existence, phenotype, and suppressive mechanisms of $CD8^+$ Tregs remain active areas of investigation. Emerging evidence suggests that populations exhibiting the phenotype $CD8^+CD28^-CD39^+CD127^-$ may possess regulatory or suppressive properties. $CD8^+CD28^-$ cells have been associated with chronic activation, senescence, and reduced effector capacity, yet may also acquire immunomodulatory features under specific conditions. However, interpreting these findings is complicated by technical challenges—most notably, that loss of CD28 expression is not unique to regulatory populations but is also observed in activated or exhausted effector T cells. This overlap complicates efforts to isolate, define, and functionally validate putative $CD8^+$ Treg subsets (46–48).

Further elucidating their molecular identity, transcriptional signatures, and developmental trajectories is therefore essential to determine whether $CD8^+$ regulatory cells represent a distinct lineage or reflect a transient activation state. Given these uncertainties, clarifying whether such $CD8^+$ regulatory populations emerge during TCR-T manufacturing or are induced following antigen encounter represents a key area for future investigation. A deeper understanding of these immunoregulatory dynamics may uncover new avenues for enhancing TCR-T persistence, mitigating premature dysfunction, and ultimately improving therapeutic efficacy.

2. Study overview

2.1. Scope

This study was conducted within the broader context of TCR-T technology development, focusing on early-stage research and preclinical discovery rather than clinical translation or manufacturing. The overarching goal was to identify and characterize antigen-specific TCRs and to investigate engineering strategies that enhance the function, persistence, and regulatory balance of TCR-T effector cells. Accordingly, this work represents a mechanistic and preclinical exploration of the immunological and bioengineering principles underlying next-generation ACT, rather than an evaluation of therapeutic efficacy or safety in human subjects.

Within this framework, TCR discovery efforts focused specifically on HLA class I-restricted receptors (HLA-A, -B, and -C) recognizing peptide–MHC class I complexes. Non-classical HLA molecules, including HLA-E, were not included within the investigative scope. TCR candidates were selected from $CD8^+$ T cells to prioritize putatively cytotoxic specificity and direct target-cell killing capacity. Although $CD4^+$ T cells were not the primary source of TCR discovery, their established role in supporting durable and effective immune responses was acknowledged, and final TCR-T products incorporated mixed $CD4^+$ and $CD8^+$ T cell populations to reflect cooperative immune dynamics.

2.2. Aims

The central aim of this study was to advance the preclinical understanding of TCR-T cell biology and explore strategies that could ultimately improve the discovery, efficacy, and durability of therapeutic TCR-T products. Collectively, these aims were designed to inform the optimization of TCR-T therapeutic products, integrating antigen discovery, receptor engineering, and immunoregulatory profiling to support next-generation ACT development.

By addressing these aims, this study establishes an integrated preclinical framework for the discovery, engineering, and immunological refinement of therapeutic TCR-T. The combination of antigen-specific TCR discovery, co-receptor engineering, and high-dimensional regulatory profiling provides a mechanistic foundation for improving both the functional performance and phenotypic stability of TCR-T products. Collectively, these findings inform the rational design of next-generation adoptive cell therapies with enhanced specificity, persistence, and clinical applicability.

2.2.1. Aim 1: Identification and functional characterization of antigen-specific TCRs

Utilizing high-dimensional mass cytometry and single-cell sequencing, a comprehensive technical pipeline was executed across hundreds of healthy and patient samples to discover and validate viral-

and tumor-specific TCRs. Peripheral blood mononuclear cells (PBMCs) from more than 100 healthy donors and 200 cancer patients across multiple indications were screened using high-dimensional mass cytometry–based assays (TargetScape) to identify putative viral- and tumor-specific T cells. Paired TCR α/β sequences were recovered from pMHC (peptide-MHC) tetramer labelled antigen-specific $CD8^+$ T cells by single-cell sequencing and cloned into lentiviral vectors for transduction into Jurkat TCRα/β-knockout reporter cells and primary human T cells to further evaluate these candidate TCR sequences. Functional validation of the candidate TCRs was performed using luminescent NFAT-reporter assays following co-culture with peptide-pulsed, HLA-matched antigen-presenting cells.

As an extension of this discovery and validation platform, epitope mapping of TCRs predicted to recognize Epstein–Barr virus (EBV) antigens was performed using overlapping peptide pools and titration assays to confirm antigen specificity and define the precise epitopes driving TCR activation. Among the tumor-reactive candidates, a mesothelin (MSLN)-specific, HLA-A*11:01–restricted TCR (A0341) was isolated from a colorectal cancer patient and selected for further evaluation. MSLN-specific TCR-T cells were generated and assessed against multiple HLA-matched cancer cell lines endogenously expressing MSLN using cytotoxicity, cytokine secretion, and proliferation assays. Ultimately, while the rigorous preclinical safety framework—involving alloreactivity testing and *in silico* modeling—identified a crucial DHRS11 cross-reactivity leading to the exclusion of the candidate Mesothelin (MSLN)-specific TCR, the established screening methodology was successfully validated for future translational development.

2.2.2. Aim 2: Characterization of immunosuppressive $CD8^+$ Treg populations in donor samples and TCR-T products

To better understand potential regulatory mechanisms influencing TCR-T product function, $CD8^+$ Treg precursor populations were profiled across healthy donors, cancer patients, and TCR-T cell products. High-dimensional mass cytometry was used to quantify $CD8^+CD28^-CD39^+CD127^-$ Treg precursors in 31 healthy donor and 196 cancer patient PBMC samples spanning multiple tumor indications. A phenotypic and functional panel was developed to capture activation, co-stimulatory, exhaustion, and transcriptional markers, enabling detailed resolution of subset heterogeneity.

To further investigate characteristics of this population of interest, modified TargetScape antibody reagent panels containing Treg biomarkers of interest were applied to an additional cohort of 6 healthy donors and 12 cancer patients. Longitudinal analysis of TCR-T manufacturing intermediates (including pre- and post-activation, mid-expansion, and harvest stages) from six healthy donors revealed dynamic emergence of $CD8^+CD28^-CD39^+CD127^-$ populations during expansion. These observations suggest that TCR-T manufacturing conditions can promote enrichment of $CD8^+$ Treg-like subpopulations, which may exert immunomodulatory or exhaustion-associated effects within the product.

2.2.3. Aim 3: Evaluation of co-stimulatory receptor engineering to enhance TCR-T function

To investigate strategies for enhancing TCR-T potency and persistence, we evaluated whether engineering auxiliary co-stimulatory receptors could improve function. Two receptors—CD27 and **4**-1BB (CD137)—were selected for assessment across multiple TCRs. Multigene lentiviral constructs were designed to enable co-expression of these receptors alongside either a benchmark WT1 A*02:01–restricted TCR or the novel MSLN A*11:01–restricted TCR. $CD8^+$ primary T cells were transduced under three conditions: TCR only, TCR+CD27, or TCR+4-1BB, and the resulting products were assessed for transduction efficiency, surface receptor expression, and phenotypic stability.

Engineered TCR-T cells were tested in cytokine secretion and degranulation assays following peptide-pulsed or antigen-expressing target cell stimulation. Serial antigen stimulation assays with tumor cell lines in short and long-term assays permitted measurement of proliferation kinetics and long-term survival. Comparisons across engineered and unmodified TCR-T cells demonstrated that CD27 co-expression enhanced activation and proliferative capacity while reducing phenotypic exhaustion over time. These findings identified CD27 as a promising co-stimulatory receptor candidate for improving next-generation TCR-T function and persistence.

---

3. Materials and Methods

Sample source and processing

Whole blood samples (TargetScape Cohort) were commercially obtained from healthy donors (San Diego Blood Bank) and individuals with different types of cancer, mainly lung cancer and melanoma (Discovery Life Science). PBMCs from each individual were isolated following a standard Ficoll gradient centrifugation protocol and frozen at −80°C in aliquots of up to 10^7cells. PBMCs were commercially purchased (STEMCELL) or prepared from Leukopaks (HemaCare).

TargetScape identification and profiling of antigen-specific T cells using mass cytometry

Peptides and MHC loading

A total of common virus (CMV, EBV, influenza, SARS-CoV-2) and cancer derived epitopes spanning six HLAs (HLA-A*01:01, HLA-A*02:01, HLA-A*03:01, HLA-A*11:01, HLA-A*24:02 and HLA-B*07:02) were selected for peptide MHC tetramer generation. Cancer epitope selection was informed by published immunodominance data, predicted peptide–HLA binding affinity (NetMHCpan), and novel peer-reviewed literature reported epitopes, with priority given to well-characterized class I-restricted epitopes. All peptides were ordered from Genscript (China) or Mimotopes (Australia) with a purity above 85% by HPLC purification and mass spectrometry. Upon receipt, peptide identity and purity were

confirmed by vendor-provided analytical certificates, and peptides were stored lyophilized at −20°C until use.

Lyophilized peptides were reconstituted at a stock concentration of 10mM in DMSO. Peptide stocks were aliquoted to minimize freeze–thaw cycles and stored at −80°C. Working dilutions were prepared immediately prior to UV exchange to maintain peptide stability. Biotinylated UV-cleavable peptide HLA monomers Rodenko (Toebes et al, 2006) for each allele were produced in house and individual peptide MHC class I complexes were generated by loading 50µM target antigen candidates onto each 100µg/mL monomer in the presence of ultraviolet (UV) light in a UV Crosslinker (Analytik Jena). Briefly, UV-mediated peptide exchange was performed by exposing monomer–conditional ligand complexes to 365 nm UV light for 30–60 minutes on ice to induce cleavage of the photolabile peptide, enabling simultaneous loading of the intended target peptide. All pMHC mixtures were incubated at 4°C overnight before tetramerization (described in "Multiplexed tetramer staining"). Successful peptide exchange was assessed indirectly by evaluating monomer stability.

Antibody staining panel setup

DN3 MAXPAR chelating polymers were loaded with heavy metal isotopes and conjugated to purified antibodies lacking carrier proteins (100µg/antibody) following the manufacturer's recommendations (Fluidigm). Staining panels were set up consisting of up to 33 antibodies binding to lineage, phenotypic and functional markers, as well as labels for live cell discrimination (cisplatin) and DNA (iridium intercalator). All labelled antibodies were titrated and tested by assessing relative marker expression intensities on relevant immune cell subsets in PBMCs from healthy donors (Leukopak, HemaCare). Total antibody mixtures were prepared for each batch (PBS, 2% fetal calf serum, 2mM EDTA, 0.05% sodium azide), aliquoted into single reactions and frozen (−80°C) before sample staining.

Multiplexed tetramer staining

pMHC monomers loaded with target antigen candidates were tetramerized using recombinant streptavidin conjugated to heavy metal loaded DN3 polymers (Newell et al, 2013) at a final molar ratio of 1:4 (total streptavidin:peptide–MHC). Following tetramerization, complexes were incubated for at least 60 minutes at 4°C and centrifuged briefly to remove potential aggregates prior to pooling.

To screen for antigen-specific CD8 T cells we set up a three-metal combinatorial tetramer staining approach resulting in a unique barcode as described previously (Newell et al, 2013; Simoni et al, 2018b; Fehlings et al, 2017, 2019). This approach enabled simultaneous detection of multiple antigen specificities within a single sample while minimizing spectral overlap, leveraging the high-dimensional detection capacity of mass cytometry (CyTOF). Each tetramer specificity was encoded by a distinct combination of three metal isotopes, permitting deconvolution during downstream computational analysis.

Tetramer mixtures containing all peptide candidates were prepared for each batch (PBS, 2% fetal calf serum, 2mM EDTA, 0.05% sodium azide), aliquoted into single reactions and frozen (−80°C) before sample staining.

Sample staining and CyTOF acquisition

PBMCs were thawed at 37°C, transferred into complete RPMI medium 10% fetal calf serum (FCS), 1% penicillin/streptomycin/glutamine, 10mM HEPES, 55µM 2-mercaptoethanol (2-ME) supplemented with 50µ/ml Benzonase (Sigma) and washed twice before depleting monocytes (CD14+) and B cells (CD19+) or undergoing "CD8 isolation" (negative depletion) using magnetic beads (Miltenyi). For each staining reaction up to $5x10^6$ enriched T cells were used in one well of a 96 well plate consisting of up to 2 donor samples combined following prior barcoding with differently labelled anti-CD45 antibodies for 20 mins at RT. Samples were stained with 100µl tetramer mixtures for 1h at RT. Cells were then washed twice and stained with heavy metal labeled antibody mixtures for 30 mins on ice and 200µM cisplatin during the last 5 mins for the discrimination of live and dead cells, then fixed in 2% paraformaldehyde in PBS overnight at 4°C. Cells were then washed and resuspended in 250nM iridium DNA intercalator (Fluidigm) in 2% paraformaldehyde/PBS at RT. Cells were pooled together, and adjusted to $5x10^5$ cells per mL in H_2O or CAS buffer (Fluidigm) together with 1% equilibration beads (Fluidigm) for acquisition on a CyTOF HELIOS or XT mass cytometer (Fluidigm).

Computational processing of TargetScape data

After mass cytometry acquisition, signals for each parameter were normalized based on EQ beads (Fluidigm) added to each sample. Each sample was manually debarcoded followed by gating on live CD8+ T cells (CD45+ DNA+ cisplatin- CD3+ cells) after gating out residual monocytes (CD14+), B cells (CD19+) and NK cells (CD56+ CD3-). Antigen-specific triple tetramer positive cells (hits) were identified based on an automated peptide-MHC gating method (Newell et al, 2013). Calling of bona fide antigen-specific T cells was further dependent on (i) the detection cut-off threshold (≤ 3 events to be detected), (ii) the background noise of unspecific CD8+ bulk T cells, and (iii) phenotypic homogeneity as unbiased objective criteria for antigen-specificity assessment (Fehlings et al, 2019). Frequency values of tetramer reactive cells were calculated based on the percentage of the parent CD8+ T cell populations. Phenotypic markers were gated individually for each sample and calculated as percent of positive cells. Analysis was performed using CYTOGRAPHER®, ImmunoScape's cloud based analytical software, GraphPad Prism and FlowJo software.

TCR sequence recovery

In vitro expanded T cells were stained with HLA multimers and surface antibodies to sort specific T cells into individual wells for single cell PCR (scPCR). A Melody flow cytometer (Becton Dickinson BD) was used for the sorting. Sorted cells were immediately frozen and stored at -80C until further use. RT reaction was performed, followed by a nested PCR protocol to amplify the variable TCR regions of the TCR alpha

and -beta chain using primers binding in the V gene. The protocol was described previously (49). TCR sequences were obtained by Sanger sequences of PCR products. Alternatively, ex vivo or in vitro expanded cells were stained with oligo-tagged multimers and surface antibodies for flow cytometry sorting and scRNA sequencing using the 10xGenomics workflow.

Functional validation of TCRs

Plasmids, lentiviral vector production, and transduction of Jurkat cells

Lentiviral vectors were produced for each TCR by transfection of the transgene plasmid along with packaging plasmids encoding the additional lentiviral components into HEK293 cells. Lentiviral vectors collected from the transfected HEK293 cells were then used to transduce each TCR into T cells (either CD8+ Jurkat TCR α/β KO reporter cells or activated CD4/CD8-enriched primary cells from a healthy donor). Transduction efficiency and expression of the introduced TCR were confirmed by flow cytometry.

Dose-response testing of transduced Jurkat cells

Antigen presenting cells expressing a selected HLA allele were seeded into 96 well plates at 50,000 cells per well. 50,000 Jurkat TCR α/β KO reporter cells that were transduced or non-transduced with the TCR to be tested were added to the antigen presenting cells; transduction efficiency was quantified by flow cytometry, to verify that at least 10% of Jurkat reporter cells express the transduced TCR. In a separate plate, peptide dilutions were prepared to the desired range of concentrations (for dose-response testing) and added to the plate containing antigen presenting cells and Jurkat cells. Plates were incubated at 37° C in a cell culture incubator for 3h50min with a final 10min of incubation at room temperature (4h incubation in total). To reveal the luciferase signal, Bio-Glo-NL™ reagent was added to all wells, reacted for 5 min and luminescence read on a SpectraMax i3x (Molecular Devices) plate reader.

Functional assessments in TCR-T

Primary cells processing and TCR-transduction

Peripheral blood mononuclear cells (PBMCs) from healthy donors were used as a source of primary T cells for the preparation of effector cells. PBMCs were isolated by density-gradient centrifugation using Ficoll-Paque and cryopreserved in fetal bovine serum with 10% DMSO until use. Prior to enrichment, cells were thawed rapidly at 37°C, washed to remove DMSO, and rested overnight in complete medium to recover viability.

CD4+ and CD8+ T cells were positively enriched from PBMC using either A) CD4 and CD8 microbeads, and LS columns and magnets from Miltenyi or B) CliniMACS CD4 and CD8 GMP MicroBeads, CliniMACS tubing set on the Miltenyi CliniMACS automated cell processing system. Purity of enriched populations was assessed by flow cytometry and routinely exceeded 90%. Cells were resuspended in AIM V medium

with 10% heat-inactivated human AB serum and 10ng/ml IL-15. Cell density was adjusted to 0.5–1.0 × 10^6 cells/mL prior to activation. For gentle T cell activation, cells were incubated with TransAct™ beads (Miltenyi) at half of the manufacturer's recommended bead-to-cell ratio.

On the same or the next day, lentiviruses encoding for the TCR of interest were added to the activated T cells and incubated for three days. Cells that were not transduced with lentivirus and were used as control cells. Transduction efficiency was quantified by flow cytometry prior to performing cell based functional assays. TCR expression was assessed using peptide–MHC tetramer staining or anti-TCR Vβ–specific antibodies, and only cultures exceeding predefined expression thresholds were advanced to functional assays.

Flow cytometry-based cytotoxicity and proliferation

TCR-transduced primary $CD4^+$ and $CD8^+$ T cells were labeled with CellTrace Violet (CTV) for 20 minutes at 37°C, washed, and resuspended in assay buffer (95% RPMI, 5% human serum albumin). Labeling efficiency and viability were confirmed prior to co-culture setup. Target cells (50,000) were seeded in 96-well plates. Effector cells were added at the effector-to-target ratios indicated in the figures. Media-only controls or cognate peptide were added at the concentrations specified in the figures. Cultures for short-term cytotoxicity assays were incubated for 20–24 hours; cultures for proliferation were cultured for the period specified in figure descriptions; all cultures were incubated for the duration of the assay at 37°C. After incubation, culture supernatants were collected and frozen at –80°C for cytokine quantification. Remaining cells were stained in-plate with 7-AAD and Annexin V APC for 15 minutes and analyzed on a flow cytometer (Thermo Fisher Scientific or BD FACS Melody). Cytotoxicity was calculated based on live target cells ($CTV^+7\text{-}AAD^-Annexin\ V^-$) relative to target-only control wells using FlowJo software: % Cytotoxicity = [(T.O. avg – assay well count of live targets)/ T.O. avg]*100. Proliferation was quantified based on dilution of CTV signal within viable effector cell populations using FlowJo proliferation modeling tools.

Quantification of cytokine secretion

IFNγ secreted by T cells into the culture medium during the cytotoxicity assay was quantified by ELISA methodology using the OptEIA IFNγ Kit from Becton Dickinson (BD**).** Assays were performed according to manufacturer instructions, including duplicte standards and triplicate samples. Plates were coated overnight, blocked, incubated with standards and samples, and developed using HRP-conjugated detection antibodies and TMB substrate. Absorbance was measured with the SpectraMax i3x (Molecular Devices) plate reader and cytokine concentration calculated based on standard curve using SoftMax Pro 7.1.2 software. EC50 concentration for was calculated using the luminescence values dose-response curve for the index peptide on and non-linear regression fit (ECF, where "F" = 50) on Prism software.

Dynamic cytolytic analysis

Real-time cytotoxicity and killing kinetics were evaluated using the xCELLigence real-time cell analysis platform. Target cells were seeded on impedance-sensing plates, and TCR-transduced effectors were added at defined effector-to-target ratios. Impedance measurements were recorded at 15-minute intervals for the duration of the assay (typically 48–96 hours), and normalized cell index values were calculated relative to pre-effector addition baseline. Changes in electrical impedance over time provided continuous, quantitative assessment of target cell lysis. Data were analyzed to extract metrics including killing onset, maximum cytolytic rate, and overall cytotoxic capacity using RTCA software and exported for statistical analysis. All experiments were performed in technical duplicate or triplicate and repeated across independent donors to ensure reproducibility.

CD8+ Treg evaluation

Retrospective phenotypic evaluation of CD8+ Treg precursor subpopulation

Mass-cytometry (CyTOF XT)-acquired TargetScape sample was manually debarcoded followed by gating on live CD8+ T cells (CD45+ DNA+ cisplatin- CD3+ cells), then by gating on CD8+ Treg precursor population (CD28- CD38+ CD127-). MFI of the CD8+ Treg precursor populations were compared, and frequency values of CD8+ Treg precursor cells were calculated based on the percentage of either the parent CD8+ or CD3+ T cell populations. Phenotypic markers were gated individually for each sample and calculated as percent of positive cells. Analysis was performed using CYTOGRAPHER® (ImmunoScape) cloud based analytical software, GraphPad Prism and FlowJo software.

High-dimensional analysis of $CD8^+$ Treg precursors

To further evaluate phenotypic and functional heterogeneity, a dual-panel mass cytometry approach was employed, incorporating both surface markers and intracellular signaling or activation markers (**Suppl. Tab. 7**). Subsets were additionally subjected to PMA/Ionomycin stimulation to assess cytokine production and activation potential. Analysis was performed using FlowJo software and CYTOGRAPHER® (ImmunoScape) cloud based analytical software.

4. Results

4.1. Discovery and characterization of antigen-specific TCRs

To enable unbiased identification and functional validation of naturally occurring, antigen-specific TCRs from accessible donor samples, we applied a high-throughput discovery and validation workflow integrating TargetScape – a multiplexed, mass cytometry-based single-cell phenotyping platform – with TCR clonotype recovery and functional validation using TCR-transduced Jurkat reporter cells. The TargetScape platform, previously described and validated for antigen-reactive T cell profiling (25,26), was employed here to agnostically screen peripheral blood mononuclear cells (PBMCs) for rare, antigen-specific TCRs of potential therapeutic relevance.

This integrated approach enabled comprehensive identification of putative antigen-specific TCR identification, paired α/β chain sequence recovery, and downstream functional assessment of the TCR activity and HLA-restricted antigen recognition. The high-dimensional immunophenotypic data generated in parallel also enabled secondary computational analyses—including feature correlation analyses and phenotypic mapping. As an initial validation of the TCR discovery workflow—and to explore the integration of machine learning approaches—epitope mapping was performed for TCRs predicted to recognize Epstein–Barr virus (EBV) antigens, providing functional confirmation of antigen specificity and demonstrating the platform's utility for systematic TCR characterization. An overview of the TCR identification, recovery, and functional validation workflow is provided in **Supplementary Figure 1**.

4.1.1. Agnostic identification and functional validation of naturally occurring viral- and cancer-specific TCRs

To agnostically detect naturally occurring, viral- and tumor-specific $CD8^+$ T cells from peripheral blood, we utilized mass cytometry-based multiplexed tetramer screening strategy of peripheral blood mononuclear cell (PBMC) samples in 410 subjects (129 healthy donor and 281 cancer patients of various indications; **Fig. 1A**) for antigen-specific CD8+ T cells against more than 500 metal-barcoded peptide–MHC (pMHC) tetramers targeting known and predicted tumor-associated antigens (TAAs), tumor-specific antigens (TSAs), and viral epitopes across six common HLA types. The pMHC multimer panel included epitopes derived from common viruses (CMV, EBV, influenza, SARS-CoV-2) as well as cancer-associated antigens spanning HLA-A*01:01, HLA-A*02:01, HLA-A*03:01, HLA-A*11:01, HLA-A*24:02, and HLA-B*07:02. A triple metal-barcoding strategy of pMHC tetramers enabled simultaneous screening of hundreds of epitopes per sample.

Mass cytometry-acquired samples were analyzed based on individual triple codes for each candidate pMHC tetramer (i.e., each peptide-MHC tetramer in the mixture was labeled with three different heavy metal isotopes) to identify $CD8^+$ T cells bearing potential viral- and cancer-specific TCRs of therapeutic

interest, including rare populations detectable at frequencies as low as 0.000036% (or ~1 in 2.8 million CD8+ cells) (**Fig. 1B**). Cancer-derived epitopes represented multiple antigen classes, including driver mutations, frameshifts, gene fusions, RNA-processing variants, and classical TAAs, allowing for broad and unbiased discovery of naturally occurring, low frequency antigen-specific T cells.

Next, selected paired TCR α/β sequences from putative antigen-specific T cells of interest were recovered with VDJ-CITESeq and transduced into Jurkat reporter cells for preliminary functional validation of TCR function with the cognate peptides. Transduction efficiency and expression of the introduced TCR were confirmed by flow cytometry, and activity of the TCR-transduced Jurkat reporters evaluated in a luminescence-based assay with peptide-pulsed targets with HLA(s) of interest for functional validation screening (**Fig. 2A**).

Using this high-throughput natural TCR discovery approach, we identified and functionally validated 117 unique TCRs recognizing HLA-restricted viral epitopes, tumor-associated antigens (TAAs), tumor-specific antigens (TSAs), neoantigens (neoAg), and tumor-associated cryptic antigens across six common HLA alleles (**Fig. 2B–D**). Across antigen classes, viral antigens (n = 34) and cancer/testis (CT) antigens (n = 28) were the most frequently recognized, followed by TAAs (n = 18) and shared splice variants (n = 9) (**Fig. 2C**). The majority of TCRs were restricted by HLA-A*02:01 (46%) and HLA-B*07:02 (25%), with additional contributions from HLA-A*01:01 (12%)**,** HLA-A*11:01 (8%)**,** HLA-A*03:01 (5%), and HLA-A*24:02 (4%) (**Fig. 2D**); notably, the distribution presented here is influenced both by the pMHC panel and donor sources used in screening.

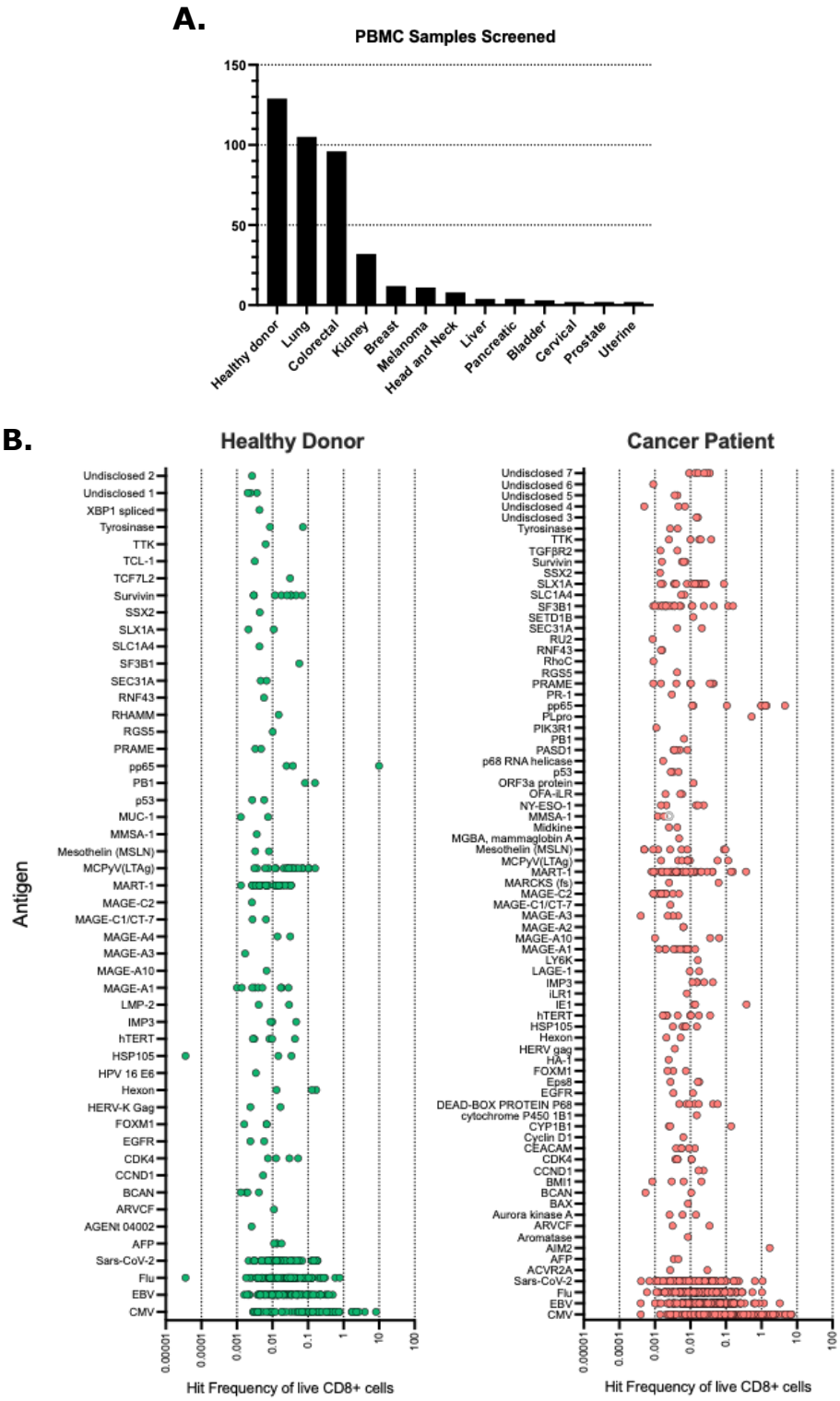

Figure 1: Putative viral- and cancer-specific T cell identification using a high-throughput mass cytometry screening approach. A) Four hundred and ten (410) total PBMC samples from 129 healthy donor and 281 cancer patients of various indications were stained with TargetScape screening panel and acquired by mass cytometry (CyTOF). B) Frequency of viral- and cancer-specific TCR hits in total CD8+ cells in healthy donor (green) and cancer patient (red) samples.

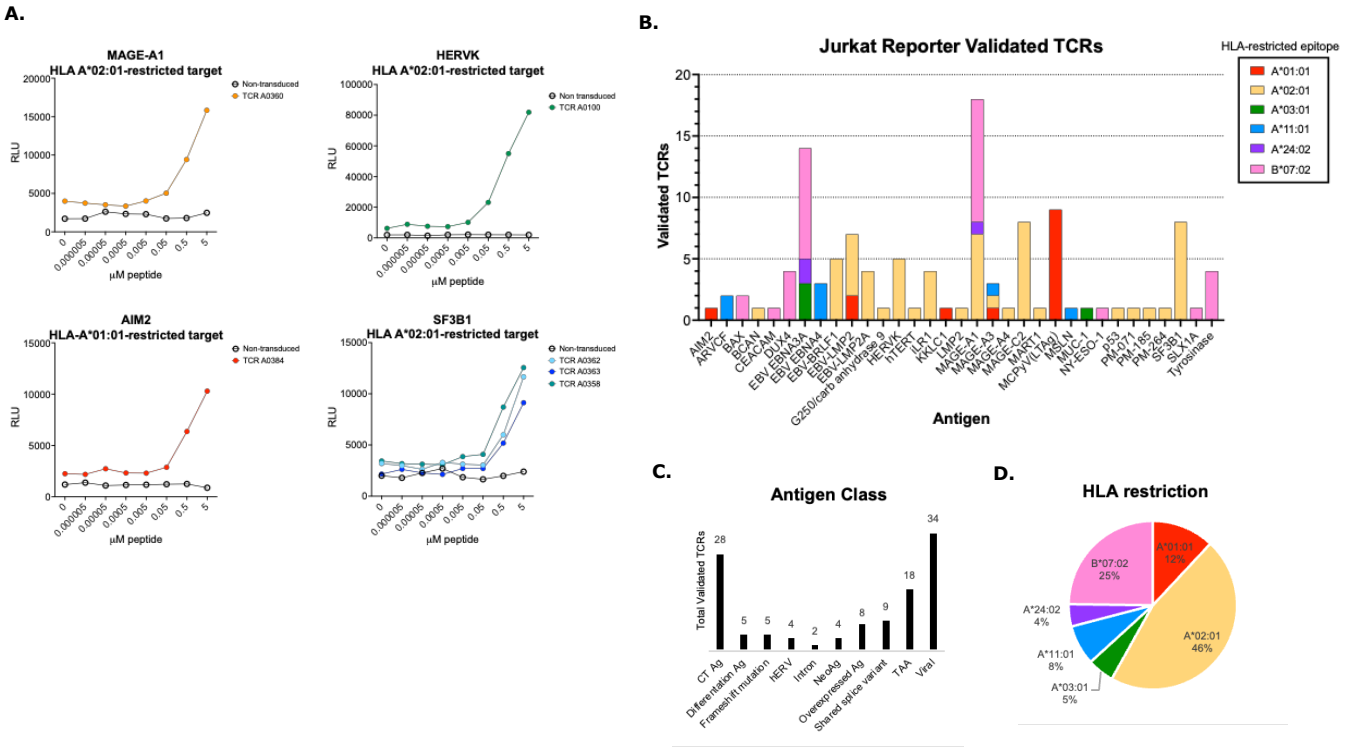

Figure 2: Overview of functionally validated TCRs identified through mass-cytometry agnostic discovery. (A) Representative functionally validated TCRs from bioluminescent assay readout of non-transduced or TCR-transduced (various unique TCRs denoted by "AXXXX" nomenclature) Jurkat reporters plated with peptide epitope of interest and target cells with the relevant HLA restriction. (B) Distribution of validated TCRs by antigen and restricting HLA allele. Each bar represents the number of TCRs validated per antigen, color-coded according to HLA restriction. (C) Classification of validated TCRs according to antigen class. (D) Distribution of validated TCRs by restricting HLA allele.

4.1.2. Functional validation of machine learning predicted EBV-specific TCRs

One of the novel aspects of the described TCR discovery workflow is its ability to integrate high-dimensional phenotypic data with computational prediction to identify antigen-specific TCRs that may be missed by conventional detection methods. To both validate the predictive power of our integrated platform and demonstrate the versatility of the screening framework, we next functionally characterized machine learning–predicted Epstein–Barr virus (EBV)-specific TCRs that were initially undetectable (i.e., unlabeled) by the primary tetramer panel. Using the high-throughput TCR discovery approach outlined above, phenotypic signatures of antigen-specific T cells were leveraged to predict viral specificity for bulk CD8⁺ T cells via machine learning, as previously described (52). To functionally validate machine learning-predicted antigen specificity, we extracted the TCR sequences from T cells predicted to be specific for EBV (**Suppl. Fig. 2**) and which, importantly, did not bind to any of the tetramers used in the staining approach - thus representing bulk CD8⁺ without known specificity. We transduced two predicted EBV-specific TCR clonotypes (TCRs designated A0015 and A0099) identified in separate healthy donors with a lentiviral vector system into TCRα/β-KO CD8⁺ Jurkat reporter cells. Each TCR reactivity was

tested using EBV protein-derived peptide pools pulsed on target cells corresponding to HLA of the respective PBMC donors (**Tab. 1**).

In predicted EBV-specific TCR A0015, we first identified a dose-specific response to Miltenyi PepTivator® EBV LMP2A pool using HLA A*02:01-restricted T2 target cells (**Fig. 3A**). To more precisely localize the activating epitope within the LMP2A protein, we next tested peptide pools, each consisting of nine overlapping 10-mer peptides (7 amino acid (AA) overlap) derived from the EBV LMP2A protein, strain B95-8 (UniProt ID: P13285) **(Suppl. Tab. 1)**. We detected a dose-specific response associated with peptide pool #1, mapping to the N-terminal region (MGSLEMVPMGAGPPSPGGDPDGYDGGNNSQY) (**Fig. 3B**). We deconvoluted the response observed in pool #1 revealed a specific response to the MGSLEMVPMG sequence (peptide P00095, **Fig. 3C**). We additionally selected the top five ranked predicted HLA A*02:01 binders of all 8-12mer epitopes possible from MGSLEMVPMG + 2 AA (MGSLEMVPMGAG) using NetMHCpan (version 4.1b) (**Suppl. Tab. 2**). We identified three homologous HLA-A*02:01–restricted LMP2-derived peptide epitopes (MGSLEMVPM(G/A)) that elicited dose-dependent $CD8^+$ T cell activation, consistent with recognition of structurally similar epitopes. (**Fig. 3C**).

A second predicted EBV-specific TCR (A0099) was tested with Miltenyi PepTivator® EBV Consensus pool using multiple target cell lines or PBMC with partial HLA-match to the original TCR source donor HD5 (**Tab. 1**). We observed dose-specific responses in two targets with partial match to HD5 on HLA-B*35:01 (**Fig. 4A**). Of note, one of the targets in which a response was observed (SDBB019 PBMC) also overlapped HLA-B*07:02 expression with HD5; however, the absence of response in another target expressing this HLA alone (Raji B*07:02) allowed us to exclude HLA-B*07:02 as the presenting allele. Next, we sought to elucidate the specific activating EBV epitope. We evaluated the literature for B*35-restricted EBV epitopes and identified four candidate peptides spanning various EBV proteins (**Tab. 2**). One epitope derived from EBV BZLF1 Lytic protein (EPLPQGQLTAY) elicited a dose-specific response (**Fig. 4B**).

Notably, neither HLA-B*35:01 nor any of the deconvoluted cognate EBV peptides for TCRs A0015 and A0099 were included in our upstream TargetScape TCR discovery screening assays. The successful functional validation of these predicted EBV-reactive TCRs demonstrates the feasibility of combining computational prediction with high-throughput functional screening to identify therapeutically relevant TCRs. This capability represents a unique feature of the platform, enabling the discovery of antigen-specific TCRs beyond the limits of preselected peptide–MHC panels, and could be expanded in the future to accelerate identification of TCRs targeting rare viral epitopes, tumor neoantigens, or other challenging antigenic landscapes.

Table 1. HLA haplotype of A) PBMC samples yielding predicted EBV-specific TCRs and B) various target cells used for allele restricted deconvolution of EBV epitopes.

A.

ML TCR# / epitope	Donor ID	HLA-A		HLA-B		HLA-C	
TCR A0015 / predicted EBV	HD10	A*02:01		A*23:01		B*35:12	
TCR A0099 / predicted EBV	HD5	A*03:01	A*68:02	B*07:02	B*44:03	Unknown	Unknown

B.

Target	Cell type	HLA-A		HLA-B		HLA-C	
T2	Cell line	A*02:01	A*02:01	N/A	N/A	N/A	N/A
Raji A*03:01	Cell line	A*03:01	A*03:01	N/A	N/A	N/A	N/A
Raji B*07:02	Cell line	N/A	N/A	B*07:02	B*07:02	N/A	N/A
SDBB025	PBMC	A*23:01	A*68:01	B*44:03	B*50:01	C*04:01	C*06:02
SDBB019	PBMC	A*01:01	A*11:01	B*08:01	B*35:01	C*04:01	C*07:01
SDBB049	PBMC	A*02:01	A*03:01	B*07:02	B*35:01	Unknown	Unknown

Table 2. Literature-derived HLA-B*35 EBV epitopes.

Peptide ID	Epitope	HLA	EBV Antigen
P00176	HPVGEADYFEY	B*35:01, B*35:08	EBNA1 Latency I, II, III
P00177	YPLHEQHGM	B*35:01	EBNA3A Latency III
P00178	YSLHEQHGM	B*35:01	EBNA3A Latency III
P00179	EPLPQGQLTAY	B*35:01	BZLF1 Lytic

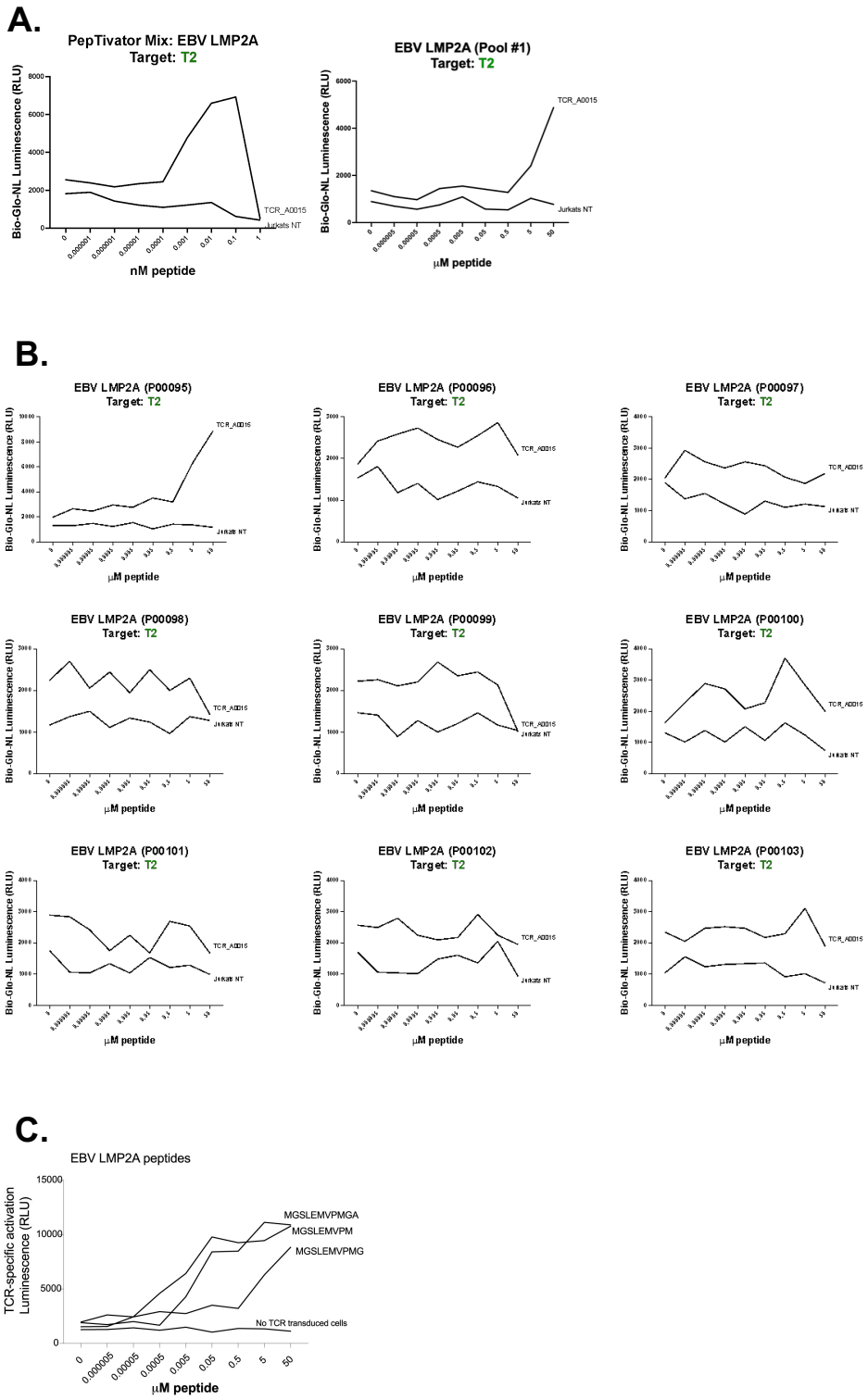

Figure 3. Functional validation and epitope mapping of machine learning–predicted EBV-specific TCR A0015. TCRα/β-KO CD8+ Jurkat reporter cells transduced with the predicted EBV-specific TCR A0015 were co-cultured with HLA-A*02:01 expressing target cell line T2 and serial dilution of various peptides. (A) Miltenyi PepTivator® EBV LMP2A peptide pool. (B) Epitope localization was refined using sequential overlapping 10-mer peptide pools (7-AA overlap) spanning the EBV

LMP2A protein (strain B95-8, UniProt P13285; see Suppl. Tab. 1). (C) Deconvolution of pool #1 identified a single activating peptide (P00095; MGSLEMVPMG); predicted HLA-A*02:01–restricted epitopes within the activating sequence (MGSLEMVPMGAG) were evaluated using NetMHCpan 4.1b (Suppl. Tab. 2).

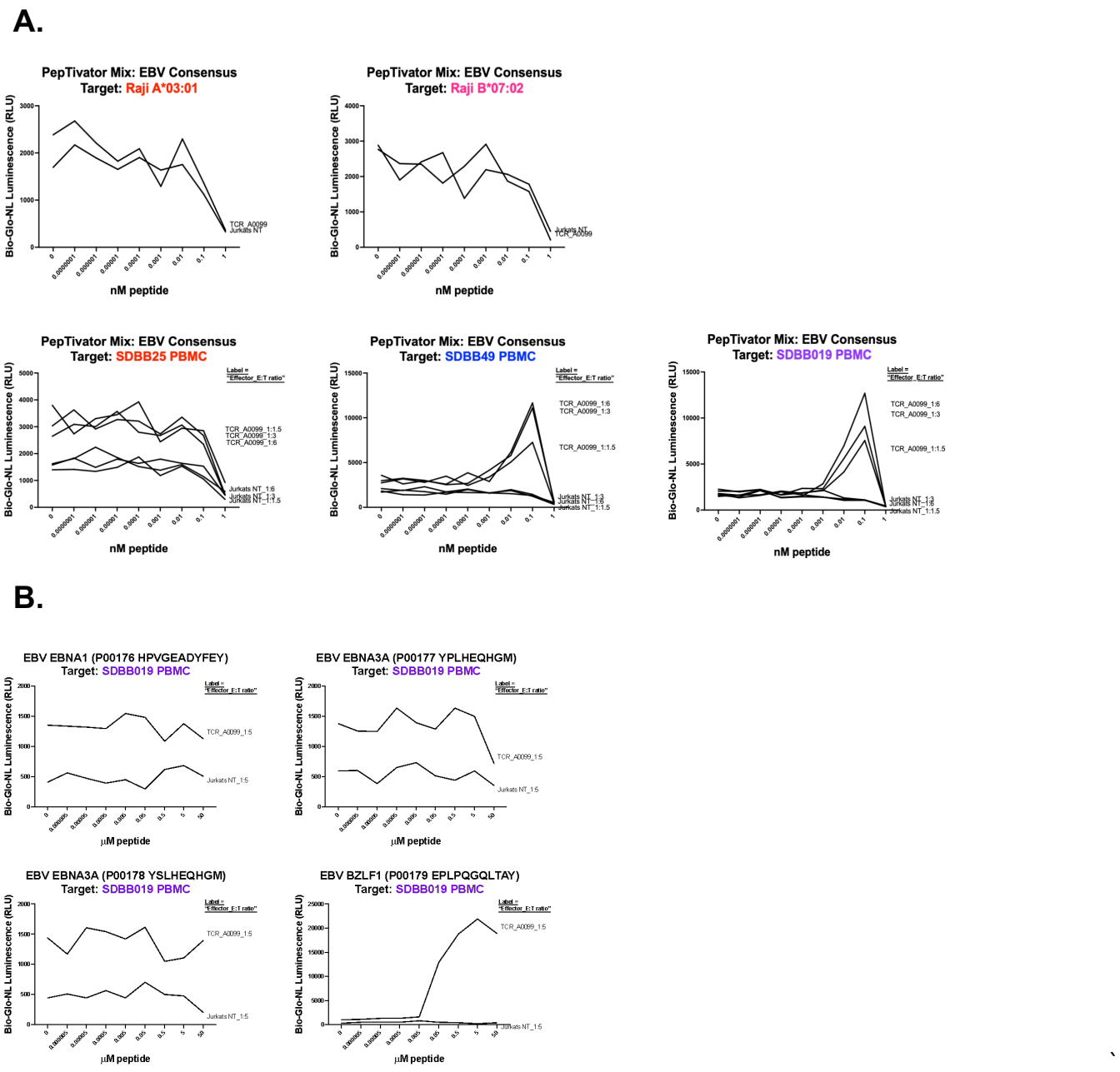

Figure 4. Functional validation and epitope deconvolution of machine learning–predicted EBV-specific TCR A0099. TCRα/β-KO CD8+ Jurkat reporter cells transduced with the predicted EBV-specific TCR A0099 were co-cultured with HLA-appropriate target cell lines or PBMCs and serial dilution of various peptides. (A) Miltenyi PepTivator® EBV Consensus peptide pool with various partial HLA-matched targets. B) Epitope deconvolution of the response in (A) was performed using reported HLA-B*35:01–restricted EBV peptides spanning various viral proteins (Table 2) and B*35:01-expressing SDBB019 target cells.

4.2. Preclinical characterization of a mesothelin-targeting TCR-T cell therapy candidate

Next, we aimed to further explore the capacity of the TCR Discovery approaches outlined above to identify a TCR with potential therapeutic application in TCR-T in oncology. A comprehensive discovery and characterization workflow was employed to isolate a naturally occurring MSLN-specific TCR and assess its preclinical efficacy and safety, as summarized in **Suppl. Fig. 2**. First, we used mass cytometry-based multiplexed tetramer staining to isolate a naturally occurring MSLN-targeting TCR (A0341) against a novel HLA A*11:01-restricted epitope. Next, we confirmed both functional activity of TCR A0341 and endogenous presentation of the epitope FTYEQLDVLK with various MSLN-expressing cancer-derived cell lines. We then performed safety profiling of off-target activity of TCR A0341.

4.2.1. Isolation and validation of a MSLN-targeting TCR

We identified ten putative MSLN-specific cells in the CD8+ population (frequency 0.006) of a single colorectal cancer patient sample that putatively recognize two potential A*11:01-restricted epitopes, FTYEQLDVLK and AIPFTYEQLDVLK (53), along with additional TCR hits against seven distinct viral control epitopes (**Fig. 1B; Fig. 5A**). The two HLA-A*11:01-restricted MSLN epitopes analyzed in this study (FTYEQLDVLK and its N-terminally extended version AIPFTYEQLDVLK) were both included based on prior experimental work identifying them as naturally processed and presented peptides in the context of HLA-A*11:01 as characterized in a study by Zhang et al. (53). Given this evidence, we included both peptide variants in our screening panel to ensure comprehensive evaluation of potential TCR targets. We observed a phenotypically distinct CD127+ signature on MSLN (FTYEQLDVLK/AIPFTYEQLDVLK) hits with unsupervised clustering when compared to viral-specific hits in the same donor (**Fig. 5B**), which may indicate a long-lived memory T cell subset (54–56). While we do not propose to draw conclusions from MSLN-specific T cells in a single patient, we include this data given the paucity of existing information on cancer antigen-specific T cell phenotype in low frequency, naturally occurring tumor-reactive T cells.

Following mass cytometry identification of MSLN hits, TCR sequence recovery was performed. PBMC from the same colorectal cancer patient were expanded *ex vivo* with beads, stained with oligo-tagged multimers and surface antibodies for flow cytometry single cell sorting (**Fig. 5C**). Paired sequences were recovered from a single clone oligo-tagged for MSLN A*11:01 FTYEQLDVLK (TCR A0341) using VDJ CITE-Seq as previously described (52). The A0341 TCR construct (**Fig. 5D**) was designed with both i) codon-optimization of TCR gene sequences, which describes gene engineering approaches that use synonymous codon changes to increase protein production (57) and ii) inclusion of an 2nd stabilizing disulfide bond between the TCR α/β constant regions (58,59) for increased TCR α/β fidelity pairing and transduction efficiency.

Initial functional validation of the putative MSLN-specific TCRs was carried out with A0341 lentiviral-transduced CD8+ TCR α/β KO Jurkat reporters with target cells of various HLA restriction (Raji A*11:01 and Raji A*03:01 engineered cell lines) and two putative target MSLN epitopes (FTYEQLDVLK and AIPFTYEQLDVLK) (**Fig. 5E,F**). While A0341 was agnostically identified with an A*11:01 tetramer, HLA-A*03:01 presentation was additionally screened as it belongs to the same supertype family as A*11:01 (60). Additionally, while A0341 TCR α/β sequences were ultimately identified using the FTYEQLDVLK epitope, a second, slightly longer version of the epitope (AIPFTYEQLDVLK, another putative HLA A*11:01 presented epitope) (53) was also tested.

We observed that a dose-dependent A0341 luciferase signal was activated only in the context of HLA A*11:01 presentation, not HLA A* 03:01, and more optimally with the 10mer epitope (FTYEQLDVLK; EC50 0.01μM) than the 13mer (AIPFTYEQLDVLK; EC50 0.91μM**).** This differential activity likely reflects structural constraints of human MHC class I peptide binding, which typically accommodates peptides of 8–11 amino acids in length (61,62). The reduced functional potency observed with the 13-mer peptide is consistent with suboptimal MHC class I presentation and suggests that the shorter 10-mer represents the physiologically relevant epitope for $CD8^+$ TCR recognition. In contrast, longer peptides such as the 13-mer may be preferentially processed or presented via MHC class II pathways, potentially enabling recognition by $CD4^+$ T cells rather than cytotoxic $CD8^+$ T cells. These findings provide a mechanistic explanation for the dominant functional relevance of the 10-mer epitope in this system despite prior prediction of the longer peptide as an HLA-A*11:01 ligand**.** To our knowledge, neither MSLN epitope has been validated for TCR recognition by another group to date.

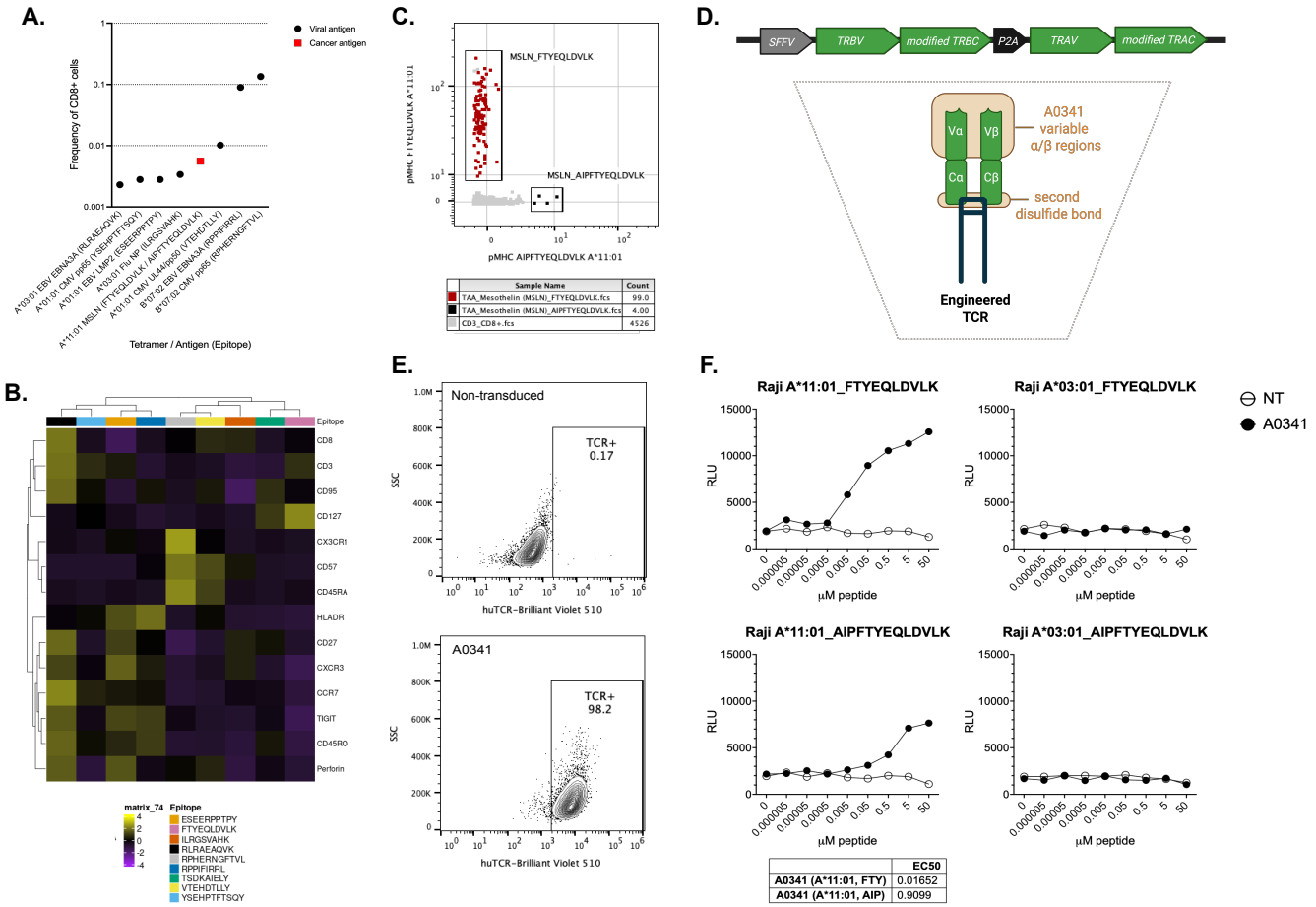

Figure 5. Isolation and functional validation of natural HLA A*11:01-restricted MSLN TCR from a colorectal cancer patient sample. PBMC from a colorectal cancer patient processed with mass cytometry workflow (**Suppl. Fig. 1**) and evaluated for putative Ag-specific T cells. A) Frequency of viral- and cancer-Ag T cells (hits) in total CD8+ cells in bulk sample; epitopes with >70% sequence similarity (including MSLN epitopes FTYEQLDVLK and AIPFTYEQLDVLK) received the same tetramer barcode and are indistinguishable at this stage. B) Heatmap of phenotypic marker expression frequencies with clustering based on Pearson's correlation coefficient. Each column represents one antigen-specific T cell population. C) FACS sorting of MSLN-epitope oligo-tagged *in vitro* expanded T cells stained with HLA multimers and surface antibodies to sort specific T cells into individual wells for scPCR. D) TCR construct design and pictorial representation of the molecular structure engineered with an additional disulfide bond. E) Transduction efficiency of Jurkat reporters +/- A0341 stained with a viability dye and anti-human TCR α/β antibody and collected on flow cytometer. F) Representative Jurkat reporter luminescence-based functional assay; Jurkat TCR α/β KO reporter cells +/- A0341 and antigen presenting cells expressing a selected HLA allele were seeded into 96 well plates (E:T = 1:1) with peptide of interest.

4.2.2. Functional assessment of MSLN TCR-T cells

CD4+ and CD8+ enriched T cells from two healthy donor leukopaks were used as a source of primary T cells for the preparation of TCR-T effector cells; two separate donors were used to preclude endogenous TCR activity specific to either donor. A0341 TCR transduction efficiency quantified by flow cytometry

with an antibody specific to the variable region of the transduced TCR (Vβ1) indicates TCR expression >50% in both donors (**Fig. 6A**). Baseline TCR Vβ1 expression in non-transduced effectors was consistent with reported normal endogenous frequency ranges (63). We observed empirically that both CD4+ and CD8+ cells were transduced with A0341, with a greater percentage of CD8+ cells showing TCR expression (TCR Vβ1+/CD8+ to TCR Vβ1+/CD4+ ratio between 1.5-3.3 in the representative data shown). When A0341 TCR-T effector cells were co-cultured with HLA-A*11:01 Raji targets cells pulsed with increasing concentrations of peptide FTYEQLDVLK, A0341 TCR-T were confirmed to exhibit dose-dependent IFN-***γ*** production (**Fig. 6B**); activity was consistent between both primary donors tested.

Next, A0341 TCR-T activity was tested against MSLN positive tumor cell lines of various indications (**Suppl. Tab. 3**). Target cell lines were selected for potential endogenous MSLN expression based on Protein Atlas reported RNA transcript (nTPM) and protein expression confirmed by flow cytometry staining. Reported HLA-A*11:01 negative (DU145 and OVCAR-3) cell lines were additionally transduced with HLA-A*11:01, expression of which was confirmed by flow cytometry staining. A0341 TCR-T from both donors demonstrated functional activity in IFNγ secretion and target cytolysis readouts against a variety of MSLN-expressing target lines covering a range of solid tumor indications (ovarian, prostate, lung, and pancreatic cancers; **Fig. 6C,D**). Generally, the relative activity of A0341 TCR-T against each tumor cell line corresponded with reported RNA transcript expression of MSLN (nTPM; **Suppl. Tab. 3**) with native or engineered expression of HLA-A*11:01 was observed to increase with higher E:T ratios and was consistent in both donors tested.

These results confirm that the A0341 TCR mediates HLA-A*11:01–restricted recognition and cytolytic activity specifically against MSLN-expressing cancer cells across multiple solid tumor types. Notably, to our knowledge, the epitope targeted here—FTYEQLDVLK presented on HLA-A*11:01—has not previously been validated by another group to date. These findings therefore establish it as a therapeutically relevant antigen for future TCR-T development.

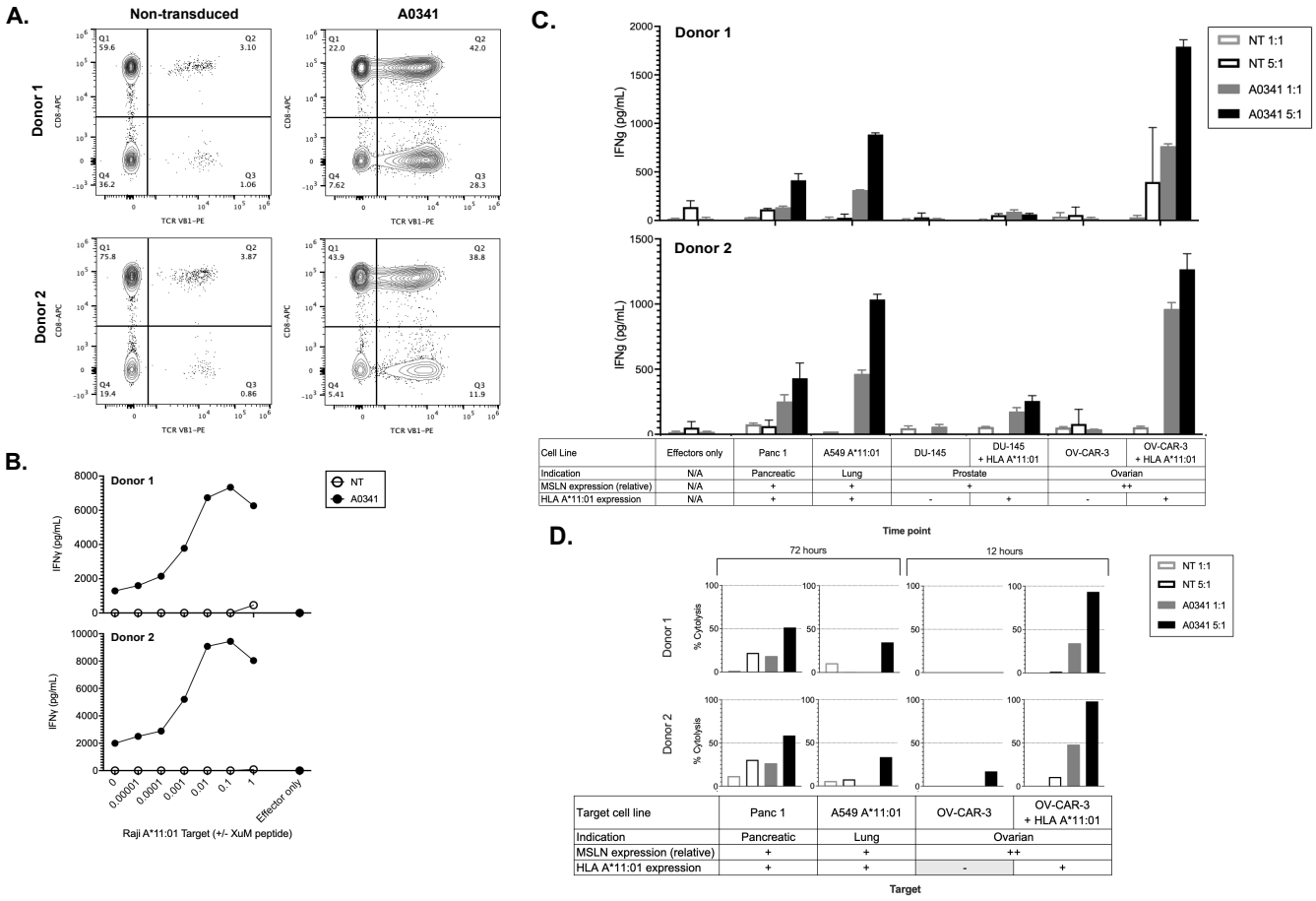

Figure 6. MSLN TCR-T tested with peptide-pulsed or endogenous MSLN Ag presenting targets. Primary effector cells were plated with indicated target cell lines (+/- HLA A*11 engineering) cells. (A) Representative transduction efficiency of A0341 TCR-transduced (TCR-T) or non-transduced effector cells from two donors were evaluated day 9 post-transduction by staining samples with a viability dye and PE-conjugated anti-human TCR Vβ1 antibody and collecting on a flow cytometer. (B) Effectors were plated (E:T = 1:1) with HLA-A*11:01 Raji targets cells and titrated peptide FTYEQLDVLK; after 22 hours, assay well supernatant was evaluated for IFNγ cytokine secretion. Results shown are representative of multiple experiments. (C) Various MSLN expressing target cell lines co-cultured with primary effectors; after 22 hours, assay well supernatant was evaluated for IFNγ cytokine secretion. (D) Cytotoxic activity against adherent cell lines engineering at various E:T ratios using xCELLigence system.

4.2.3. Off-target characterization of MSLN TCR-T cells

Evaluation of on-target activity, described above, is an important first step in characterization of a therapeutic TCR candidate. Following confirmation of activity, it is critically important to next assess the potential for off-target activity. Off-target reactivity refers to the unintended activation of immune cells, such as T cells, against non-target tissues or antigens that share structural similarities with the intended target, potentially leading to damage to healthy cells. This can occur due to shared epitopes between different pathogens or between self and non-self antigens such as in autoimmunity (34). Both alloreactive and cross-reactive responses are examples of off-target TCR activity.

4.2.3.1. Evaluation of alloreactivity

Alloreactivity refers to the response of T cells against foreign antigens, mainly peptide presented on foreign MHC molecules not encountered during thymic development (64,65). To determine potential alloreactivity of A0341 TCR-T, a comprehensive lymphoblastoid cell line (LCL) target panel was generated (**Suppl. Tab. 4**) including at least one sample covering each of the top ten most frequent HLA-A, -B, and -C alleles for North America, Europe, and North-East Asia (source: Allele Frequency Net Database as of June 7th, 2022), and reactivity of A0341 to this panel of cells was evaluated. No significant HLA allele alloreactivity was detected by IFNg activity above the threshold of paired non-transduced (NT) effector control in either primary donor screened (**Fig. 7**).

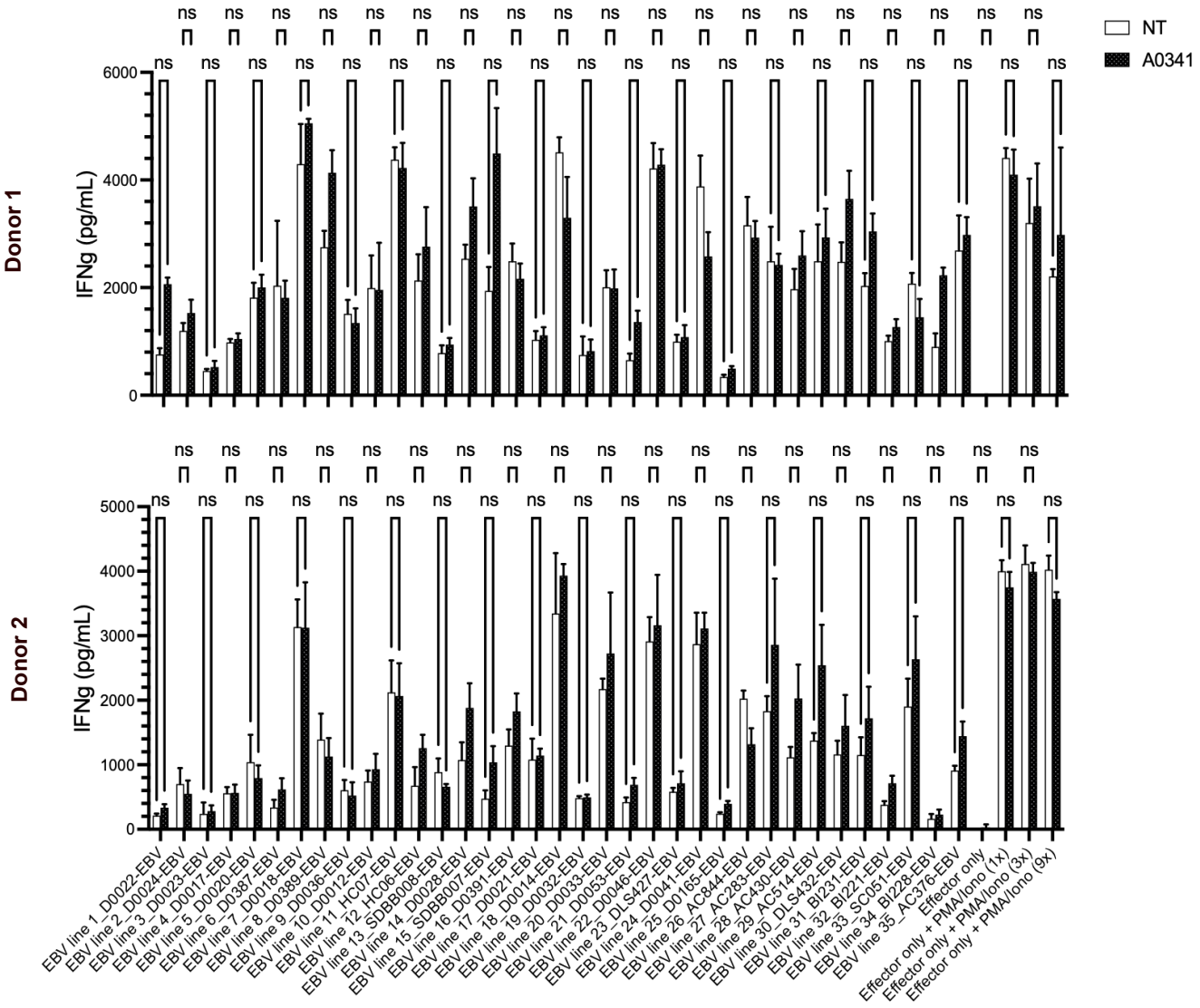

Figure 7. Mapping the alloreactivity profile of A0341 TCR-T. A0341 TCR-T or non-transduced effectors from two primary donors were co-incubated with a panel of EBV-transformed LCL cells with a known HLA type (listed in Supplementary Table 1). Supernatants collected after 22h of co-culture were analyzed for IFNγ content by ELISA. Statistical analysis of Kolmogorov-Smirnov multiple unpaired t tests ($p < 0.05$) performed using Prism software.

4.2.3.2. Cross-reactivity assessment

To address the need for comprehensive and physiologically relevant epitope determination in cross-reactivity screening, we utilized two different motif-based approaches to obtain peptides to be tested: 1) the standard alanine-scan whereby single amino acid (AA) substitutions for alanine at each position in the index peptide are tested *in vitro* to identify the critical residues required for TCR recognition (31,66–68) and 2) a structurally informed, computational modeling approach (overview in **Suppl. Fig. 3**).

As pointed out by Karapetyan (35), while A-scan is a commonly utilized approach, it has limitations that can restrict its ability to detect all cross-reactive peptides. At the same time, the field of computational methods for cross reactivity prediction is in its infancy (69) and existing methods are not applicable in our use case, for example the state-of-the-art method CrossDome (70) allows only 9-mers as input. Therefore, we devised a simple structure-guided computational method, which uses a recently developed variation of the structural prediction tool Alphafold (71): As TCR antigen specificity and activation involves specific contacts between amino acid residues in the TCR complementarity determining regions (CDRs) and pMHC (72,73), the structure-based approach entails prediction of the TCR-pMHC 3D structure of the index peptide in complex with the TCR under investigation with TCRDOCK (71). Next, an interaction motif highlighting which amino acids of the epitope are likely to be in contact with the TCR is computed. For motif generation, we focused on the top 2 positions with the highest number of non-van der Waals interactions. This motif can be augmented with literature knowledge on which positions are relevant for HLA binding (74).

Motifs derived by either method were then used as input to ScanProsite (75) to retrieve candidate epitopes from the human peptidome, however output lists can be prohibitively large to screen entirely. As peptide-HLA binding is governed by anchor residues within the peptide that engage defined pockets in the HLA binding groove, epitopes may be further filtered and ranked according to their predicted HLA-binding affinity using computational tools such as such as NetMHCPan (76) or HLAthena (77) to inform immunogenic epitope selection for a given HLA (78).

4.2.3.2.1. Cross-reactive epitope identification using Alanine- and X-scan

A-scan peptide analogs were screened in Jurkat reporters (**Fig. 8A**) and in two primary donors transduced with MSLN TCRs A0341 (**Fig. 8B**). As indicated by the relative TCR activity for each substituted position (**Fig. 8C**), an alanine substitution was tolerated in at least two A0341-transduced donor T cells at seven

out of ten positions resulting in the A-scan tolerated motif “x-x-Y-E-x-x-x-x-x-K”. A ScanProsite motif search for this motif yields 1,601 unique additional epitopes. From the epitopes in this list, we obtained HLA-A*11:01 binding predictions and selected the top 15 ranked epitopes (**Suppl. Tab. 5**) for X-scan functional testing in primary cells. Although background IFNγ levels in the absence of peptides were generally high in TCR-T cells generated from Donor 1, only stimulation with the HLA-A*11:01 restricted peptide ASYEIGYILK (RNF17) induced IFNγ production above background levels. Similarly, stimulation with the HLA-*A11:01 restricted peptide ASYEIGYILK (RNF17) induced IFNγ production from TCR-T cells generated from Donor 2, albeit at low levels (**Fig. 8D**). Taken together, of the 15 epitopes screened, ASYEIGYILK (RNF17) emerged as a potentially cross-reactive epitope.

4.2.3.2.2. Cross-reactive epitope identification using TCR-pMHC structural modeling

Using TCRDOCK, we predicted 3D structures of the A0341 TCR in complex with the index peptide (FTYEQLDVLK) loaded onto HLA-A*11:01 (**Fig. 8E**). From the obtained TCR-pMHC structures, we derived the interaction profile “x-x-x-E-x-x-x-x-x-L-x” (**Fig. 8F**), which augmented with literature information on positions relevant for HLA binding, i.e. P2, P3 and P10 for a 10mer, yields the motif “x-T-Y-E-x-x-x-x-x-L-K”. Of note, the DHRS11 epitope (ATYEQMKCLK) elucidated from the *in silico* modeling was also recovered using the A-scan approach, however the list of potential cross-reactive epitopes generated from this motif (1,602) would be prohibitive to screen entirely. Subsequent ranking based on predicted HLA A*11:01 binding placed ATYEQMKCLK (DHRS11) epitope at #62 (**Suppl. Tab. 5**), a sufficiently low enough position that it was not captured for initial cross-reactivity screening. Alternatively, by using the structural modeling we were able to identify this cross-reactive epitope independent of *in vitro* A-scan library screening and without the pre- or co-requisite of testing all preceding peptides as ranked by predicted HLA A*11:01 binding.

4.2.3.2.3. Cross-reactive epitope evaluation

Putative cross-reactive epitopes ASYEIGYILK and ATYEQMKCLK derived from the RNF17 and DHRS11 proteins respectively, were selected for further validation testing based on initial A0341 off-target screening (**Fig. 8D**) and TCR-pMHC structural modeling, the two methods described above. When increasing titrations of ASYEIGYILK and ATYEQMKCLK peptides were exogenously presented by HLA-A*11:01 Raji target cells, only ATYEQMKCLK elicited IFNγ production in TCR-T cells from both donors 1 and 2 -in a dose-response dependent manner (**Fig. 9A**).

We further evaluated A0341 cross-reactivity in the context of endogenous DHRS11 expression. Leukemia-derived K562 cells do not express MSLN but do express DHRS11 (**Fig. 9B,C**).

We found that A0341 activation, resulting in target cell cytolysis, was induced by A*11-transduced K562 cells alone, indicating off-target reactivity mediated by endogenously presented DHRS11 on HLA-A*11:01 molecules (**Fig. 9D,E**).

The epitope ATYEQMKCLK is derived from the Dehydrogenase/Reductase SDR Family Member 11 (DHRS11) protein, a 17β-hydroxysteroid dehydrogenase which catalyzes the production of the 11-oxygenated and traditional androgens. DHRS11 expression has been reported in a variety of tissues with highest expression reported in gastrointestinal tract (duodenum, small intestine, colon), followed by rectum, testis, kidney, brain and heart (79,80). Off-target activity of A0341 was confirmed using a leukemia cell line with low reported DHRS11 expression relative to primary gastrointestinal tissue (particularly duodenum and small intestine), conferring TCR A0341 with an unfavorable clinical risk to benefit ratio that would bring challenges to further clinical advancement of this candidate.

In summary, we identified TCR A0341, which targets a novel HLA-A*11:01–restricted MSLN epitope (FTYEQLDVLK), as a candidate for preclinical evaluation. A0341 exhibited potent cytolytic activity against MSLN-expressing tumor cells, confirming FTYEQLDVLK as a therapeutically relevant target; however, off-target reactivity to a DHRS11-derived epitope (ATYEQMKCLK) raises safety concerns that preclude its further clinical development.

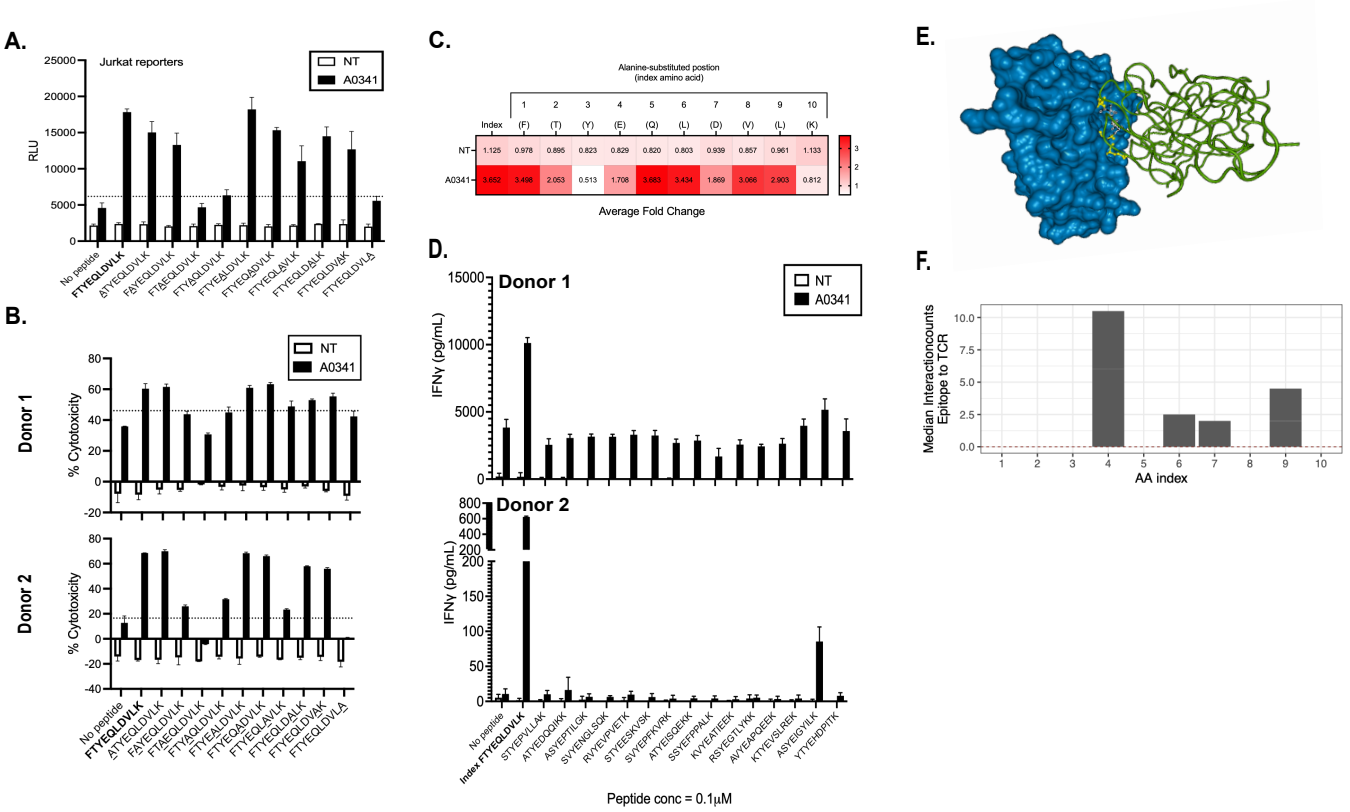

Figure 8. Cross-reactive epitope determination. A-B) A-scan analogs of index peptide tested with cells +/- TCR A0341 in both A) Jurkat reporter (E:T = 1:1, peptide concentration 0.05 µM) and B) two primary effector donors (E:T = 1:1, 1 µM peptide concentration); dashed black line indicates 130% of transduced TCR effector plated with no peptide as minimum threshold cutoff for determination of a "tolerated" AA residue change; representative data are mean and SD of triplicate conditions. C) Heat map of average fold increase of response of A-scan results from (A-C) normalized by respective no peptide conditions. D) Potential cross-reactive epitope screening of the top 15 predicted HLA-A*11:01 10mers (NetMHCPan4.1) from conventional A-scan. E) TCR-pMHC 3D structure A0341-(FTYEQLDVLK)-HLA A*11:01 complex. Green represents TCR A0341, blue is HLA A*11:01 and index MSLN epitope FTYEQLDVLK; amino acids predicted to be interacting with the TCR are highlighted in yellow. F) Interaction motif for A0341 TCR.

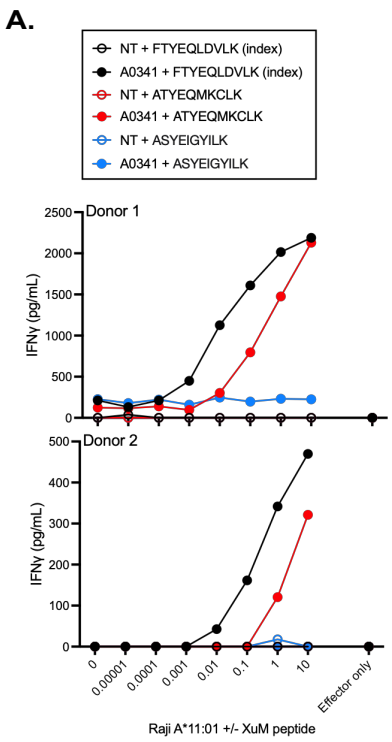

	EC50
Donor 1 FTYEQLDVLK (index)	0.01566
Donor 1 ATYEQMKCLK (DHRS11)	0.5577
Donor 2 FTYEQLDVLK (index)	0.3555
Donor 2 ATYEQMKCLK (DHRS11)	1.056

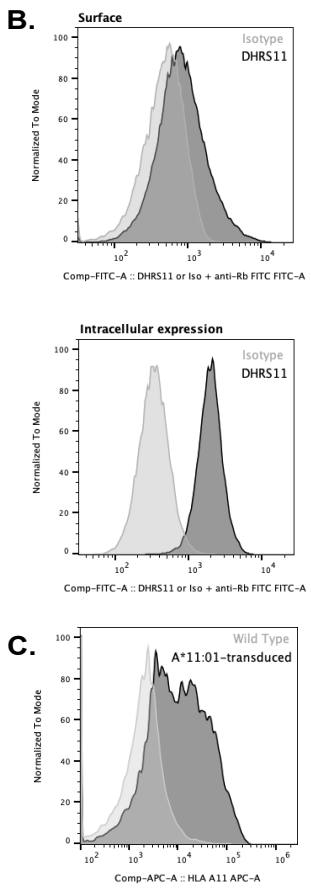

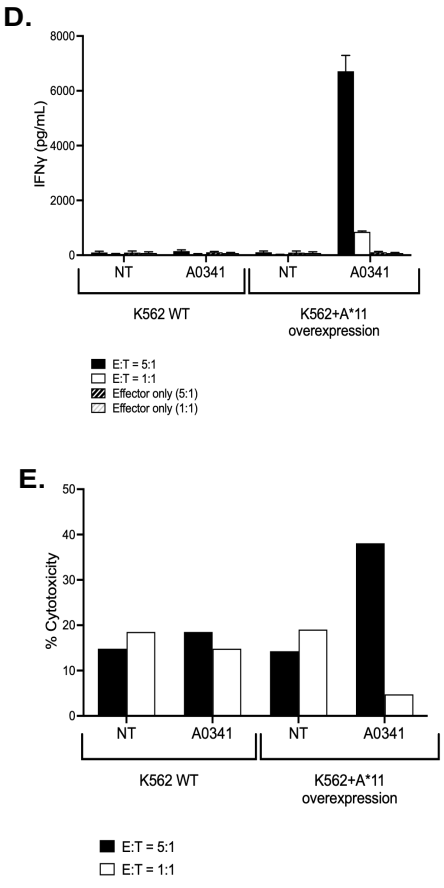

Figure 9. DHRS11 cross-reactive epitope characterization. A) Comparative dose response evaluation of potential cross-reactive peptides vs. index MSLN peptide FTYEQLDVLK. Primary effector cells were plated at an E:T of 1:1 with HLA-A*11:01 Raji target cells and titrated peptide; after 22 hours, assay well supernatant was evaluated for interferon gamma (IFNγ) cytokine secretion. B-C) K562 phenotype; B) surface and intracellular expression of DHRS11 and C) HLA A*11 expression in WT and HLA A*11:01-transduced cells. D-E) Functional cross-reactive screening of A0341 TCR-T against K562 +/- HLA A*11:01; after 22 hours, (D) assay well supernatant was evaluated for interferon gamma (IFNγ) cytokine secretion and (E) remaining cell pellet fraction stained with two viability dyes and collected by flow cytometer for evaluation of cytotoxic activity.

4.3 Immunological profiling and functional augmentation in TCR-T cell therapy

4.3.1. Characterization of CD8+ regulatory T cell precursor population

To better understand potential regulatory mechanisms influencing TCR-T product function, $CD8^+$ regulatory T cell (Treg) precursor populations were profiled across healthy donors, cancer patients, and TCR-T cell products. To investigate potential immunoregulatory $CD8^+$ T cell subsets of therapeutic relevance, we focused on a putative $CD8^+$ regulatory T cell (Treg) precursor population, defined by the immunophenotype $CD3^+CD8^+CD28^-CD39^+CD127^-$and previously associated with suppressive and exhaustion features (81). For clarity, we refer to this population as a $CD8^+$ Treg "precursor" subset throughout, since phenotypic marker expression alone does not confirm immunosuppressive function.

Building upon previously generated TargetScape high-dimensional mass cytometry datasets (**Suppl. Fig. 1**), we performed a retrospective analysis of this subset across healthy donors and cancer patients to establish a baseline understanding of its frequency, phenotypic diversity, and potential involvement in antigen-specific immune responses. We next employed a customized TargetScape panel incorporating candidate $CD8^+$ Treg–associated biomarkers, selected based on both internal analyses and previously reported features of this subpopulation. Finally, we extended these analyses to TCR-T cell products, examining the presence and phenotypic evolution of this subset across multiple stages of *in vitro* TCR-T cell production.

4.3.1.1. CD8+ Treg precursor population in healthy donors and cancer patients

To define the distribution of $CD8^+$ Treg precursors across donor sources, we first retrospectively quantified their frequency within TargetScape datasets encompassing 31 healthy donors and 196 cancer patients representing multiple disease indications. Frequencies were calculated as a proportion of total $CD8^+$ T cells to account for prior CD14/CD19 microbead depletion or $CD8^+$ enrichment steps (Miltenyi $CD8^+$ T Cell Isolation Kit, Cat# 130-096-495), which remove non-$CD8^+$ lineages and thus preclude direct normalization to PBMCs.

Across all samples, the frequency of $CD8^+$ Treg precursors varied substantially (range: 0.036–21.6% of total $CD8^+$ cells), with higher overall frequencies observed in cancer patients compared to healthy donors—consistent with previous findings (82,83). The mean frequency was 0.4850% in healthy donors and 1.831% in cancer patient samples (**Fig. 10A**). When stratified by cancer indication, $CD8^+$ Treg precursor frequencies displayed variable patterns (**Fig. 10B**); however, limited sample sizes (as few as n = 1 in some groups) constrained statistical power for comparisons across indications.

Given that the TargetScape dataset included agnostic peptide–MHC (pMHC) screening, we had the unique opportunity to assess $CD8^+$ Treg precursor representation among TargetScape-identified viral-

and cancer-related antigen-specific TCR hits, as little is known about antigen-specificity of this population. Few of the viral antigen-specific populations contained detectable CD8⁺ Treg precursors, with more limited detection, if any, in cancer antigen specific populations (**Suppl. Fig. 4**). This may reflect both the inherently low frequency of antigen-specific TCR hits—particularly for cancer-associated antigens—and the rarity of the CD8⁺ Treg precursor subset, which in combination may be below the limit of detection.

To more precisely define phenotypic differences, we analyzed mean electron intensity (MEI) values for multiple markers included in the TargetScape panel, comparing bulk CD8⁺ cells and CD8⁺ Treg precursors from 30 healthy donors and 55 cancer patients. To minimize reagent-related variability, only samples stained using a single batch of prepared TargetScape were included in this analysis. Statistical analysis using two-way ANOVA with Tukey's multiple comparison test (**Fig. 11A***)* and Holm–Šídák or unpaired t-tests (**Fig. 11B–C**) identified significant MEI for several markers, which were subsequently included in follow-up panels for further evaluation below as potential biomarkers.

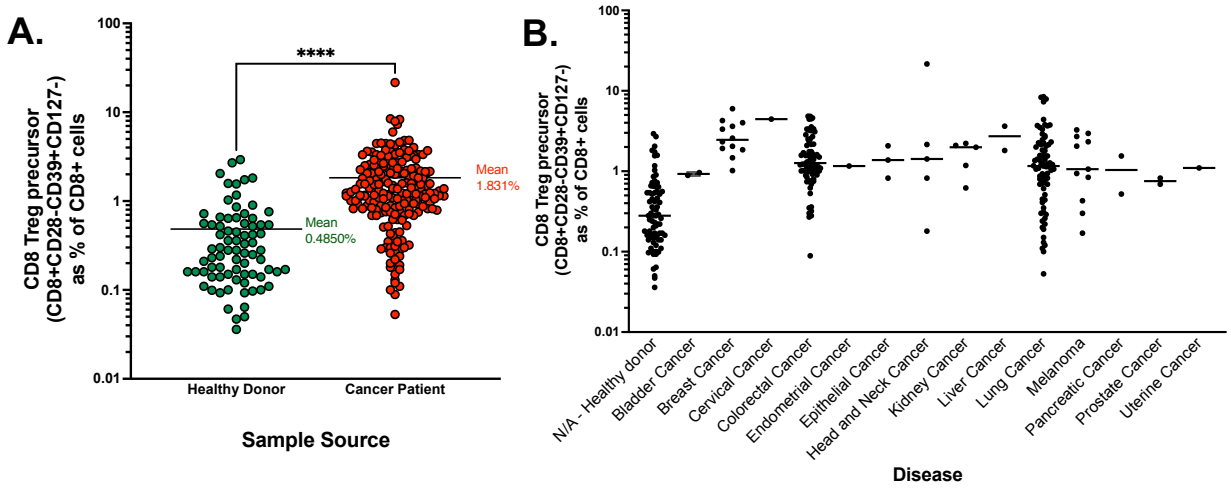

Figure 10: CD8+ Treg precursor frequencies in healthy donor and cancer patient samples. TargetScape samples from healthy donors and cancer patients of various indications were stained with a screening panel containing cell surface markers and collected on a CyTOF mass cytometer. A sample cohort of 31 healthy donor and 196 cancer patient samples of various indications were analyzed for the presence of CD8+ Treg precursors (CD8+/CD28-/CD39+/CD127-) in total CD8+ cells and visualized by frequency in (A) healthy donors versus consolidated cancer patients and B) various indications.

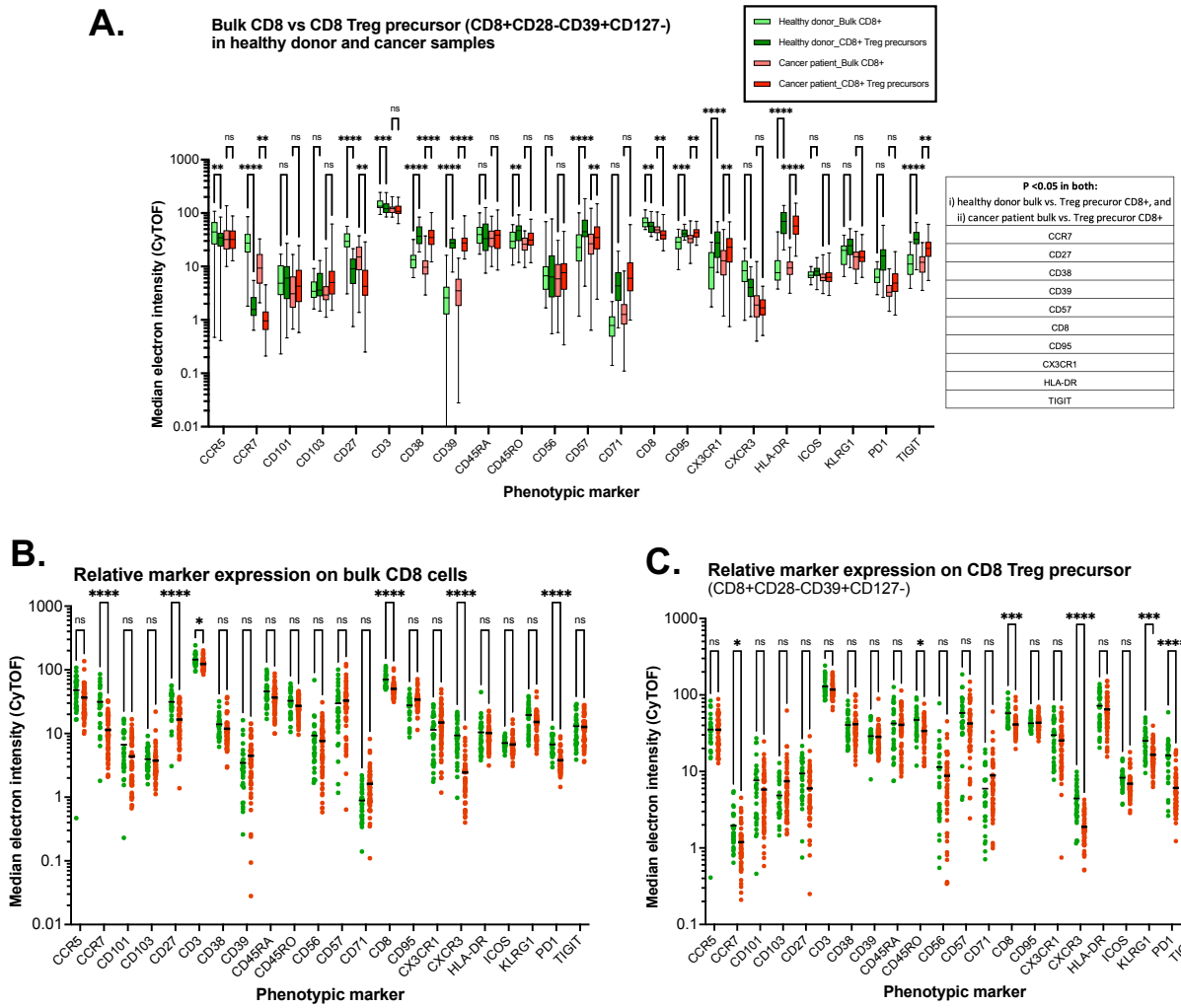

	P value
CXCR3	<0.000001
PD1	<0.000001
CCR7	<0.000001
CD27	<0.000001
CD8	<0.000001
CD3	0.001173

	P value
CXCR3	<0.000001
PD1	<0.000001
CD8	0.000012
KLRG1	0.000013
TIGIT	0.000036
CD45RO	0.000700
CCR7	0.000735

Figure 11: Relative phenotypic marker expression CD8+ Treg precursor in healthy donor and cancer patient samples. Comparison of median electron intensity (MEI) of various TargetScape panel phenotypic markers on CD8+ Treg precursor populations in 30 healthy donor and 55 cancer patient samples. A) Bulk versus Treg precursor CD8+ population in comparisons in both healthy donor and cancer patient samples; statistical analysis of 2-way ANOVA Tukey multiple comparison ($P < 0.05$) performed using Prism software. B) Relative marker comparisons on either bulk CD8+ cells (B) or CD8+ Treg precursor cells (C); statistical analysis of Holm-Šídák multiple unpaired t tests ($P < 0.05$) performed using Prism software; yellow highlighted table cells (C) indicate unique markers with significant MEI differences in CD8+ Treg precursors in healthy donor versus cancer patients and which do not appear to be due to differences in bulk vs. Treg precursor CD8+ differences (A) or to differences in bulk CD8+.

4.3.1.2. Characterization of CD8+ subset within high-frequency CD8+ Treg precursor individuals

Next, we evaluated potential in-house samples for use in further phenotypic and functional characterization of $CD8^+$ Treg precursor cells. Given the overall low abundance of CD8+ Treg precursor cells in most donor sources, six healthy donor and twelve cancer patient samples representing multiple disease indications and exhibiting relatively high $CD8^+$ Treg precursor frequencies (>1.83% of $CD8^+$ cells, corresponding to the mean frequency observed in cancer patient samples per **Fig. 10A**) selected for further analysis are summarized in **Suppl. Tab. 6**.

To comprehensively profile these populations, we designed a TargetScape high-dimensional cytometry panel, designed to measure lineage, activation, exhaustion, and functional markers in putative $CD8^+$ Treg cells. A modification of this panel included an arm with non-specific PMA/Ionomycin stimulation to assess inducible effector functions such as cytokine production. Full panel compositions are provided in **Suppl. Tab. 7**.

Focusing on the $CD8^+$ compartment, we compared the $CD8^+$ Treg precursor population with other canonical $CD8^+$ T cell subsets, including naïve (Tn), stem cell memory (Tscm), central memory (Tcm), effector memory (Tem), and terminal effector/Temra (Te). Unsupervised high-dimensional analysis revealed that $CD8^+$ Treg precursors possess a distinct phenotypic signature, independent of whether the source sample was derived from a healthy donor or a cancer patient (**Suppl. Fig. 5**). No additional biomarkers distinguishing healthy donor from cancer patient origin were identified beyond those previously observed in the retrospective cohort analysis (**Fig. 11**), which may reflect the smaller number of samples analyzed here (n = 18) compared to the prior dataset (n = 85).

We next evaluated marker expression patterns within bulk $CD8^+$ T cells relative to the $CD8^+$ Treg precursor population. When hierarchical clustering was performed (omitting Treg subgating markers CD28, CD39, and CD127 from consideration for unbiased clustering), $CD8^+$ Treg precursors formed a nearly independent cluster, distinct from other $CD8^+$ subsets, with closest phenotypic similarity to $CD8^+$ Tem cells (**Fig. 12A**).

To further investigate the activation profile of $CD8^+$ Treg precursors, we compared marker expression following non-specific PMA/Ionomycin stimulation relative to unstimulated conditions. As the only significant induction observed upon stimulation was an increase in IFNγ expression, subsequent analyses focus on the stimulated condition alone (**Suppl. Fig. 6**). Unsupervised clustering of stimulated PBMCs demonstrated that $CD8^+$ Treg precursors shared HLA-DR and PD-1 expression features with classical $CD4^+$ Tregs, while their overall expression profile again remained most similar to the $CD8^+$ Tem subset (**Fig. 12B**).

Given the phenotypic similarity between CD8⁺ Treg precursors and Tem cells, as well as the expression of activation- and exhaustion-associated markers, we next included terminal effector (Te) cells in a focused phenotypic comparison to determine whether the Treg precursor subset aligns with or diverges from exhaustion-associated differentiation patterns.

A detailed phenotypic comparison of CD8⁺ Treg precursors with Te and Tem subpopulations in unstimulated samples revealed differential expression of CD28, CD39, HLA-DR, and IL-7RA (**Fig. 12C**). CD8⁺ Treg precursors exhibited lower CD28 and IL-7RA relative to Tem cells, but higher levels than Te cells, while CD39 and HLA-DR were elevated compared with both Tem and Te subsets. These expression patterns suggest that CD8⁺ Treg precursors may represent an intermediate or transitional population between Tem and Te differentiation states; however, the distinct marker profile also supports the alternative interpretation that this subset may follow a unique lineage trajectory, separate from classical effector differentiation. This observation is consistent with prior hypotheses proposing a potential exhausted-to-regulatory differentiation pathway, linking features of exhaustion with immunoregulatory function (81).

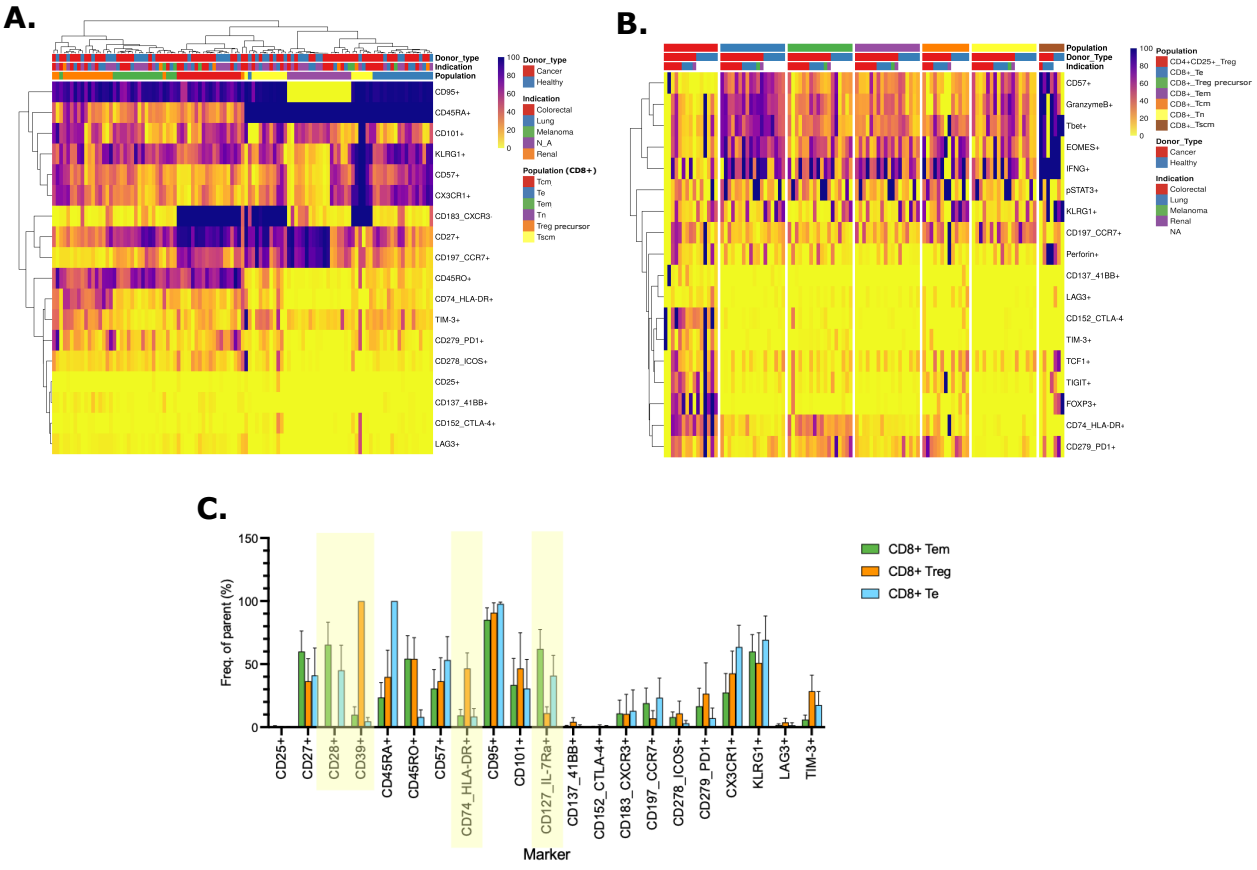

Figure 12. Phenotypic clustering of CD8⁺ Treg precursors relative to canonical CD8⁺ T cell subsets. (A) Unsupervised hierarchical clustering heatmap of marker expression across CD8⁺ T cell subsets from selected healthy donor and cancer patient PBMC samples. Shown are CD8⁺ Treg precursors (CD8⁺CD28⁻CD39⁺CD127⁻) and canonical CD8⁺ subsets: naïve (Tn;

$CD45RA^+RO^-CD95^-CXCR3^-$), stem cell memory (Tscm; $CD45RA^+RO^-CD95^+CXCR3^+$), central memory (Tcm; $CD45RA^-RO^+CD28^+CXCR3^+$), effector memory (Tem; $CD45RA^-RO^+CXCR3^-$), and terminal effector (Te; $CD45RA^+RO^-CD95^+CXCR3^-$) populations. Clustering was performed using expression values from all markers in the TargetScape panel except those used for $CD8^+$ Treg subgating (CD28, CD39, CD127) to allow unbiased comparison. Donor type, disease indication, and population identity are annotated above the heatmap. **(B)** Heatmap showing unsupervised clustering of phenotypic marker expression across $CD4^+$ and $CD8^+$ subsets following PMA/Ionomycin stimulation. Columns represent individual donor samples, and rows represent surface and intracellular markers included in the activation arm of the TargetScape panel. Annotated bars indicate donor type, disease indication, and subset classification. **(C)** Bar graph summarizing marker expression frequencies (% of parent population) for $CD8^+$ effector memory (Tem; green), $CD8^+$ Treg precursor (orange), and $CD8^+$ terminal effector (Te; blue) subsets. Data are shown for all measured markers; shaded regions highlight selected markers of interest. Bars indicate mean ± SD across analyzed donor samples.

4.3.1.3. CD8+ Treg precursor population in TCR-T cell products

To investigate the emergence of CD8+ T regulatory-like phenotypes within TCR-engineered T cell (TCR-T) products, we profiled longitudinal samples derived from six primary donors collected across key stages of production: pre-activation (day 0; d0) and post-transduction expansion (d7, d9, and d14). Across donors, the frequency of a $CD8^+CD28^-CD39^+CD127^-$ subset—consistent with a previously described $CD8^+$ Treg precursor phenotype—was highest in post-transduction TCR-T products and increased progressively over time in culture (**Fig. 13A**). Of note, at later time points (d9–d14), $CD8^+$ cells comprised a greater proportion of the overall cell product, thus the $CD8^+$ Treg precursor population becoming a more substantial component of the total TCR-T product (**Fig. 13B**).

Post-transduction TCR-T (i.e., d7, d9, d14) samples were non-specifically expanding at the time of sample collection, resulting different phenotypic signatures between pre- and post-transduction (**Supp. Fig. 7**). Comparative high-dimensional analysis of the TCR-T $CD8^+$ compartment in the expanded post-transduction samples revealed that this Treg precursor–like subset shared the greatest phenotypic similarity with effector memory (Tem) cells across all time points examined (**Fig. 13C)**. Notably, post-transduction "CD8+ Treg precursor" cells were distinguishable from conventional Tem and terminal effector (Te) populations primarily by the absence of CD28 expression (**Fig. 13D)**.

These findings suggest that $CD8^+$ Treg precursor–like cells emerge during TCR-T production, potentially reflecting expansion-induced shifts in differentiation state. However, the interpretation of these data is limited by technical challenges in isolating this population for functional evaluation. Specifically, the use of CD28 negativity as a defining marker is insufficient, because various $CD8^+$ population downregulate CD28 during activation and proliferation (84,85). This dynamic loss of CD28 across activated and differentiating populations complicates the reliable purification of bona fide Treg precursors, as defined here, from expanded TCR-T cultures. As a result, functional assays targeting $CD28^-$ cells risk contamination with conventional CD8+ subset populations, limiting the ability to definitively determine the immunoregulatory capacity of this subset within the final TCR-T product.

Nonetheless, these observations indicate that TCR-T production can give rise to a dynamically emerging subpopulation with potential immunosuppressive properties, underscoring the importance of accounting for such cells when evaluating the efficacy and functional composition of engineered T cell products, and opens avenues for exploration of methods to enhance functionality by reducing the presence of this population in the final product.

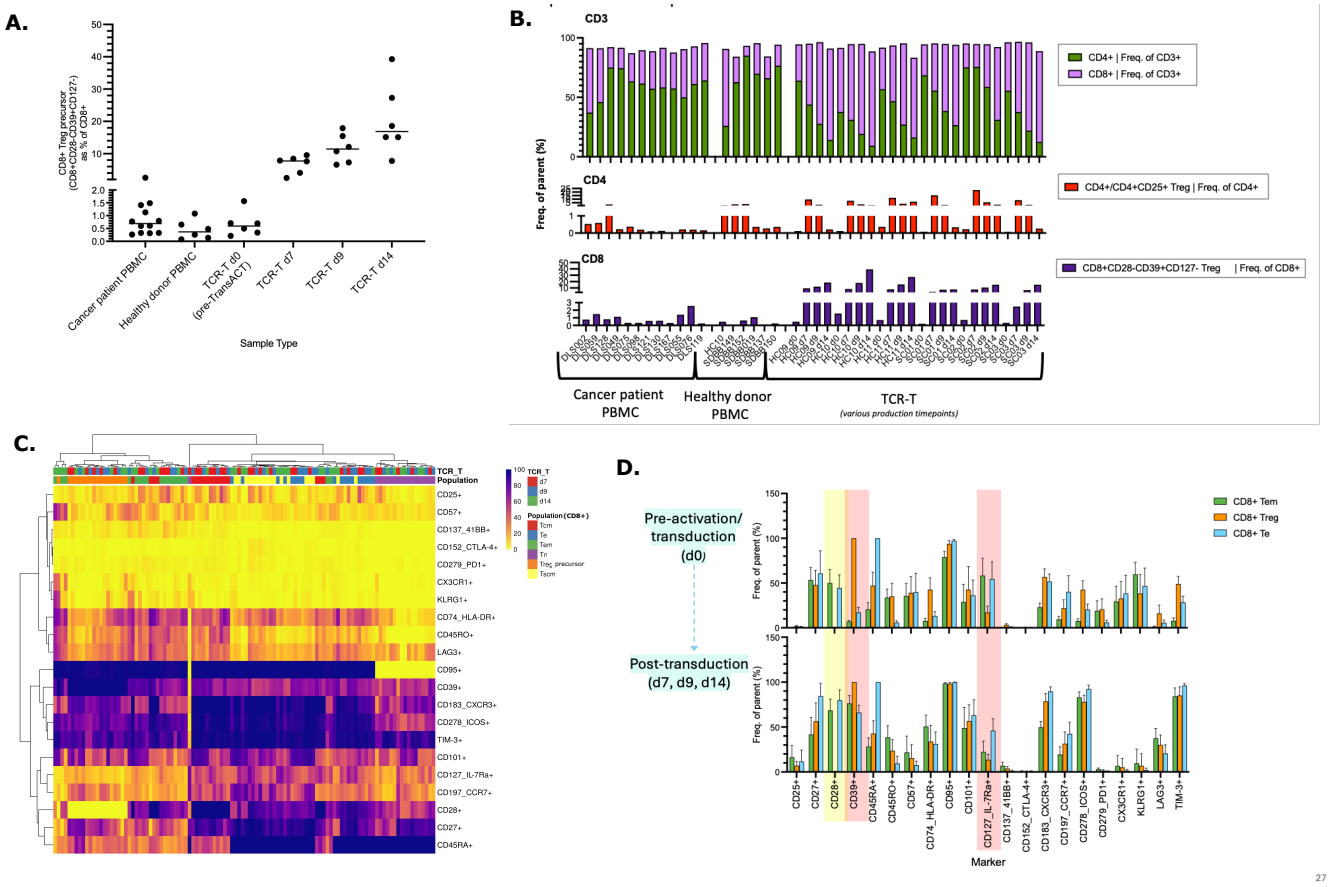

Figure 13. Phenotypic characterization of CD8⁺ Treg precursor–like populations in TCR-engineered T cell (TCR-T) products. (A) Frequency of CD8⁺ Treg precursor–like cells (CD8⁺CD28⁻CD39⁺CD127⁻) across cancer patient PBMCs, healthy donor PBMCs, and TCR-T cell products collected at indicated time points (day 0, day 7, day 9, and day 14) following TCR transduction and expansion. Each point represents an individual donor sample; horizontal bars indicate the mean. (B) Distribution of CD3⁺, CD4⁺, and CD8⁺ subsets within cancer patient PBMCs, healthy donor PBMCs, and TCR-T cell products. Stacked bar plots show frequencies of total CD4⁺ and CD8⁺ T cells within CD3⁺ lymphocytes (top), CD4⁺CD25⁺ Tregs as a fraction of CD4⁺ T cells (middle), and CD8⁺CD28⁻CD39⁺CD127⁻ cells as a fraction of CD8⁺ T cells (bottom). (C) Unsupervised hierarchical clustering heatmap of marker expression profiles within the CD8⁺ compartment of TCR-T products collected at day 0 (pre-activation/transduction), day 7, day 9, and day 14 (post-transduction). Shown subsets include CD8⁺CD28⁻CD39⁺CD127⁻ Treg precursors and canonical CD8⁺ populations. Donor and timepoint annotations are shown above the heatmap. (D) Comparative expression frequencies (% of parent population) of indicated markers for CD8⁺ effector memory (Tem; green), CD8⁺ Treg precursor (orange), and CD8⁺ terminal effector (Te; blue) subsets at pre-activation (day 0, top) and post-

transduction (days 7–14, bottom) time points. Shaded regions highlight selected markers. Bars represent mean ± SD across analyzed donor samples.

4.3.2. Engineering and functional evaluation of co-stimulatory receptors in TCR-T

We next sought to identify co-stimulatory receptor candidates that could enhance the activity and persistence of therapeutic T cells. Given their potential to counterbalance inhibitory signaling within the tumor microenvironment, members of the tumor necrosis factor receptor superfamily (TNFRSF) were prioritized for evaluation. From internal mass cytometry datasets, we observed that CD27 expression—a TNFRSF member constitutively expressed on most $CD8^+$ T cells and tumor-infiltrating lymphocytes—was significantly reduced on bulk $CD8^+$ T cells from cancer patients compared to healthy donors (**Fig. 11B**). This finding prompted us to focus on CD27, alongside another TNFRSF co-stimulatory receptor, 4-1BB, as promising candidates for engineering strategies designed to enhance the function and persistence of autologous TCR-T cell therapy products.

4.3.2.1. Co-receptor construct design and expression in TCR-T effectors

To investigate whether engineering of co-stimulatory receptors (co-receptors, or CoR) could enhance T cell performance, we designed and evaluated a panel of lentiviral constructs incorporating tumor necrosis factor receptor superfamily (TNFRSF) members CD27 (TNFRSF7) and 4-1BB (CD137; TNFRSF9). For initial proof-of-concept testing to verify expression of this intended co-receptor, we designed co-receptor constructs either alone or as multigene constructs in combination with a benchmark therapeutic TCR (Intellia NTLA5001 Wilm's Tumor-1(WT-1)/HLA-A*02:01-specific TCR, herein identified as "TCR A0418")(86) as outlined in **Fig. 14A**.

Following lentiviral vector generation, primary human CD4+/CD8+ T cells derived from healthy donor leukopaks were transduced and expanded under standard TCR-T manufacturing conditions to assess co-receptor transduction efficiency and expression kinetics. Flow cytometric analysis confirmed expression and provided insights into the baseline kinetics of each co-receptor throughout the culture period (**Fig. 14B**). 4-1BB was observed to have a transient increase expression in both baseline (control non-transduced) and 4-1BB CoR-transduced conditions, with a peak in expression observed at d3, consistent with known expression patterns following T cell activation (87); however, even with dynamic expression kinetics 4-1BB expression was increased in 4-1BB CoR-transduced relative to control non-transduced conditions (**Fig. 14B-C**). Baseline CD27 expression exhibited relatively stable expression in donor 1 and gradual decrease over the time course evaluated in donor 2 indicating (**Fig. 14B)**. When CD27 observed as percentage of the population no noticeable differences were observed in CD27 CoR-transduced conditions; however, a marked increase in median fluorescence intensity (MFI) indicated increased surface expression of the introduced receptor (**Fig. 14C-D**).

Importantly, A0418 TCR expression was reduced by >50% in tri-gene TCR α/β + CoR constructs compared to the TCR-only condition, suggesting potential competition for transcriptional or translational machinery (**Fig. 14C**). In contrast, co-receptor expression remained stable and unaffected by the presence of the TCR transgene (**Fig. 14C-D**).

To overcome the suboptimal TCR transduction efficiency observed in the multigene constructs, we next implemented a simultaneous co-transduction approach. In this modified workflow, primary T cells were co-transduced with separate TCR and CoR lentiviral vectors concurrently following overnight activation**.** By day 9 post-transduction, no significant differences in T cell viability or fold expansion were observed among conditions, indicating that dual-vector transduction did not impair overall product yield (**Fig. 14E**). Co-transduced TCR+CoR TCRVB expression levels – though reduced compared to TCR alone – were restored to values comparable to those observed in TCR-only controls, while CoR expression for both transduced CD27 and 4-1BB remained elevated as indicated by MFI and percentage of the population, respectively.

Collectively, these findings demonstrate that simultaneous co-transduction effectively mitigates the TCR expression deficit seen in sequential dual-vector transduction while preserving stable co-receptor expression and normal T cell proliferation. Based on these results, we advanced both the CD27 and 4-1BB co-receptor constructs to downstream functional evaluation.

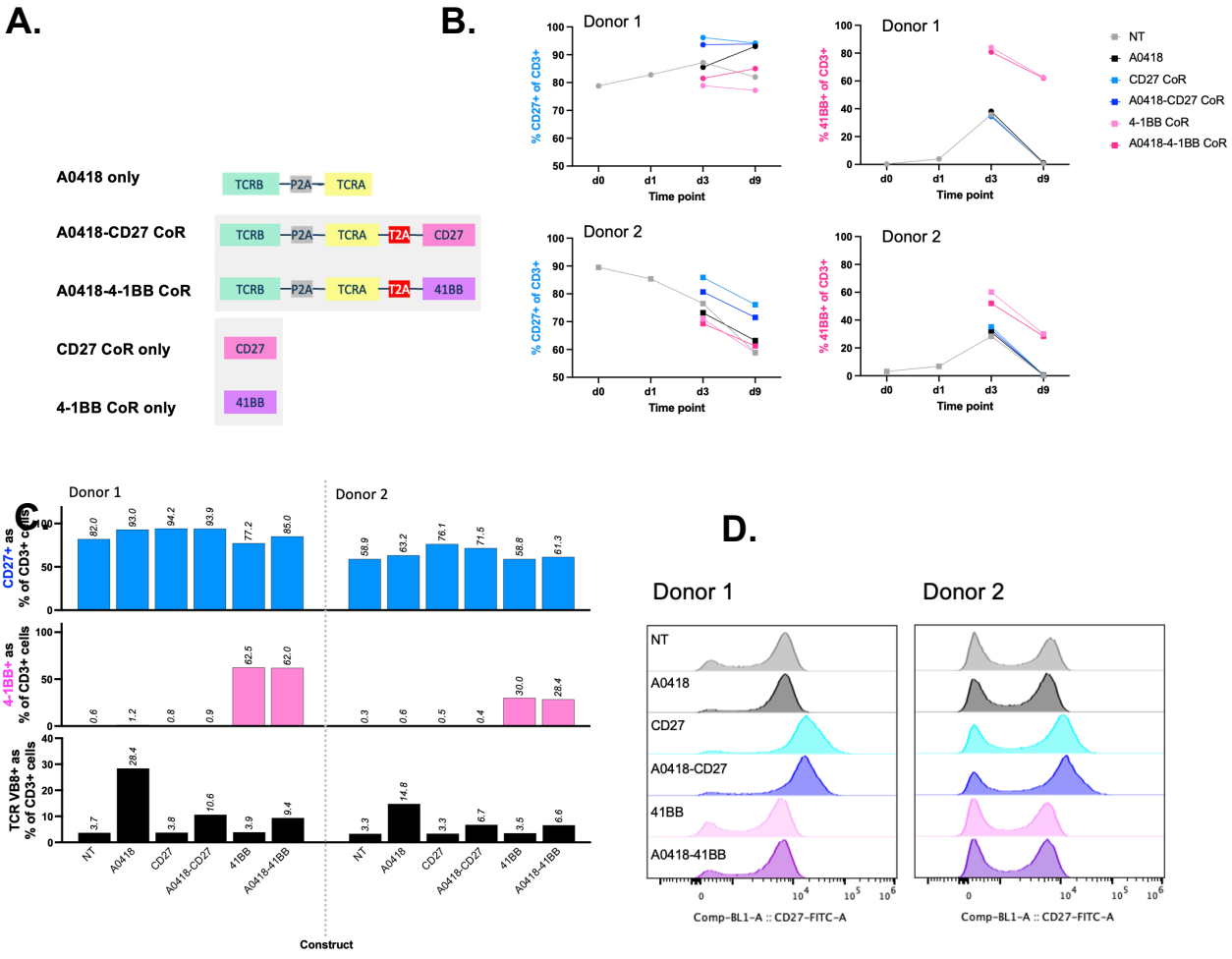

E.

	Effector	TCRVB+ (% of live cells)	CD27 (Mfi)	4-1BB+ (% of live cells)	Fold expnasion (d9/d0)	Viability (% of cells)
Donor 1	NT	3	5012	1	44	96
	A0418	23	6221	1	37	98
	A0418-CD27 co-transduction	12	10034	1	42	99
	A0418-41BB co-transduction	10	4700	62	61	99
	CD27	4	10034	1	49	99
	41BB	4	5012	63	44	98
Donor 2	NT	3	3415	1	47	100
	A0418	16	3415	1	34	99
	A0418-CD27 co-transduction	10	6090	1	39	100
	A0418-41BB co-transduction	10	4345	28	47	99
	CD27	3	9800	1	37	100
	41BB	4	3542	30	42	99

Figure 14. Design and expression characterization of CD27 and 4-1BB co-receptor constructs in primary T cells. (A) Schematic representation of lentiviral constructs used for co-receptor (CoR) engineering. Constructs include the WT1/HLA-A*02:01-specific TCR (A0418) alone or in combination with CD27 and/or 4-1BB CoRs, as well as single-gene CoR constructs. Multicistronic constructs incorporate 2A self-cleaving peptides separating the TCR α- and β-chains and co-

receptor transgenes. (B) Kinetic assessment of CD27 and 4-1BB surface expression following transduction of healthy donor $CD4^+/CD8^+$ T cells with indicated constructs. Line plots show the percentage of $CD27^+$ (left) or 4-$1BB^+$ (right) cells within the $CD8^+$ population over time (days 0, 3, and 9) for two representative donors. (C) Bar graphs summarizing $CD27^+$ (top) and 4-$1BB^+$ (middle) cell frequencies and $TCR\beta^+$ expression (bottom) within $CD8^+$ T cells across constructs for two donors at day 9 post-transduction. (D) Representative flow cytometry histograms showing relative fluorescence intensity for CD27 expression across constructs in donors 1 and 2. (E) Summary transduction and expansion metrics for T cells subjected to single- or co-transduction with TCR (A0418) and co-receptor vectors. Shown are percentages of $TCR\beta^+$ and 4-$1BB^+$ cells, CD27 median fluorescence intensity (MFI) values, fold expansion, and post-transduction viability at day 9 of expansion.

4.3.2.2. Functional evaluation of co-receptor–modified TCR-T effectors

To determine whether CoR engineering could enhance antigen-specific T cell activity, we evaluated the functional performance of WT1- and MSLN-specific TCR-T cells co-expressing CD27 or 4-1BB compared with unmodified TCR-T counterparts. Functional readouts included IFNγ ELISA to assess cytokine release and xCELLigence assays to quantify cytolytic activity against HLA-appropriate target cells.

4.3.2.2.1. WT1 A*02:01 TCR-T ± CD27 or 4-1BB co-receptors

TCR-T cells expressing the WT1-specific TCR (A0418) were generated with or without CD27 or 4-1BB CoR co-expression in primary donor-derived CD4+/CD8+ cells and assessed function across peptide-pulsed and endogenous WT1-expressing targets (**Fig. 15**; summary of WT-1 target cell lines in **Suppl. Tab. 8**).

In donor 1 effector cells, A0418-CD27 demonstrated comparable IFNγ secretion to A0418 alone, whereas A0418-4-1BB showed a diminished maximal response (**Fig. 15A**). In contrast, donor 2 effectors exhibited reduced cytokine production with A0418-CD27 and markedly decreased activity with A0418-4-1BB. When assessed across endogenous WT1-expressing tumor targets, the strongest IFNγ responses were observed against K562+A*02 cells, followed by COV434+A*02 targets (**Fig. 15B**). Interestingly, detectable activation was observed with Raji A*02 (no peptide) targets when singularly or co-transduced with CD27. Given prior flow cytometric analyses demonstrating high expression of the CD27 ligand (CD70) on Raji cells (**Suppl. Tab. 8**), this may reflect ligand-mediated, non-TCR-dependent activation. In xCELLigence dynamic cytolytic assays, A0418 co-expressing CD27 or 4-1BB showed variable effects across adherent target lines (**Fig. 15C**). Slightly enhanced cytolysis was observed against Panc-1 targets with CoR constructs compared to A0418 alone. Modest reductions in background signal were noted against the COV434 wild-type line, with some evidence of improved cytolytic activity against COV434+A*02 targets at low effector-to-target ratios (1:1) in A0418-CD27 cells.

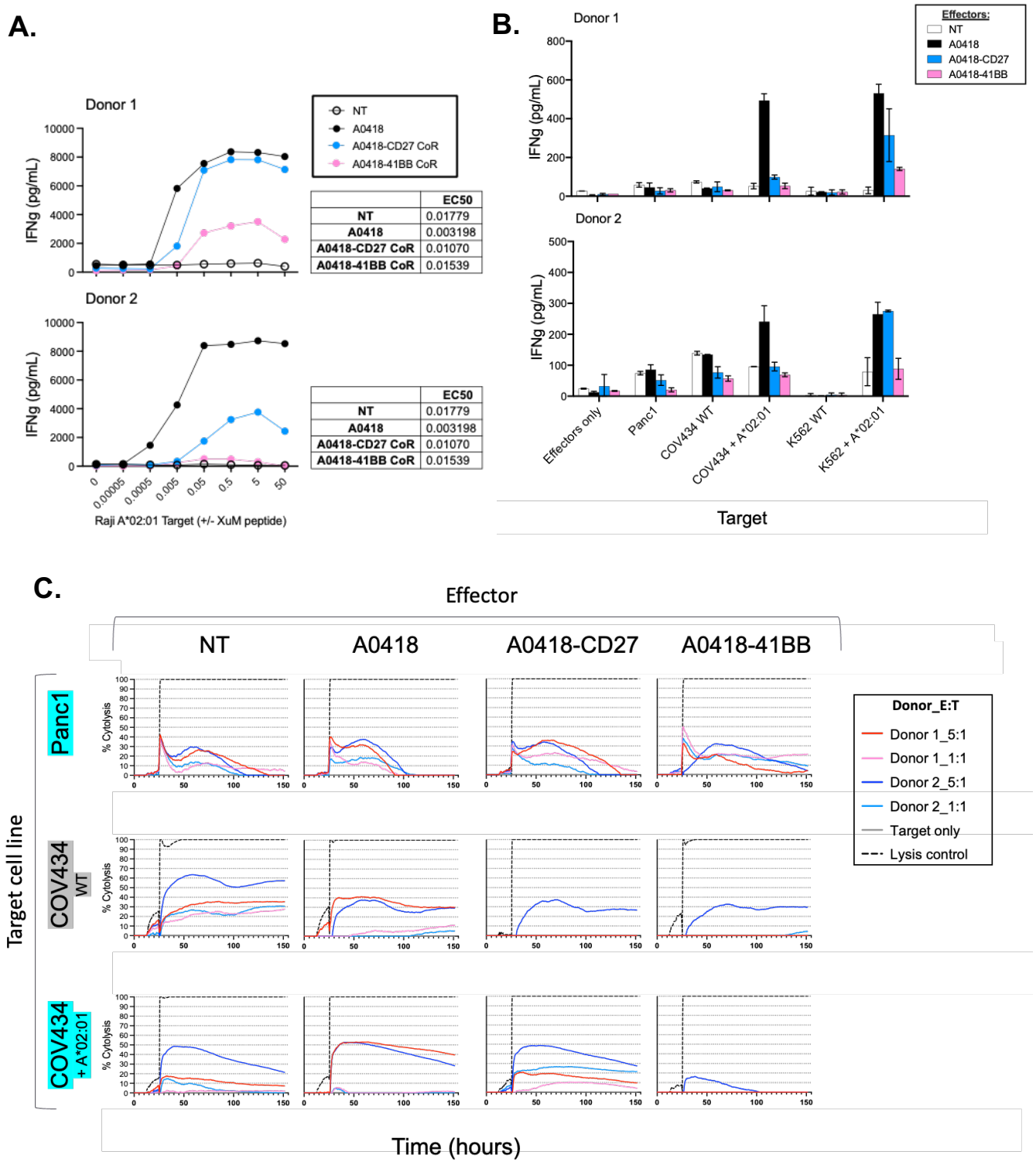

Figure 15. Functional assessment of WT1-specific TCR-T cells with CD27 or 4-1BB co-receptor co-expression
(A) Dose-dependent IFN-γ production by donor-derived WT1/A*02:01 TCR-T cells (A0418) with or without CD27 or 4-1BB co-receptors following stimulation with peptide-pulsed Raji A*02:01 target cells. IFN-γ levels were quantified by ELISA, and EC50 values were determined by nonlinear regression.(B) IFN-γ secretion 24 hours following TCR A0418±CoR effector cells in

response to endogenous WT1-expressing target lines at E:T = 5:1. (C) Real-time cytolytic activity of effector cells against adherent tumor targets (Panc-1, COV434, COV434+A*02:01) measured by xCELLigence impedance-based assays. Target cell index traces are shown over time for effector-to-target (E:T) ratios of 5:1 and 1:1. Dashed lines represent lysis controls. Data are representative of two independent donors.

4.3.2.2.2. MSLN A*11:01 TCR-T ± CD27 or 4-1BB co-receptors

To determine whether similar trends extended to a second antigen model, we generated MSLN-targeting TCR-T cells (using prior in-house characterized MSLN/A*11:01 TCR A0341) with or without CD27 or 4-1BB CoR and assessed function across peptide-pulsed and endogenous MSLN-expressing targets (**Fig. 16;** summary of target cell lines in **Suppl. Tab. 9**).

Transduction confirmed intended CoR expression; again, we noted a decreased transduction expression in the exogenous TCRVB (**Fig. 16A**) All A0341 constructs exhibited broadly comparable dose-dependent peptide responses (**Fig. 16B**). When evaluated against tumor targets naturally expressing MSLN, A0341-CD27 effectors showed modestly enhanced IFNγ secretion relative to A0341 alone across several lines (**Fig. 16C**). In xCELLigence dynamic cytolytic assays, A0341-CD27 demonstrated improved and more sustained killing of A549 A*11 and Panc-1 targets compared to A0341 alone; a more modest but similar effect was also observed with DU-145 cells (**Fig. 16D**).

Collectively, these results indicate that incorporation of co-stimulatory receptors CD27 or 4-1BB into TCR-T constructs produced variable functional outcomes across cognate peptide-HLA dose-response and target settings, with minimal enhancement occasionally observed in 4-1BB–modified cells. CD27 co-expression occasionally improved cytokine release and sustained cytolytic activity, although these effects were not consistently associated with expression of the cognate ligand CD70 on target cells. These findings suggest that CoR engineering may modulate TCR-T function through ligand-dependent and/or ligand-independent mechanisms. Given the more durable enhancement observed with CD27 co-expression in xCELLigence time-course assays, subsequent studies focused on CD27-modified TCR-T cells to assess potential long-term functional benefits and TCR-independent activity.

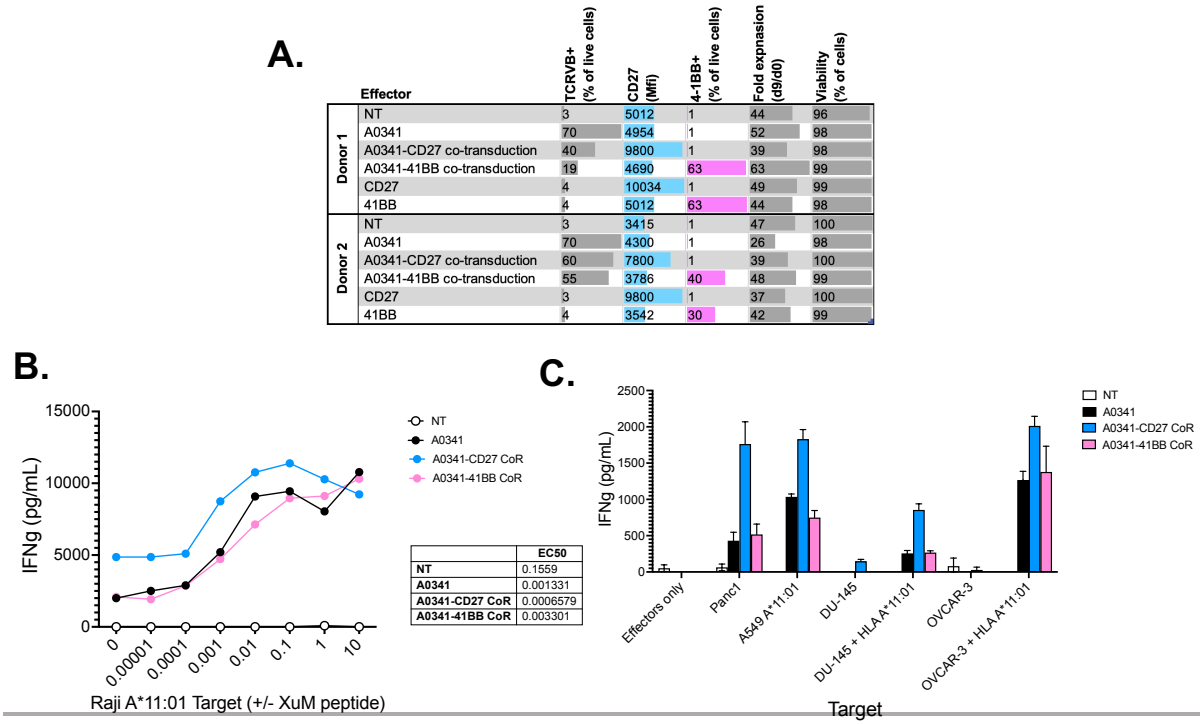

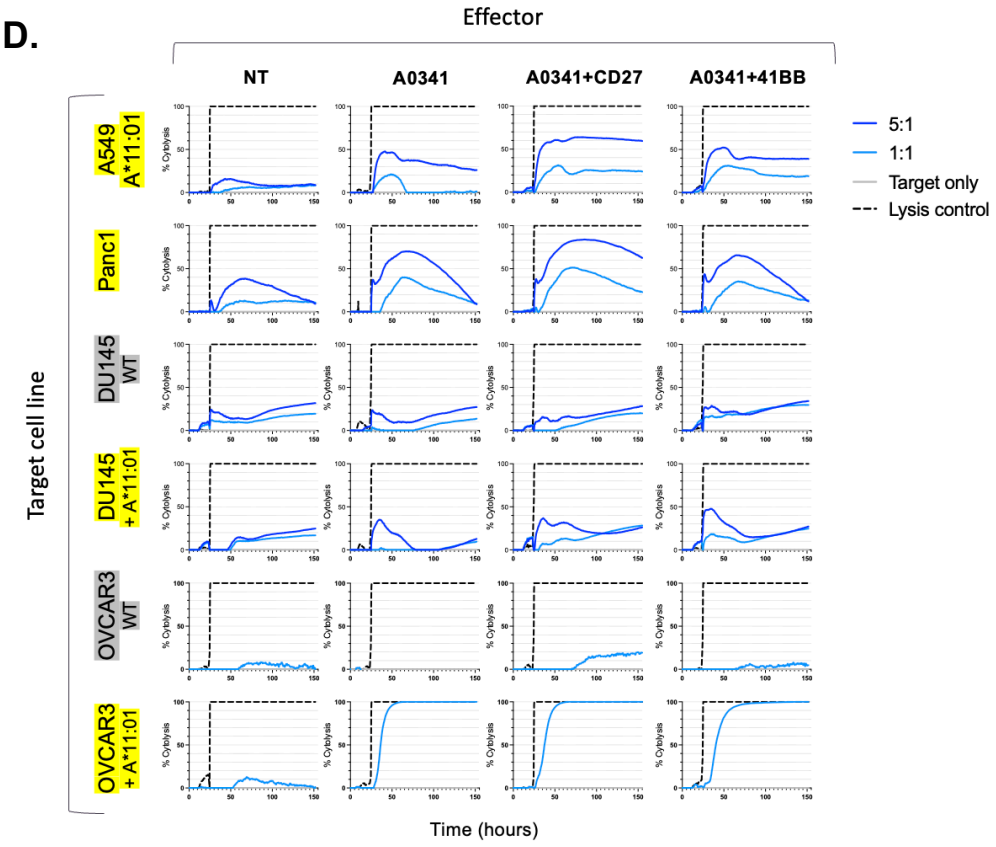

Figure 16. Functional assessment of MSLN-specific TCR-T cells with CD27 or 4-1BB co-receptor co-expression. (A) Flow cytometric analysis of transduction efficiency and co-receptor expression in MSLN/A*11:01-specific TCR-T cells (A0341) with

or without CD27 or 4-1BB co-receptors in primary donor-derived T cells. (B) Dose-dependent IFN-γ secretion by A0341±CoR effectors following stimulation with peptide-pulsed Raji A*11:01 target cells, quantified by ELISA with corresponding EC50 values determined by nonlinear regression. (C) IFN-γ production by A0341 constructs in response to endogenous MSLN-expressing tumor cell lines. (D) Real-time cytolytic activity of A0341±CoR effectors against adherent MSLN-expressing tumor cell lines using xCELLigence impedance-based assays. Target cell index traces are shown for effector-to-target (E:T) ratios of 5:1 and 1:1; dashed lines denote lysis controls. Data shown are representative of two independent donors.

4.3.2.3. Durability assessment of CD27-modified TCR-T effectors

To further assess a possible durable advantage of CoR modification, TCR-T effectors ± CD27 were assessed for proliferative capacity and persistence under both non-specific activation and in coculture with respective endogenously presenting target cell lines (**Suppl. Tab. 8-9**).

Under non-specific stimulation using CD3/CD28 TransAct beads (Miltenyi), CD27-only transduced effectors exhibited the highest proliferative capacity by day 9 (**Fig. 17A**), consistent with enhanced responsiveness to generalized activation signals. Dual TCR+CD27 transduced effectors also demonstrated modestly increased proliferation compared with their respective TCR-only counterparts. No substantial proliferation differences were observed between the $CD4^+$ and $CD8^+$ subsets, indicating that CD27-mediated expansion effects are inducible across the $CD3^+$ T cell compartment.

When assessed for persistence in long-term coculture with tumor cell lines**,** across all TCR/target combinations tested, CD27-engineered effectors generally demonstrated greater durability and maintained higher viable cell numbers over time relative to their unmodified counterparts (**Fig. 17B**). The most consistent distinction observed between $CD27^+$ and control effectors was an increase in normalized $CD3^+$ cell counts over time**,** suggestive of improved persistence.

Notably, this increased persistence did not appear to be driven by TCR-specific activation; elevated CD3+ cells in the TCR+CD27-modified effectors did not correspond to the frequency of $TCRV\beta^+$ cells (as a percentage of $CD3^+$) (**Fig. 17C**). This observation held true for most TCR/target combinations tested, apart from A0418/COV434, potentially reflecting higher affinity interactions specific to that pairing. Furthermore, CD27-only transduced effectors (lacking TCR transduction) also exhibited enhanced persistence, reinforcing the idea that CD27-mediated effects may operate independently of TCR-specific signaling (**Fig. 17A-B**).

Neither was this CD27-modified increase in cell persistence due to enhanced and/or non-specific proliferating cell subsets (in the TCR+CD27 or CD27 only conditions, respectively) (**Suppl. Fig. 8A**). At later time points (up to day 19 post-activation), the persistence advantage of CD27-transduced effectors remained evident, indicating a durable and sustained effect. However, CD27 surface expression did not consistently remain elevated at extended time points, particularly in TCR+CD27 transduced effectors, suggesting that functional effects may persist despite modest expression levels (**Suppl. Fig. 8B**).

Persistence benefits associated with CD27-transduced TCR-T cells were observed across both primary donors tested, although the effect was more consistent in donor 2 across all target types and TCRs (A0341/MSLN and A0418/WT1). Donor 1 showed similar trends but primarily with MSLN-targeting A0341 effectors. This donor-specific variability aligns with prior characterization; Donor 1 displays relatively high, sustained baseline CD27 expression, whereas Donor 2 exhibits lower and more transient expression (**Fig. 14B,D**). Consistent with this, the CD27 CoR construct appeared to provide the greatest benefit in Donor 2, where endogenous CD27 expression is limited.

Collectively, these data suggest that CD27 co-receptor expression enhances effector persistence in TCR-engineered T cells, potentially through general survival or persistence mechanisms rather than TCR-dependent synergy. This benefit appears consistent across multiple donors and sustained over extended culture periods, supporting CD27 as a promising functional augmentation approach for TCR-T products.

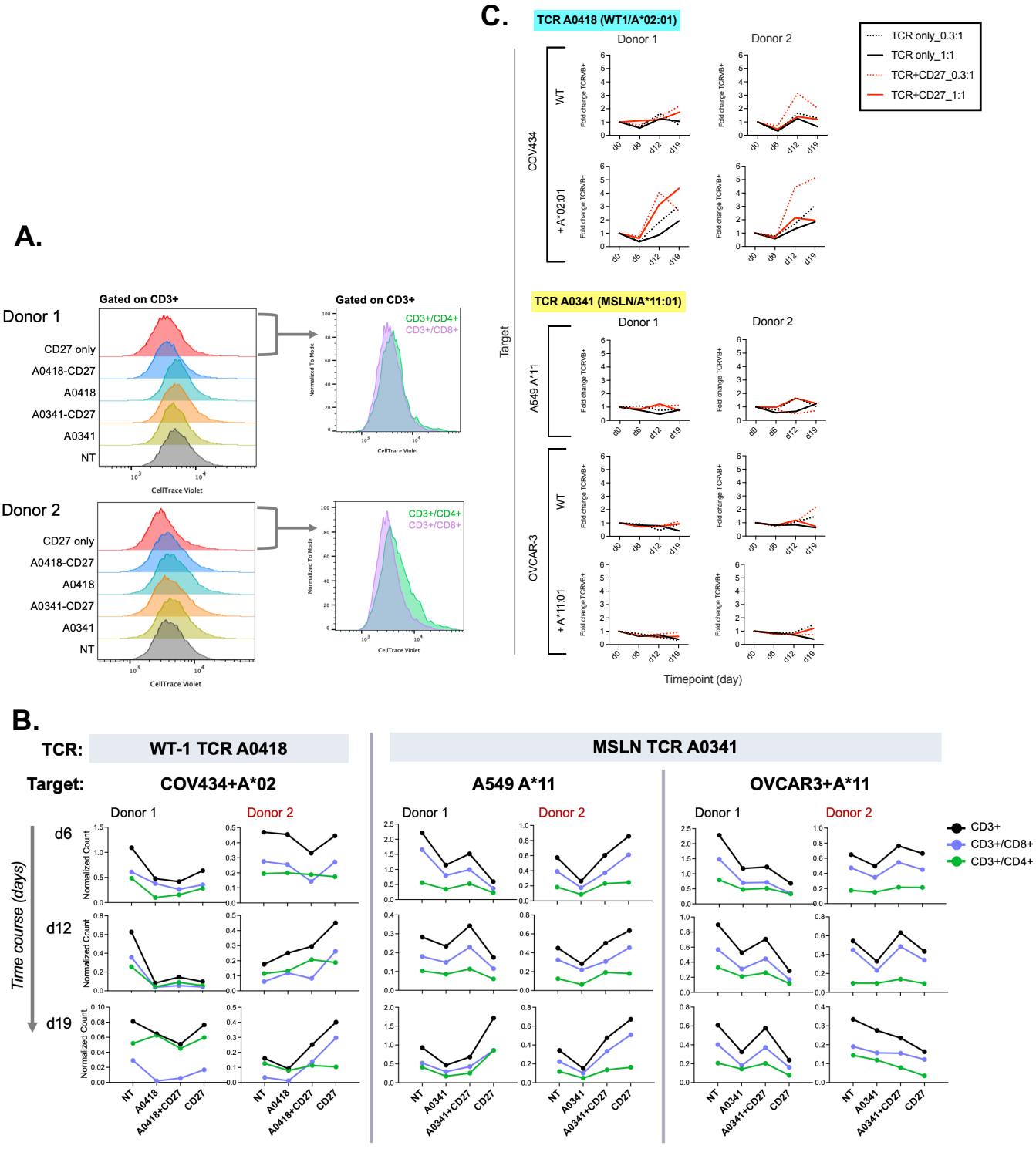

Figure 17. Assessment of proliferative capacity and persistence of CD27-engineered TCR-T effectors. (A) Flow cytometric analysis of proliferative responses following non-specific stimulation with CD3/CD28 TransAct beads. Relative proliferation dye (CellTrace Violet) dilution profiles are shown for $CD3^+$ gated populations from two donors, with representative overlays illustrating $CD3^+CD4^+$ and $CD3^+CD8^+$ subsets. (B-C) Longitudinal evaluation of WT1-specific (A0418) and MSLN-specific (A0341) TCR-T cells ± CD27 co-receptor cocultured with respective HLA-matched and endogenous antigen-presenting target

cell lines. (B) Normalized $CD3^+$, $CD3^+CD8^+$, and $CD3^+CD4^+$ effector frequencies in coculture with tumor cell lines across indicated time points (days 6, 12, and 19). (C) $TCRV\beta^+$ cell frequency within $CD3^+$ populations over time. Graphs represent donor-matched comparisons of TCR-only versus TCR+CD27 effectors at effector-to-target (E:T) ratios of 0.3:1 and 1:1. Data are representative of two independent donors and show mean values from duplicate wells per condition.

---

5. Discussion

Adoptive T cell receptor (TCR)-based therapy represents a promising frontier in cancer immunotherapy, offering the potential to target intracellular antigens inaccessible to antibody or CAR-based strategies. Yet, despite growing clinical interest, the therapeutic impact of TCR-T therapies in solid tumors remains constrained by persistent barriers in novel TCR discovery, safety validation, and sustained functionality within immunosuppressive solid tumor microenvironments (TMEs). This work sought to address these challenges through a multi-faceted research approach that spans the discovery of antigen-specific TCRs, preclinical candidate characterization, and rational engineering to enhance T cell persistence and function.

5.1. Expanding the translational landscape for antigen-specific TCR discovery

One of the central limitations in TCR-T therapy lies in the availability of technologies to discover and characterize diverse, therapeutically relevant, and safely targetable antigen-specific receptors. The high-throughput discovery approach developed in this work demonstrates a scalable route to broaden the antigenic and HLA landscape for therapeutic TCRs. Importantly, it exemplifies a transition from empiric, antigen-by-antigen screening toward agnostic, multiplexed identification of naturally occurring TCRs. This approach holds implications for the field: by recovering TCRs across multiple antigen classes and HLA alleles, it may enable more equitable access to TCR-T therapy across underserved patient populations and tumor indications.

Furthermore, the predictive capacity to infer antigen specificity from phenotypic signatures, as demonstrated with the exploration of EBV-specific TCRs, opens new avenues for immune monitoring and diagnostic applications. While this approach remains nascent and its accuracy depends on the availability of sufficient training data for each target antigen class—an especially challenging limitation in tumor contexts due to the scarcity of well-annotated circulating T cell datasets—it nonetheless holds significant promise. If expanded across additional viral or tumor contexts, such models could inform precision immunotherapy design or even *in situ* monitoring of therapeutic efficacy. In this way, the discovery pipeline established here extends beyond TCR identification and applications to TCR-T development—it contributes a conceptual foundation for data-integrated immunological discovery relevant to cell therapy, infectious disease, and vaccine research.

5.2. Toward safer and more rationally designed TCR-T therapies

Clinical enthusiasm for TCR-T therapy is balanced by caution driven from the risk of off-target and alloreactive toxicities, which remain difficult to predict and mitigate. This project contributes to an emerging paradigm of integrated safety evaluation, wherein orthogonal assays—ranging from peptide mutagenesis to *in silico* structure-based modeling—are leveraged early in development to anticipate and exclude problematic receptor candidates. This strategy exemplifies a "fail early, fail fast" framework that can streamline preclinical decision-making and reduce the translational risk of clinical TCR-T programs.

More broadly, this work underscores a shift in the field to systematic risk management and predictive modeling. As advances in TCR-T engineering and manufacturing propel these therapies toward broader clinical translation, the incorporation of computational, biophysical, and high-throughput validation tools will be critical to ensuring safety without stifling innovation. The structural–computational approach outlined here, while a proof of concept, provides a pathway toward scalable preclinical screening pipelines that can refine TCR selection with higher confidence and speed.

5.3. Functional optimization and the challenge of persistence in the TME

Even with highly specific receptors, TCR-T therapies face substantial functional attrition in the TME, where chronic antigen exposure and inhibitory signaling drive exhaustion and loss of effector potential. Addressing this limitation requires both mechanistic understanding and rational engineering of T cell persistence. The dual strategy approach adopted here—profiling immunoregulatory $CD8^+$ subsets and testing co-stimulatory receptor (CoR) augmentation—illustrates two diverse routes to potentially enhance therapeutic durability.

The phenotypic and temporal characterization of $CD8^+$ regulatory T cell–like subsets adds to a growing recognition that not all $CD8^+$ cells within TCR-T are uniformly cytotoxic, and further study is required to optimize final infused cell products. Regulatory or suppressive fractions may emerge during *ex vivo* expansion and could limit product potency after infusion. Understanding the differentiation pathways, biomarkers, and functional impact of these subsets will be essential to refining T cell manufacturing protocols. These insights may also inform clinical monitoring strategies to ensure consistency and predict patient response.

In parallel, the engineering of TCR-T cells with additional co-stimulatory domains—specifically CD27 and 4-1BB—illustrates how insights from CAR-T optimization can inform next-generation TCR-T design. The observed benefits of CD27 incorporation are consistent with its known roles in promoting T cell survival, enhancing cytokine production, and mitigating activation-induced exhaustion. Notably, the apparent CD70–independent activity of CD27 observed in this study suggests a mechanism of signaling that does not rely solely on CD70 ligand availability. While we cannot rule out contributions from as-yet

uncharacterized ligands, these CD70-independent effects may provide an advantage in tumors lacking CD70 expression, potentially broadening the therapeutic applicability of CD27-engineered TCR-T cells.

As CD27 expression is downregulated in cancer patient–derived T cells, its exogenous inclusion may be particularly advantageous in autologous TCR-T settings, where endogenous costimulatory signaling is impaired. More broadly, such modular receptor design may serve as a flexible template for T cell optimization across adoptive cell therapy platforms, supporting the development of durable, polyfunctional effector populations without compromising specificity.

5.4. Broader implications and future directions

Taken together, this work exemplifies a translationally oriented model for TCR-T cell therapy development—one that integrates discovery, safety, and functional optimization into a cohesive experimental continuum—contributing to a growing movement toward rationally designed adoptive cell therapies that are not only potent and precise, but also predictable and manufacturable.

Beyond immediate translational relevance, these findings also enrich the broader field of T cell immunology. The link between phenotypic signatures and antigen specificity deepens understanding of T cell differentiation; the discovery of suppressive $CD8^+$ subsets during manufacturing raises questions about lineage plasticity; and the demonstration of co-stimulatory enhancement reinforces the importance of integrating synthetic and natural signaling mechanisms. Each of these advances—while arising from TCR-T development—feeds back into fundamental immunology, informing both mechanistic and clinical research.

Future studies should seek to expand the antigen discovery pipeline to additional HLA alleles and clinically relevant target antigens, incorporate machine learning–guided safety prediction, refine co-stimulatory designs and investigate mechanistic underpinnings based on systems-level modeling of T cell exhaustion and persistence. As advances in antigen discovery, receptor engineering, and cell manufacturing intersect, the prospect of clinically durable and safe TCR-T cell therapies for solid tumors is rapidly moving from concept to clinical reality.

In sum, this dissertation contributes not only a set of empirical findings but a translational framework—a roadmap for the next generation of TCR-T therapies that are rationally designed, computationally guided, and biologically optimized for efficacy and safety in the clinic.

5.5. Limitations

While this research provides important insights into the early-stage development and optimization of TCR-engineered T cell (TCR-T) products, several limitations must be acknowledged.

Research Delimitation

The study focused on the in vitro evaluation of TCR-engineered effector cells derived from healthy human primary $CD4^+$ and $CD8^+$ T cells. Excluded from this investigation were clinical-grade manufacturing processes, or patient infusion studies. These omissions reflect deliberate delimitations of scope consistent with early-stage research and development study. Variables such as clinical persistence, systemic immunogenicity, and *in vivo* toxicity could not be addressed using standard *in vitro* methodologies and were therefore reserved for future translational studies.

In addition, TCR discovery was intentionally restricted to HLA class I molecules (HLA-A, -B, and -C), and did not include class II-restricted TCRs or non-classical HLA molecules such as HLA-E. The identification pipeline prioritized $CD8^+$-derived TCRs with putative cytotoxic function and did not include a parallel discovery strategy for $CD4^+$ helper-specific TCRs. While $CD4^+$ T cells were incorporated into final mixed TCR-T products due to their established role in supporting effective immune responses, CD4-mediated antigen specificity and helper-optimized TCR engineering were not independently investigated.

Experimental Design and Model Limitations

The study was restricted to *in vitro* and *in silico* experimental systems and therefore does not fully capture the physiological complexity of the tumor microenvironment (TME) or the *in vivo* immune response. While such systems provide controlled conditions for mechanistic investigation, they lack the spatial, metabolic, and cellular heterogeneity that characterizes human tumors. Consequently, findings relating to TCR-T effector function, persistence, and co-stimulatory enhancement should be interpreted as preclinical observations rather than predictors of clinical efficacy.

Similarly, the absence of *in vivo* testing precludes evaluation of pharmacokinetic and pharmacodynamic parameters, including TCR-T expansion, tissue trafficking, and long-term persistence. These properties can significantly influence therapeutic outcomes but cannot be reliably modeled *in vitro*. Follow-up studies incorporating appropriate models, especially for the CD27 co-stimulatory identified herein as a promising candidate for further study, will therefore be essential to validate the translational relevance of these results.

Sample Representation and HLA Diversity

A further limitation stems from the demographic and genetic characteristics of the donor samples used. All PBMC samples were collected from adult donors residing within the United States, leading to potential sampling bias that may limit global representativeness. While the inclusion of six HLA types captured a significant proportion of the world's population, other HLA variants and their associated peptide-binding repertoires were not evaluated. This limitation may result in underrepresentation of

certain antigen–HLA combinations and reduced generalizability of the identified TCRs to non-U.S. or ethnically diverse populations.

Specificity and Cross-Reactivity Constraints

Although machine learning–based predictions and *in silico* peptide–MHC–TCR interaction modeling were used to support the identification of candidate antigen-specific TCRs, these computational predictions carry inherent uncertainty. The possibility of cross-reactivity with unrelated peptides, particularly those derived from peptides with similar motifs to the target epitope, cannot be fully ruled out. Functional validation assays, while robust, may not identify all potential off-target interactions, particularly those arising from low-affinity or context-dependent binding.

Donor Age and Immune State

All donor samples used in this study were obtained from adults, with no inclusion of pediatric cohorts. As age is known to influence T cell repertoire diversity, activation potential, and exhaustion profiles, the absence of age-related variability restricts the generalizability of these findings. Likewise, healthy donor samples were used for TCR-T functional studies, which may not accurately reflect the immune dysfunction or T cell exhaustion commonly observed in cancer patients.

Technical and Methodological Constraints

As with any complex cellular study, technical variability represents a potential confounding factor. Transduction efficiency, vector design, and culture conditions can influence T cell phenotype and function. Although care was taken to standardize protocols across experiments, variables such as minor batch-to-batch variations in reagents, primary donor cell characteristics, viral titers, and cytokine supplementation may have contributed to experimental variability.

Interpretation and Generalizability

Finally, the findings presented herein should be interpreted within the context of early-stage, proof-of-concept research. The observed effects of co-stimulatory receptor engineering—particularly the influence of CD27 on TCR-T function—reflect controlled *in vitro* conditions and may not directly translate to the dynamic environments encountered *in vivo*. Furthermore, as the study did not assess interactions with the tumor microenvironment or with immunosuppressive stromal factors, the durability and efficacy of these engineered constructs in clinical settings remain to be determined.

Collectively, these limitations delineate the boundaries of inference for this study. They highlight the need for future research integrating *in vivo* validation, expanded HLA coverage, and clinical-grade manufacturing optimization to confirm and extend the biological relevance of these findings.

6. Conclusions

In this study, we demonstrate the utility of a multi-pronged, translationally oriented approach for the discovery, preclinical characterization, and functional optimization of therapeutic T cell receptors (TCRs) targeting a broad range of antigens and HLA alleles. Applying this approach, we successfully recovered antigen-specific TCRs spanning diverse antigen classes—including viral, tumor-associated, and tumor-specific antigens—across six of the most common HLA class I alleles represented in global populations. Among these, we identified and characterized a naturally occurring mesothelin (MSLN)-specific TCR restricted by HLA-A*11:01, an allele underrepresented in current TCR-T cell therapy pipelines. This TCR recognized a novel HLA-A*11:01-restricted MSLN-derived epitope and demonstrated potent antigen-specific cytotoxicity against tumor cells, underscoring its therapeutic relevance in solid malignancies. However, comprehensive safety assessment revealed cross-reactivity with the off-target antigen DHRS11, highlighting the critical importance of integrating broad off-target screening in early TCR discovery workflows.

Beyond this specific candidate, the platform established here provides a scalable and modular framework for the discovery of clinically relevant TCRs paired with rigorous preclinical safety and efficacy evaluation. Through integration of multi-omic, functional, and computational assays, this framework enables systematic identification of rare antigen-specific receptors and facilitates their translation into preclinical development pipelines, addressing a major bottleneck in adoptive T cell therapy. Functional validation of machine learning–predicted EBV-specific TCRs—undetected by upstream screening—demonstrates the platform's ability to uncover therapeutically relevant TCRs beyond preselected peptide–MHC panels. This approach could be extended to accelerate discovery of TCRs targeting rare viral epitopes, tumor neoantigens, or other challenging antigenic landscapes. Moreover, the predictive capacity to infer antigen specificity from phenotypic signatures highlights a potential avenue for immune monitoring and diagnostics, though performance will depend on expanding training datasets across antigen and HLA classes, particularly in tumor contexts where annotated data remain limited.

Parallel engineering strategies focused on improving TCR-T function revealed that co-expression of selected co-stimulatory receptors—particularly CD27—can enhance activation, cytokine secretion, and persistence of TCR-T cells within tumor-challenged contexts. This finding supports the concept of CD27 co-receptor engineering as a rational approach to augment TCR-T potency and persistence, with potential applicability across tumor contexts where chronic antigen exposure drives T cell dysfunction.

In parallel, immunophenotypic profiling of TCR-T manufacturing cultures uncovered the dynamic emergence of $CD8^{+}CD28^{-}CD39^{+}CD127^{-}$ regulatory T cell–like precursors during expansion. While these cells exhibit phenotypic overlap with effector-memory and terminal effector subsets—complicating functional isolation and interpretation—their increasing prevalence during TCR-T production suggests a potentially immunosuppressive influence on product phenotype. The known downregulation of CD28

upon T cell activation and proliferation further complicates their delineation but underscores the importance of monitoring such subsets to ensure functional consistency of therapeutic products. Together, these findings highlight that engineered T cell therapies are not static entities, but evolving ecosystems shaped by differentiation dynamics and manufacturing conditions. Further exploration and manipulation of these factors to control product composition may result in beneficial phenotypic parameters.

Collectively, this work establishes a unified experimental and analytical framework for end-to-end TCR discovery, validation, and functional optimization. The integration of scalable antigen screening, predictive modeling, co-stimulatory receptor engineering, and immunoregulatory profiling provides a foundation for rationally designing TCR-T cell therapies that are both potent and safe.

---

7. References

1. Liu S, Jiang W, Sheng J, Wang L, Cui M. Adoptive cell therapy for cancer: combination strategies and biomarkers. Front Immunol. 2025 Aug 1;16:1603792. doi:10.3389/fimmu.2025.1603792 PubMed PMID: 40821802; PubMed Central PMCID: PMC12354659.

2. Qian J, Liu Y. Recent advances in adoptive cell therapy for cancer immunotherapy. Front Immunol. 2025 Sep 22;16:1665488. doi:10.3389/fimmu.2025.1665488 PubMed PMID: 41058692; PubMed Central PMCID: PMC12497837.

3. Sanjary M, Shokati A, Rahnama MA, Khaseb S, Ahmadvand M. Engineering adoptive cell therapy for solid tumors. Med Oncol. 2025 Sep 28;42(11):500. doi:10.1007/s12032-025-03067-8

4. Wieczorek M, Abualrous ET, Sticht J, Álvaro-Benito M, Stolzenberg S, Noé F, et al. Major Histocompatibility Complex (MHC) Class I and MHC Class II Proteins: Conformational Plasticity in Antigen Presentation. Front Immunol. 2017;8:292. doi:10.3389/fimmu.2017.00292 PubMed PMID: 28367149; PubMed Central PMCID: PMC5355494.

5. Robins HS, Campregher PV, Srivastava SK, Wacher A, Turtle CJ, Kahsai O, et al. Comprehensive assessment of T-cell receptor β-chain diversity in αβ T cells. Blood. 2009 Nov 5;114(19):4099–107. doi:10.1182/blood-2009-04-217604 PubMed PMID: 19706884; PubMed Central PMCID: PMC2774550.

6. Weng N ping. Numbers and odds: TCR repertoire size and its age changes impacting on T cell functions. Semin Immunol. 2023 Sep;69:101810. doi:10.1016/j.smim.2023.101810 PubMed PMID: 37515916; PubMed Central PMCID: PMC10530048.

7. Chen L, Hu Y, Zheng B, Luo L, Su Z. Human TCR repertoire in cancer. Cancer Med. 2024 Sep 6;13(17):e70164. doi:10.1002/cam4.70164 PubMed PMID: 39240157; PubMed Central PMCID: PMC11378360.

8. Cohen CJ, Gartner JJ, Horovitz-Fried M, Shamalov K, Trebska-McGowan K, Bliskovsky VV, et al. Isolation of neoantigen-specific T cells from tumor and peripheral lymphocytes. J Clin Invest. 2015 Oct 1;125(10):3981–91. doi:10.1172/JCI82416 PubMed PMID: 0.

9. Cafri G, Yossef R, Pasetto A, Deniger DC, Lu YC, Parkhurst M, et al. Memory T cells targeting oncogenic mutations detected in peripheral blood of epithelial cancer patients. Nat Commun. 2019 Jan 25;10(1):449. doi:10.1038/s41467-019-08304-z

10. Pulliam T, Jani S, Jing L, Ryu H, Jojic A, Shasha C, et al. Circulating cancer-specific CD8 T cell frequency is associated with response to PD-1 blockade in Merkel cell carcinoma. Cell Reports Medicine. 2024 Feb 20;5(2):101412. doi:10.1016/j.xcrm.2024.101412

11. Manfredi F, Stasi L, Buonanno S, Marzuttini F, Noviello M, Mastaglio S, et al. Harnessing T cell exhaustion and trogocytosis to isolate patient-derived tumor-specific TCR. Sci Adv. 9(48):eadg8014. doi:10.1126/sciadv.adg8014 PubMed PMID: 38039364; PubMed Central PMCID: PMC10691777.

12. Mariuzza RA, Wu D, Pierce BG. Structural basis for T cell recognition of cancer neoantigens and implications for predicting neoepitope immunogenicity. Front Immunol. 2023;14:1303304. doi:10.3389/fimmu.2023.1303304 PubMed PMID: 38045695; PubMed Central PMCID: PMC10693334.

13. Wang Z, Gu Y, Sun X, Huang H. Computation strategies and clinical applications in neoantigen discovery towards precision cancer immunotherapy. Biomark Res. 2025 Jul 9;13(1):96. doi:10.1186/s40364-025-00808-9 PubMed PMID: 40629481; PubMed Central PMCID: PMC12239460.

14. Golikova EA, Alshevskaya AA, Alrhmoun S, Sivitskaya NA, Sennikov SV. TCR-T cell therapy: current development approaches, preclinical evaluation, and perspectives on regulatory challenges. J Transl Med. 2024 Oct 4;22(1):897. doi:10.1186/s12967-024-05703-9 PubMed PMID: 39367419; PubMed Central PMCID: PMC11451006.

15. Meza Pacheco MF, Tai LH. Reprogramming the tumor microenvironment to boost adoptive T cell therapy. Front Immunol. 2025 Oct 23;16:1677548. doi:10.3389/fimmu.2025.1677548 PubMed PMID: 41208982; PubMed Central PMCID: PMC12589096.

16. Adaptimmune [Internet]. 2024 [cited 2025 Dec 10]. Adaptimmune Reports Q2 2024 Financial and Business Updates. Available from: https://www.adaptimmune.com/investors-and-media/news-center/press-releases/detail/273/adaptimmune-reports-q2-2024-financial-and-business-updates

17. Immatics Announces Updated Phase 1b Clinical Data on ACTengine® IMA203 TCR-T Targeting PRAME in Melanoma Patients and Provides Update on Upcoming SUPRAME Phase 3 Trial | Immatics N.V. [Internet]. [cited 2025 Dec 10]. Available from: https://investors.immatics.com/news-releases/news-release-details/immatics-announces-updated-phase-1b-clinical-data-actenginer/

18. Sanomachi T, Katsuya Y, Nakatsura T, Koyama T. Next-Generation CAR-T and TCR-T Cell Therapies for Solid Tumors: Innovations, Challenges, and Global Development Trends. Cancers (Basel). 2025 Jun 11;17(12):1945. doi:10.3390/cancers17121945 PubMed PMID: 40563595; PubMed Central PMCID: PMC12191048.

19. Baulu E, Gardet C, Chuvin N, Depil S. TCR-engineered T cell therapy in solid tumors: State of the art and perspectives. Sci Adv. 2023 Feb 15;9(7):eadf3700. doi:10.1126/sciadv.adf3700

20. Ma P, Jiang Y, Zhao G, Wang W, Xing S, Tang Q, et al. Toward a comprehensive solution for treating solid tumors using T-cell receptor therapy: A review. European Journal of Cancer. 2024 Sep;209:114224. doi:10.1016/j.ejca.2024.114224

21. Smithy JW, Blouin A, Diamond LC, Postow M. Ensuring equity in the era of HLA-restricted cancer therapeutics. J Immunother Cancer. 2022 Nov;10(11):e005600. doi:10.1136/jitc-2022-005600

22. Sanchez-Mazas A, Nunes JM, Di D, Dominguez EA, Gerbault P, Faye NK, et al. The most frequent HLA alleles around the world: A fundamental synopsis. Best Practice & Research Clinical Haematology. 2024 Jun 1;37(2):101559. doi:10.1016/j.beha.2024.101559

23. Hurley CK, Kempenich J, Wadsworth K, Sauter J, Hofmann JA, Schefzyk D, et al. Common, intermediate and well-documented HLA alleles in world populations: CIWD version 3.0.0. HLA. 2020;95(6):516–31. doi:10.1111/tan.13811

24. Ordóñez NG. Application of Mesothelin Immunostaining in Tumor Diagnosis. The American Journal of Surgical Pathology. 2003 Nov;27(11):1418.

25. Lamberts LE, de Groot DJA, Bense RD, de Vries EGE, Fehrmann RSN. Functional Genomic mRNA Profiling of a large cancer data base demonstrates mesothelin overexpression in a broad range of tumor types. Oncotarget. 2015 Jul 1;6(29):28164–72. PubMed PMID: 26172299; PubMed Central PMCID: PMC4695051.

26. Frierson HF, Moskaluk CA, Powell SM, Zhang H, Cerilli LA, Stoler MH, et al. Large-scale molecular and tissue microarray analysis of mesothelin expression in common human carcinomas. Human Pathology. 2003 Jun 1;34(6):605–9. doi:10.1016/S0046-8177(03)00177-1

27. Klampatsa A, Dimou V, Albelda SM. Mesothelin-targeted CAR-T cell therapy for solid tumors. Expert Opinion on Biological Therapy. 2021 Apr 3;21(4):473–86. doi:10.1080/14712598.2021.1843628 PubMed PMID: 33176519.

28. Sun Y, Li F, Sonnemann H, Jackson KR, Talukder AH, Katailiha AS, et al. Evolution of CD8+ T Cell Receptor (TCR) Engineered Therapies for the Treatment of Cancer. Cells. 2021 Sep 10;10(9):2379. doi:10.3390/cells10092379 PubMed PMID: 34572028; PubMed Central PMCID: PMC8469972.

29. Wooldridge L, Ekeruche-Makinde J, van den Berg HA, Skowera A, Miles JJ, Tan MP, et al. A Single Autoimmune T Cell Receptor Recognizes More Than a Million Different Peptides. Journal of Biological Chemistry. 2012 Jan;287(2):1168–77. doi:10.1074/jbc.M111.289488

30. Khosravi-Maharlooei M, Obradovic A, Misra A, Motwani K, Holzl M, Seay HR, et al. Cross-reactive public TCR sequences undergo positive selection in the human thymic repertoire. J Clin Invest. 2019 Jun 3;129(6):2446–62. doi:10.1172/JCI124358 PubMed PMID: 0.

31. Cameron BJ, Gerry AB, Dukes J, Harper JV, Kannan V, Bianchi FC, et al. Identification of a Titin-Derived HLA-A1–Presented Peptide as a Cross-Reactive Target for Engineered MAGE A3–Directed T Cells. Sci Transl Med. 2013 Aug 7;5(197):197ra103. doi:10.1126/scitranslmed.3006034 PubMed PMID: 23926201; PubMed Central PMCID: PMC6002776.

32. Linette GP, Stadtmauer EA, Maus MV, Rapoport AP, Levine BL, Emery L, et al. Cardiovascular toxicity and titin cross-reactivity of affinity-enhanced T cells in myeloma and melanoma. Blood.

2013 Aug 8;122(6):863–71. doi:10.1182/blood-2013-03-490565 PubMed PMID: 23770775; PubMed Central PMCID: PMC3743463.

33. Morgan RA, Chinnasamy N, Abate-Daga DD, Gros A, Robbins PF, Zheng Z, et al. Cancer regression and neurologic toxicity following anti-MAGE-A3 TCR gene therapy. Journal of immunotherapy (Hagerstown, Md : 1997). 2013 Feb;36(2):133. doi:10.1097/CJI.0b013e3182829903 PubMed PMID: 23377668.

34. Zhao ZS, Granucci F, Yeh L, Schaffer PA, Cantor H. Molecular Mimicry by Herpes Simplex Virus-Type 1: Autoimmune Disease After Viral Infection. Science. 1998 Feb 27;279(5355):1344–7. doi:10.1126/science.279.5355.1344

35. Karapetyan AR, Chaipan C, Winkelbach K, Wimberger S, Jeong JS, Joshi B, et al. TCR Fingerprinting and Off-Target Peptide Identification. Front Immunol. 2019 Oct 22;10:2501. doi:10.3389/fimmu.2019.02501 PubMed PMID: 31695703; PubMed Central PMCID: PMC6817589.

36. Donnadieu E, Luu M, Alb M, Anliker B, Arcangeli S, Bonini C, et al. Time to evolve: predicting engineered T cell-associated toxicity with next-generation models. J Immunother Cancer. 2022 May 1;10(5):e003486. doi:10.1136/jitc-2021-003486 PubMed PMID: 35577500.

37. Kotturi MF, Assarsson E, Peters B, Grey H, Oseroff C, Pasquetto V, et al. Of mice and humans: how good are HLA transgenic mice as a model of human immune responses? Immunome Research. 2009 Jun 17;5(1):3. doi:10.1186/1745-7580-5-3

38. Kosti P, Maher J, Arnold JN. Perspectives on Chimeric Antigen Receptor T-Cell Immunotherapy for Solid Tumors. Front Immunol. 2018 May 22;9:1104. doi:10.3389/fimmu.2018.01104 PubMed PMID: 29872437; PubMed Central PMCID: PMC5972325.

39. Topp MS, Riddell SR, Akatsuka Y, Jensen MC, Blattman JN, Greenberg PD. Restoration of CD28 Expression in CD28− CD8+ Memory Effector T Cells Reconstitutes Antigen-induced IL-2 Production. J Exp Med. 2003 Sep 8;198(6):947–55. doi:10.1084/jem.20021288

40. Daniel-Meshulam I, Horovitz-Fried M, Cohen CJ. Enhanced antitumor activity mediated by human 4-1BB-engineered T cells. International Journal of Cancer. 2013;133(12):2903–13. doi:10.1002/ijc.28320

41. Melo V, Nelemans LC, Vlaming M, Lourens HJ, Wiersma VR, Bilemjian V, et al. EGFR-selective activation of CD27 co-stimulatory signaling by a bispecific antibody enhances anti-tumor activity of T cells. Front Immunol. 2023 Jul 20;14. doi:10.3389/fimmu.2023.1191866

42. Flieswasser T, Camara-Clayette V, Danu A, Bosq J, Ribrag V, Zabrocki P, et al. Screening a Broad Range of Solid and Haematological Tumour Types for CD70 Expression Using a Uniform IHC Methodology as Potential Patient Stratification Method. Cancers. 2019 Oct;11(10):1611. doi:10.3390/cancers11101611

43. Daniel-Meshulam I, Horovitz-Fried M, Cohen CJ. Enhanced antitumor activity mediated by human 4-1BB-engineered T cells. International Journal of Cancer. 2013;133(12):2903–13. doi:10.1002/ijc.28320

44. Karlsson M, Zhang C, Méar L, Zhong W, Digre A, Katona B, et al. A single-cell type transcriptomics map of human tissues. Sci Adv. 2021 Jul;7(31):eabh2169. doi:10.1126/sciadv.abh2169 PubMed PMID: 34321199; PubMed Central PMCID: PMC8318366.

45. Grimmig T, Gasser M, Moench R, Zhu LJ, Nawalaniec K, Callies S, et al. Expression of Tumor-mediated CD137 ligand in human colon cancer indicates dual signaling effects. OncoImmunology. 2019 Dec 2;8(12):e1651622. doi:10.1080/2162402X.2019.1651622 PubMed PMID: 31741755.

46. Niederlova V, Tsyklauri O, Chadimova T, Stepanek O. CD8+ Tregs revisited: A heterogeneous population with different phenotypes and properties. European Journal of Immunology. 2021;51(3):512–30. doi:10.1002/eji.202048614

47. Mishra S, Srinivasan S, Ma C, Zhang N. CD8+ Regulatory T Cell – A Mystery to Be Revealed. Front Immunol. 2021 Aug 18;12:708874. doi:10.3389/fimmu.2021.708874 PubMed PMID: 34484208; PubMed Central PMCID: PMC8416339.

48. Huff WX, Kwon JH, Henriquez M, Fetcko K, Dey M. The Evolving Role of CD8+CD28− Immunosenescent T Cells in Cancer Immunology. Int J Mol Sci. 2019 Jun 8;20(11):2810. doi:10.3390/ijms20112810 PubMed PMID: 31181772; PubMed Central PMCID: PMC6600236.

49. Dash P, Wang GC, Thomas PG. Single-Cell Analysis of T-Cell Receptor αβ Repertoire. In: Shaw AC, editor. Immunosenescence: Methods and Protocols [Internet]. New York, NY: Springer; 2015 [cited 2025 Dec 10]. p. 181–97. Available from: https://doi.org/10.1007/978-1-4939-2963-4_15 doi:10.1007/978-1-4939-2963-4_15

50. Newell EW, Sigal N, Nair N, Kidd BA, Greenberg HB, Davis MM. Combinatorial tetramer staining and mass cytometry analysis facilitate T-cell epitope mapping and characterization. Nat Biotechnol. 2013 Jul;31(7):623–9. doi:10.1038/nbt.2593 PubMed PMID: 23748502; PubMed Central PMCID: PMC3796952.

51. Fehlings M, Simoni Y, Penny HL, Becht E, Loh CY, Gubin MM, et al. Author Correction: Checkpoint blockade immunotherapy reshapes the high-dimensional phenotypic heterogeneity of murine intratumoural neoantigen-specific CD8+ T cells. Nat Commun. 2018 Jul 26;9(1):3000. doi:10.1038/s41467-018-05468-y PubMed PMID: 30050138; PubMed Central PMCID: PMC6062571.

52. Schmidt F, Fields HF, Purwanti Y, Milojkovic A, Salim S, Wu KX, et al. In-depth analysis of human virus-specific CD8+ T cells delineates unique phenotypic signatures for T cell specificity prediction. Cell Reports. 2023 Oct;42(10):113250. doi:10.1016/j.celrep.2023.113250

53. Finton KAK, Brusniak MY, Jones LA, Lin C, Fioré-Gartland AJ, Brock C, et al. ARTEMIS: A Novel Mass-Spec Platform for HLA-Restricted Self and Disease-Associated Peptide Discovery. Front Immunol.

2021 Apr 23;12:658372. doi:10.3389/fimmu.2021.658372 PubMed PMID: 33986749; PubMed Central PMCID: PMC8111693.

54. Kaech SM, Tan JT, Wherry EJ, Konieczny BT, Surh CD, Ahmed R. Selective expression of the interleukin 7 receptor identifies effector CD8 T cells that give rise to long-lived memory cells. Nat Immunol. 2003 Dec;4(12):1191–8. doi:10.1038/ni1009

55. Huster KM, Busch V, Schiemann M, Linkemann K, Kerksiek KM, Wagner H, et al. Selective expression of IL-7 receptor on memory T cells identifies early CD40L-dependent generation of distinct CD8+ memory T cell subsets. Proceedings of the National Academy of Sciences. 2004 Apr 13;101(15):5610–5. doi:10.1073/pnas.0308054101

56. Micevic G, Daniels A, Flem-Karlsen K, Park K, Talty R, McGeary M, et al. IL-7R licenses a population of epigenetically poised memory CD8+ T cells with superior antitumor efficacy that are critical for melanoma memory. Proceedings of the National Academy of Sciences. 2023 Jul 25;120(30):e2304319120. doi:10.1073/pnas.2304319120

57. Scholten KBJ, Kramer D, Kueter EWM, Graf M, Schoedl T, Meijer CJLM, et al. Codon modification of T cell receptors allows enhanced functional expression in transgenic human T cells. Clin Immunol. 2006 May;119(2):135–45. doi:10.1016/j.clim.2005.12.009 PubMed PMID: 16458072.

58. Kuball J, Dossett ML, Wolfl M, Ho WY, Voss RH, Fowler C, et al. Facilitating matched pairing and expression of TCR chains introduced into human T cells. Blood. 2007 Mar 15;109(6):2331–8. doi:10.1182/blood-2006-05-023069

59. Cohen CJ, Li YF, El-Gamil M, Robbins PF, Rosenberg SA, Morgan RA. Enhanced Antitumor Activity of T Cells Engineered to Express T-Cell Receptors with a Second Disulfide Bond. Cancer Res. 2007 Apr 15;67(8):3898–903. doi:10.1158/0008-5472.CAN-06-3986 PubMed PMID: 17440104; PubMed Central PMCID: PMC2147081.

60. Sidney J, Peters B, Frahm N, Brander C, Sette A. HLA class I supertypes: a revised and updated classification. BMC Immunology. 2008 Jan 22;9(1):1. doi:10.1186/1471-2172-9-1

61. Trolle T, McMurtrey CP, Sidney J, Bardet W, Osborn SC, Kaever T, et al. The length distribution of class I restricted T cell epitopes is determined by both peptide supply and MHC allele specific binding preference. J Immunol. 2016 Feb 15;196(4):1480–7. doi:10.4049/jimmunol.1501721 PubMed PMID: 26783342; PubMed Central PMCID: PMC4744552.

62. Ekeruche-Makinde J, Miles JJ, van den Berg HA, Skowera A, Cole DK, Dolton G, et al. Peptide length determines the outcome of TCR/peptide-MHCI engagement. Blood. 2013 Feb 14;121(7):1112–23. doi:10.1182/blood-2012-06-437202 PubMed PMID: 23255554; PubMed Central PMCID: PMC3653566.

63. McLean-Tooke A, Barge D, Spickett GP, Gennery AR. T cell receptor Vβ repertoire of T lymphocytes and T regulatory cells by flow cytometric analysis in healthy children. Clin Exp Immunol. 2008

Jan;151(1):190–8. doi:10.1111/j.1365-2249.2007.03536.x PubMed PMID: 17983445; PubMed Central PMCID: PMC2276915.

64. Brzostek J, Gascoigne NRJ. Thymic Origins of T Cell Receptor Alloreactivity. Transplantation. 2017 Jul;101(7):1535. doi:10.1097/TP.0000000000001654

65. Morris GP, Ni PP, Allen PM. Alloreactivity is limited by the endogenous peptide repertoire. Proceedings of the National Academy of Sciences. 2011 Mar;108(9):3695–700. doi:10.1073/pnas.1017015108

66. Bijen HM, Steen DM van der, Hagedoorn RS, Wouters AK, Wooldridge L, Falkenburg JHF, et al. Preclinical Strategies to Identify Off-Target Toxicity of High-Affinity TCRs. Molecular Therapy. 2018 May 2;26(5):1206–14. doi:10.1016/j.ymthe.2018.02.017 PubMed PMID: 29567312.

67. Hickman ES, Lomax ME, Jakobsen BK. Antigen Selection for Enhanced Affinity T-Cell Receptor-Based Cancer Therapies. J Biomol Screen. 2016 Sep;21(8):769–85. doi:10.1177/1087057116637837 PubMed PMID: 26993321.

68. Oates J, Hassan NJ, Jakobsen BK. ImmTACs for targeted cancer therapy: Why, what, how, and which. Molecular Immunology. 2015 Oct 1;Therapeutic Antibodies: Discovery, Design and Deployment67(2, Part A):67–74. doi:10.1016/j.molimm.2015.01.024

69. Antunes DA, Baker BM, Cornberg M, Selin LK. Editorial: Quantification and prediction of T-cell cross-reactivity through experimental and computational methods. Front Immunol. 2024;15:1377259. doi:10.3389/fimmu.2024.1377259 PubMed PMID: 38444853; PubMed Central PMCID: PMC10912571.

70. Fonseca AF, Antunes DA. CrossDome: an interactive R package to predict cross-reactivity risk using immunopeptidomics databases. Front Immunol. 2023 Jun 12;14:1142573. doi:10.3389/fimmu.2023.1142573 PubMed PMID: 37377956; PubMed Central PMCID: PMC10291144.

71. Bradley P. eLife. eLife Sciences Publications Limited; 2023. Structure-based prediction of T cell receptor:peptide-MHC interactions. doi:10.7554/eLife.82813

72. Rudolph MG, Stanfield RL, Wilson IA. How TCRs Bind MHCs, Peptides, and Coreceptors. Annual Review of Immunology. 2006 Apr 23;24(Volume 24, 2006):419–66. doi:10.1146/annurev.immunol.23.021704.115658

73. Krogsgaard M, Davis MM. How T cells “see” antigen. Nat Immunol. 2005 Mar;6(3):239–45. doi:10.1038/ni1173

74. Moll A, Hildebrandt A, Lenhof HP, Kohlbacher O. BALLView: a tool for research and education in molecular modeling. Bioinformatics. 2006 Feb 1;22(3):365–6. doi:10.1093/bioinformatics/bti818

75. de Castro E, Sigrist CJA, Gattiker A, Bulliard V, Langendijk-Genevaux PS, Gasteiger E, et al. ScanProsite: detection of PROSITE signature matches and ProRule-associated functional and structural residues in proteins. Nucleic Acids Res. 2006 Jul 1;34(Web Server issue):W362–5. doi:10.1093/nar/gkl124 PubMed PMID: 16845026; PubMed Central PMCID: PMC1538847.

76. Ishii K, Davies JS, Sinkoe AL, Nguyen KA, Norberg SM, McIntosh CP, et al. Multi-tiered approach to detect autoimmune cross-reactivity of therapeutic T cell receptors. Sci Adv. 9(30):eadg9845. doi:10.1126/sciadv.adg9845 PubMed PMID: 37494434; PubMed Central PMCID: PMC10371023.

77. Sarkizova S, Klaeger S, Le PM, Li LW, Oliveira G, Keshishian H, et al. A large peptidome dataset improves HLA class I epitope prediction across most of the human population. Nat Biotechnol. 2020 Feb;38(2):199–209. doi:10.1038/s41587-019-0322-9 PubMed PMID: 31844290; PubMed Central PMCID: PMC7008090.

78. Foldvari Z, Knetter C, Yang W, Gjerdingen TJ, Bollineni RC, Tran TT, et al. A systematic safety pipeline for selection of T-cell receptors to enter clinical use. npj Vaccines. 2023 Aug 22;8(1):1. doi:10.1038/s41541-023-00713-y

79. Endo S, Miyagi N, Matsunaga T, Hara A, Ikari A. Human dehydrogenase/reductase (SDR family) member 11 is a novel type of 17β-hydroxysteroid dehydrogenase. Biochemical and Biophysical Research Communications. 2016 Mar 25;472(1):231–6. doi:10.1016/j.bbrc.2016.01.190

80. Kudo Y, Endo S, Tanio M, Saka T, Himura R, Abe N, et al. Antiandrogenic Effects of a Polyphenol in Carex kobomugi through Inhibition of Androgen Synthetic Pathway and Downregulation of Androgen Receptor in Prostate Cancer Cell Lines. International Journal of Molecular Sciences. 2022 Jan;23(22):22. doi:10.3390/ijms232214356

81. Fenoglio D, Belgioia L, Parodi A, Missale F, Bacigalupo A, Tarke A, et al. Development of Exhaustion and Acquisition of Regulatory Function by Infiltrating CD8+CD28− T Lymphocytes Dictate Clinical Outcome in Head and Neck Cancer. Cancers. 2021 May 6;13(9):2234. doi:10.3390/cancers13092234

82. Filaci G, Fenoglio D, Fravega M, Ansaldo G, Borgonovo G, Traverso P, et al. CD8 $^{+}$ CD28 $^{-}$ T Regulatory Lymphocytes Inhibiting T Cell Proliferative and Cytotoxic Functions Infiltrate Human Cancers. J Immunol. 2007 Oct 1;179(7):4323–34. doi:10.4049/jimmunol.179.7.4323

83. Parodi A, Battaglia F, Kalli F, Ferrera F, Conteduca G, Tardito S, et al. CD39 is highly involved in mediating the suppression activity of tumor-infiltrating CD8+ T regulatory lymphocytes. Cancer Immunol Immunother. 2013 May;62(5):851–62. doi:10.1007/s00262-013-1392-z

84. Effros RB. Loss of CD28 expression on T lymphocytes: a marker of replicative senescence. Dev Comp Immunol. 1997;21(6):471–8. doi:10.1016/s0145-305x(97)00027-x PubMed PMID: 9463780.

85. Borthwick NJ, Lowdell M, Salmon M, Akbar AN. Loss of CD28 expression on CD8+ T cells is induced by IL-2 receptor γ chain signalling cytokines and type I IFN, and increases susceptibility to

activation-induced apoptosis. Int Immunol. 2000 Jul 1;12(7):1005–13. doi:10.1093/intimm/12.7.1005

86. Ruggiero E, Liu D, Prodeus A, Becker AM, Foisey M, Balwani I, et al. NTLA5001, a T Cell Product Candidate with CRISPR-Based Targeted Insertion of a High-Avidity, Natural, WT1-Specific TCR, Shows Efficacy in *In Vivo* Models of AML and ALL. Blood. 2020 Nov 5;136:32–3. doi:10.1182/blood-2020-143119

87. Pollok KE, Kim YJ, Zhou Z, Hurtado J, Kim KK, Pickard RT, et al. Inducible T cell antigen 4-1BB. Analysis of expression and function. J Immunol. 1993 Feb 1;150(3):771–81. PubMed PMID: 7678621.

8. Supplementary Materials

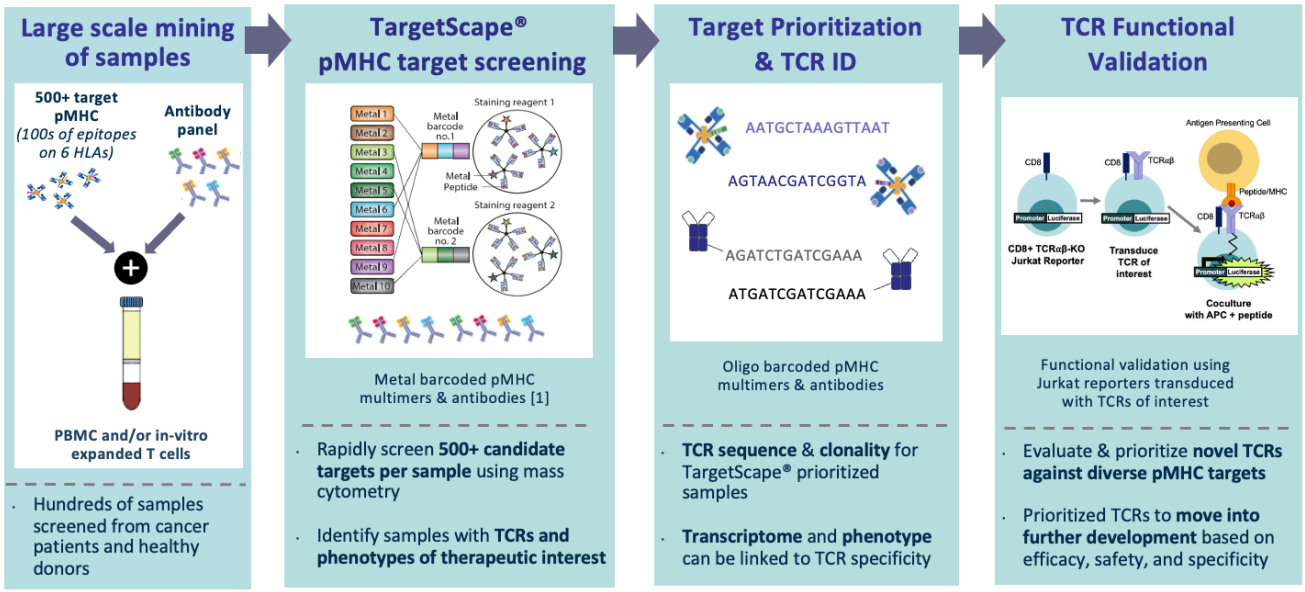

Supplementary Figure 1. High-throughput putative antigen-specific TCR discovery and functional validation workflow overview. Peripheral blood mononuclear cells (PBMC) underwent multiplexed mass cytometry screening with 500+ metal-barcoded peptide-MHC tetramers across common HLA alleles to agnostically detect $CD8^+$ T cells targeting tumor-associated or tumor-specific antigens. Sequences of putative antigen-specific TCRs were recovered with VDJ-CITESeq and transduced into Jurkat reporters for preliminary functional validation with the cognate peptide of interest.

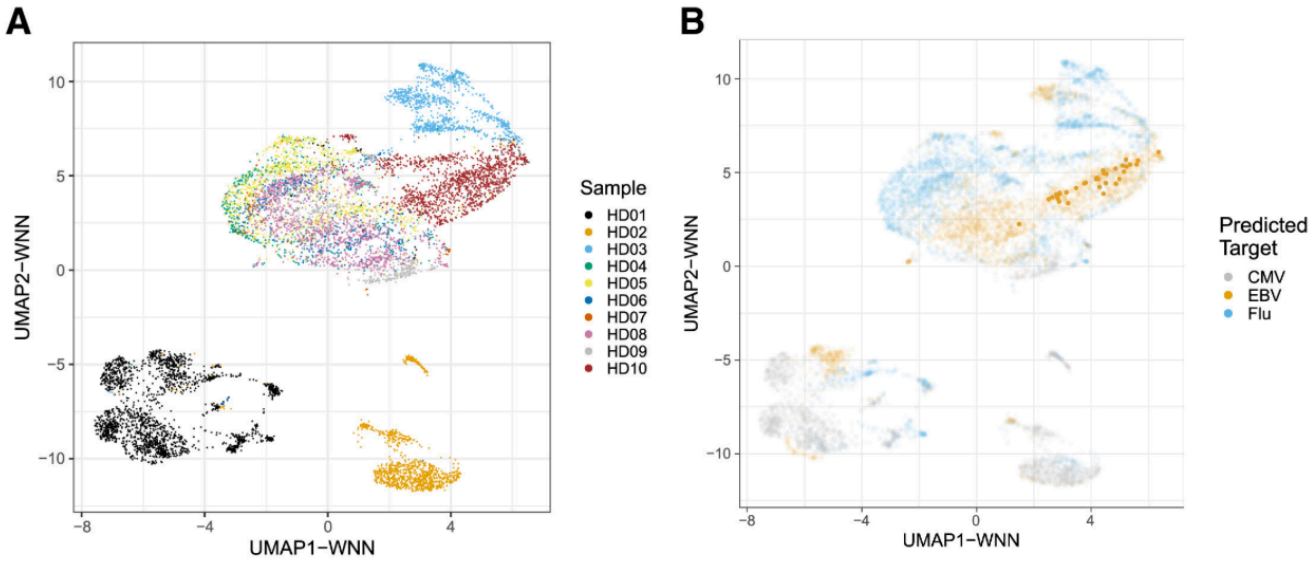

Supplementary Figure 2. Applications of a machine learning model to validate viral specificity in predicted EBV-specific TCRs. From a previously described machine learning model (52): (A) UMAP in weighted nearest-neighbor (WNN) space for the TAP validation cohort colored by donor ID. (B) UMAP in WNN space for the TAP validation cohort colored by predicted target specificity of the T cells. Enlarged dots represent predicted EBV-specific T cells that were used for functional TCR validation.

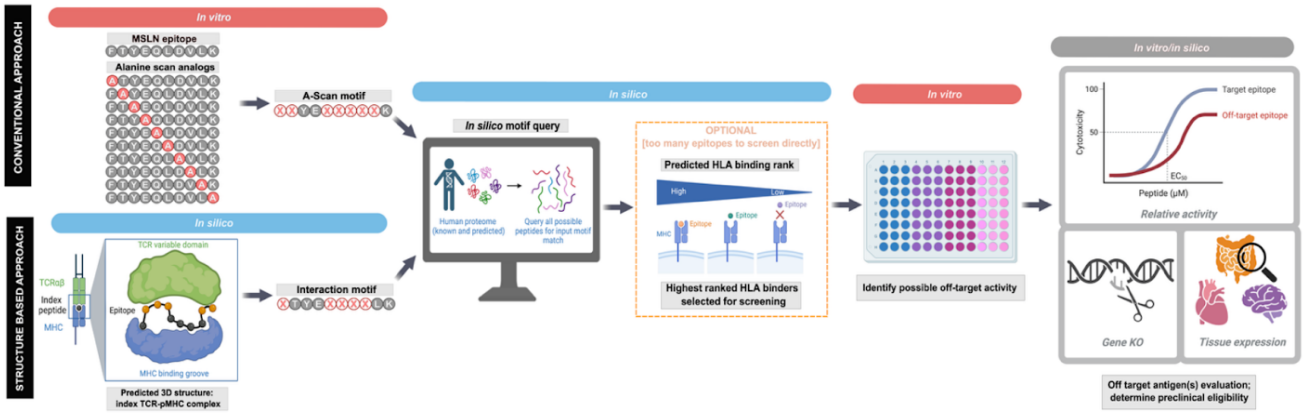

Supplementary Figure 3. Schematic representation of conventional A-scan and structure-based cross-reactive motif predictions.

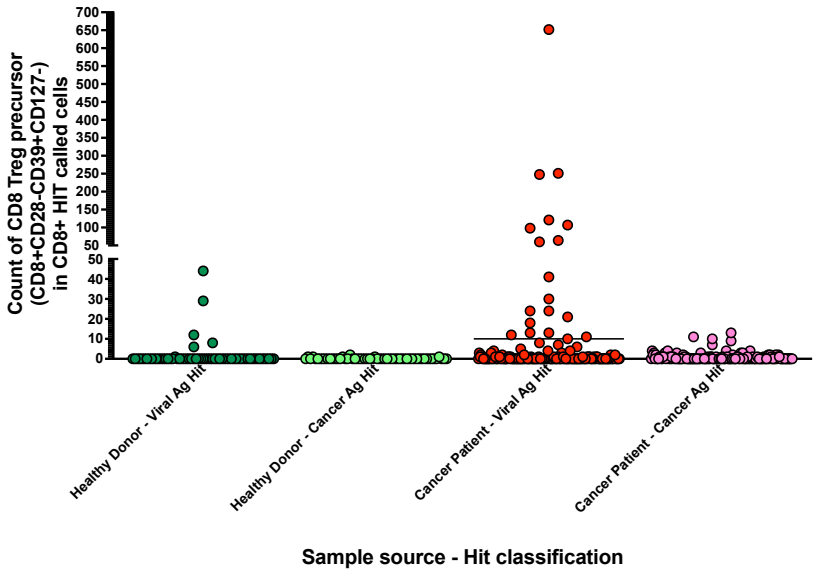

Supplementary Figure 4. CD8+ Treg precursor cells within antigen-specfic hits in healthy donor and cancer patient samples. TargetScape samples from healthy donors and cancer patients of various indications were stained with a screening panel containing cell surface markers and collected on a mass cytometer (CyTOF). A sample cohort of 31 healthy donor and 196 cancer patient samples of various indications were analyzed for the presence of CD8+ Treg precursors (CD8+/CD28-/CD39+/CD127-) in total CD8+ cells and visualized by frequency in viral- and cancer-antigen hits.

A.

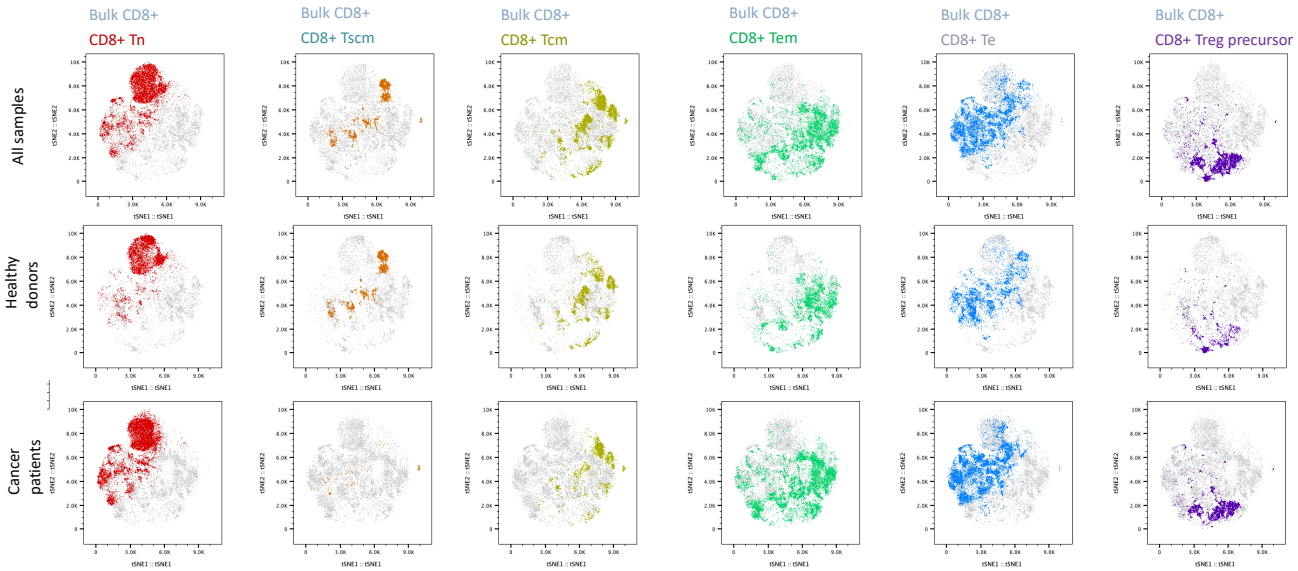

B.

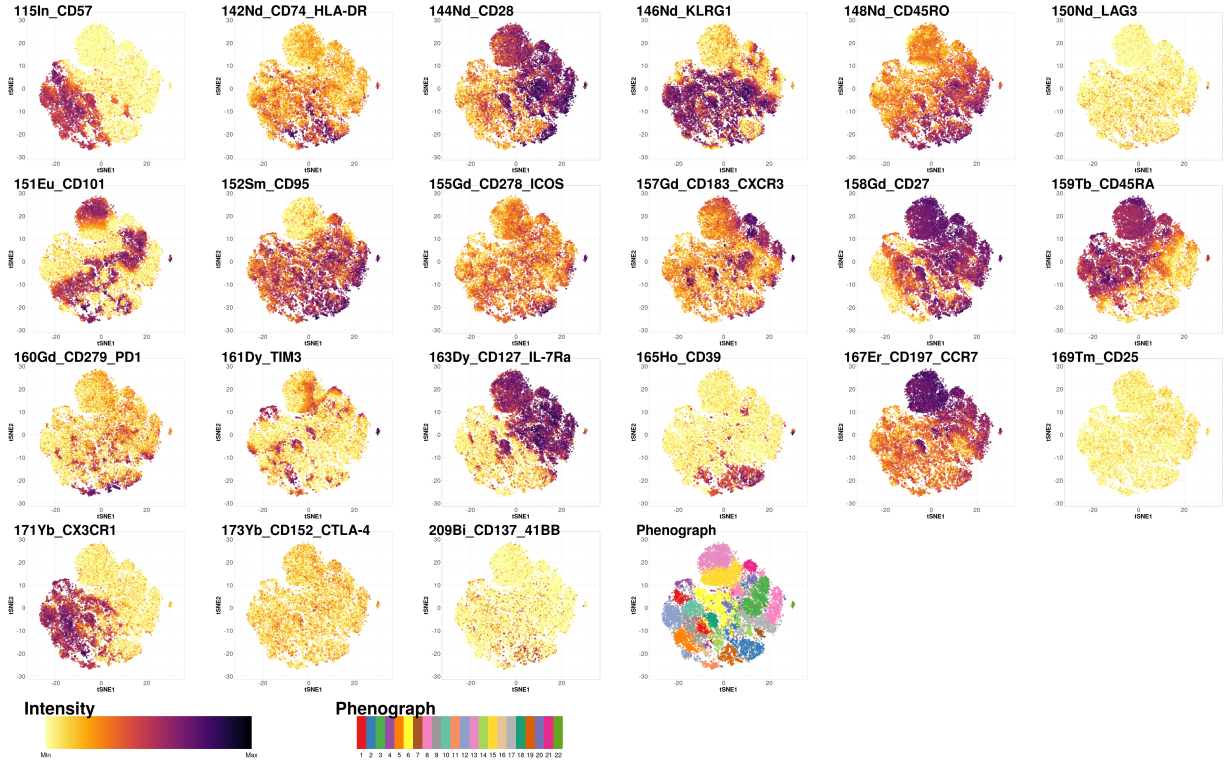

Supplementary Figure 5: High dimensional analysis of phenotypic marker expression CD8+ Treg precursor in healthy donor and cancer patient samples. Unbiased high dimensional analysis with tSNE visualization of phenotypic markers in a pilot cohort of 6 healthy donors and 12 cancer patient samples as visualized by A) CD8+ Treg precursor and other canonical CD8+

populations in healthy donor and cancer patient samples and B) non-gating individual markers heat map and phenograph overlay in all samples.

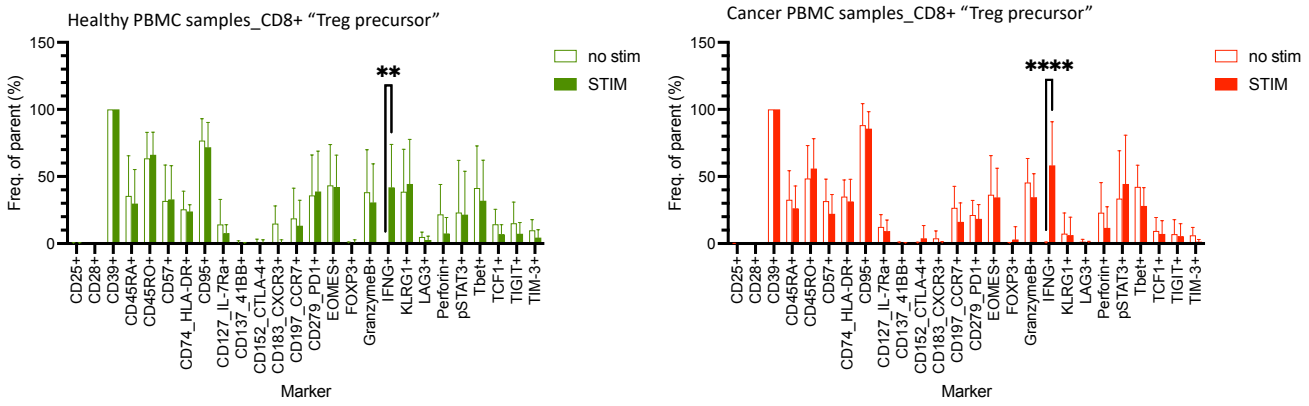

Supplementary Figure 6. Phenotypic comparison of CD8⁺ Treg precursor cells under unstimulated and stimulated conditions. Flow cytometric analysis of marker expression in CD8⁺ Treg precursor populations (CD8⁺CD28⁻CD39⁺CD127⁻) from healthy donor (left) and cancer patient (right) PBMC samples following PMA/Ionomycin stimulation (STIM) versus unstimulated controls (no stim). Bar graphs depict the frequency of parent CD8⁺ Treg precursor cells expressing each indicated activation or regulatory marker. Data represent mean ± SD across biological replicates. Statistical significance was assessed by paired testing between stimulated and unstimulated samples for each marker.

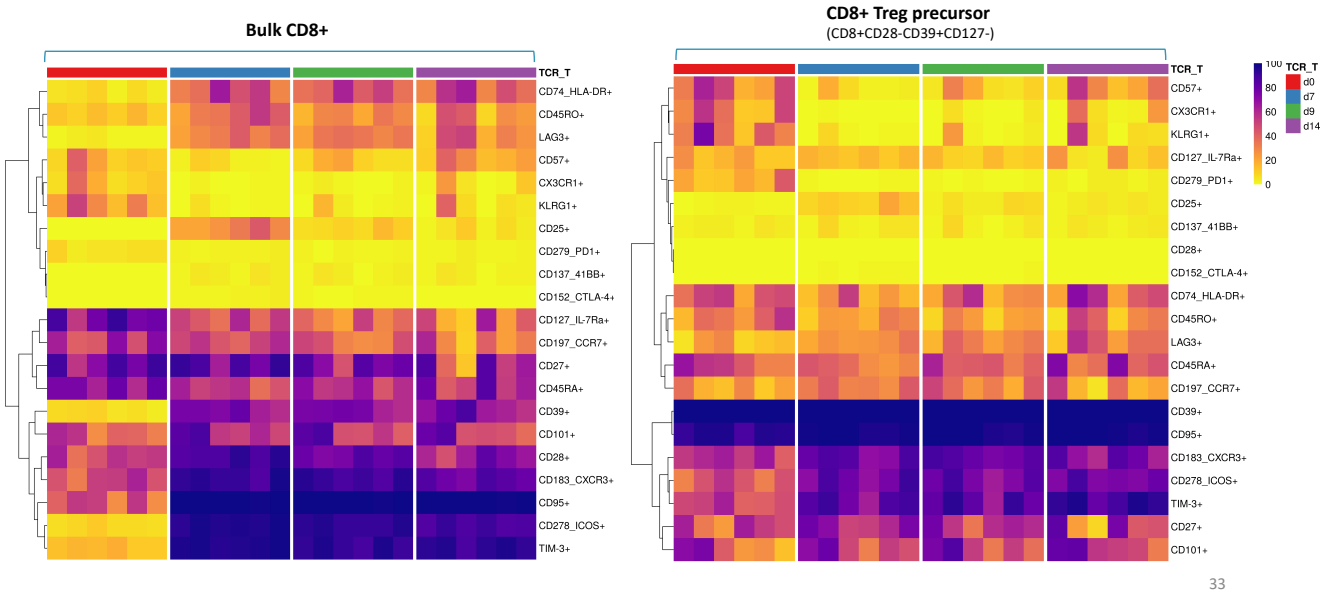

Supplementary Figure 7. High-dimensional clustering of CD8⁺ T cell subsets pre- and post–TCR-T transduction. Unsupervised hierarchical clustering heatmaps comparing expression of immune regulatory and activation markers in bulk CD8⁺ T cells (left) and CD8⁺ Treg precursor populations (right; CD8⁺CD28⁻CD39⁺CD127⁻) from primary donor samples collected pre-transduction (day 0) and post-transduction (expanded TCR-T product). Marker expression intensity is shown as normalized z-scores across donors. Dendrograms illustrate phenotypic relationships among subsets based on Euclidean distance clustering. Heatmap color scales represent relative marker expression intensity.

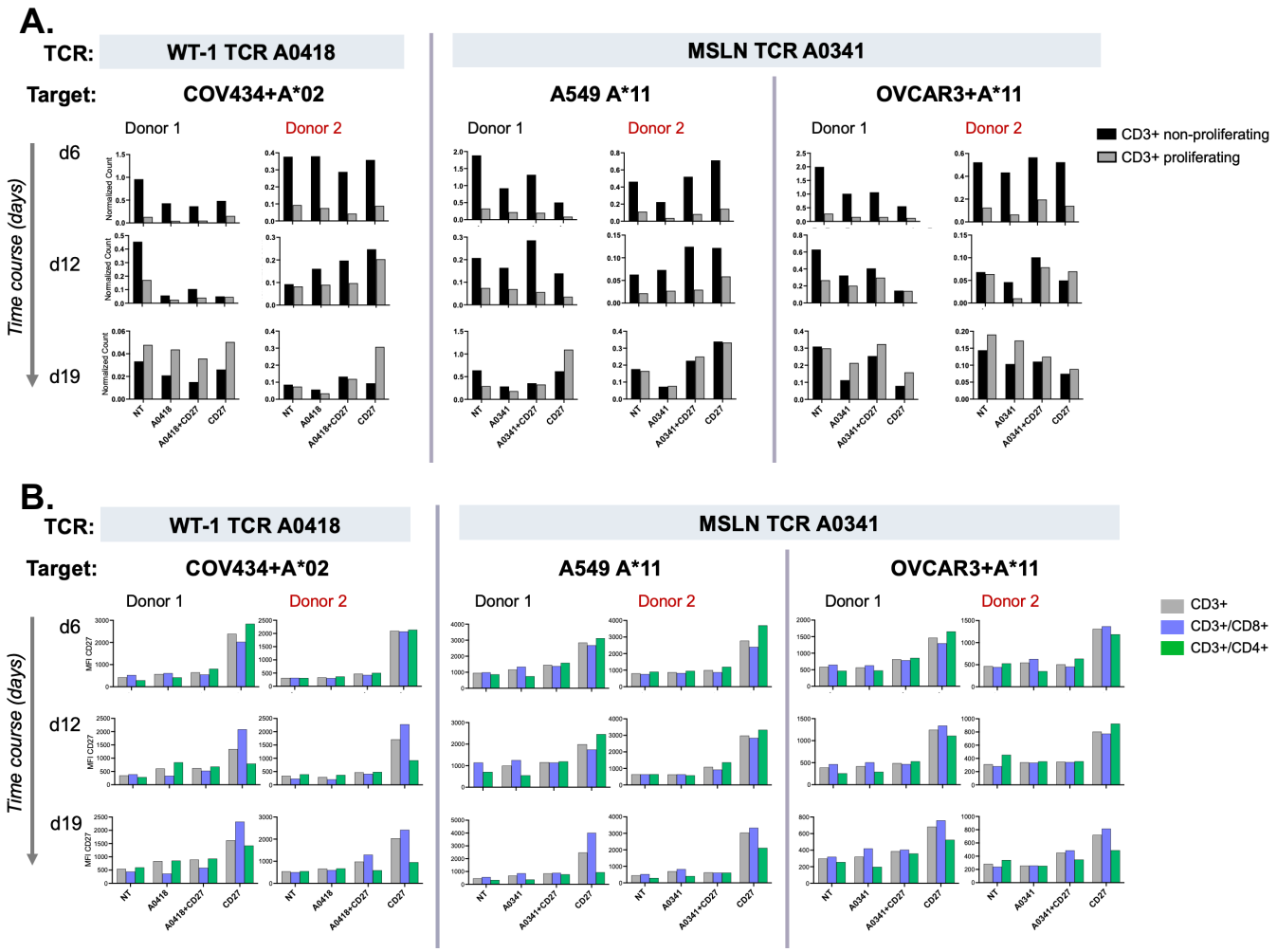

Supplementary Figure 8. Characterization of proliferative subsets and CD27 expression dynamics in CD27-engineered TCR-T cells. Effector subsets in coculture with HLA-matched target cells over time (days 6, 12, and 19). WT1-specific (A0418) and MSLN-specific (A0341) TCR-T cells ± CD27 co-receptor were assessed in two independent donors across indicated tumor target lines. (A) Quantification of proliferating (CellTrace Violet^{low}) and non-proliferating (CellTrace violet^{high}) CD3$^+$; bar graphs represent normalized proportions of proliferating versus non-proliferating CD3$^+$ populations. (B) Flow cytometric quantification of CD27 surface expression on total CD3$^+$, CD3$^+$CD8$^+$, and CD3$^+$CD4$^+$ T cell subsets. Mean fluorescence intensity (MFI) values are plotted for each donor and condition.

Supplementary Table 1. EBV LMP2A screening peptides. Overlapping 10-mer peptides (7 amino acid overlap) derived from the EBV LMP2A protein, strain B95-8 (UniProt ID: P13285).

ID	Peptide Sequence
P00095	MGSLEMVPMG
P00096	LEMVPMGAGP
P00097	VPMGAGPPSP
P00098	GAGPPSPGGD
P00099	PPSPGGDPDG
P00100	PGGDPDGYDG

P00101	DPDGYDGGNN
P00102	GYDGGNNSQY
P00103	GGNNSQYPSA
P00104	NSQYPSASGS
P00105	YPSASGSSGN
P00106	ASGSSGNTPT
P00107	SSGNTPTPPN
P00108	NTPTPPNDEE
P00109	TPPNDEERES
P00110	NDEERESNEE
P00111	ERESNEEPPP
P00112	SNEEPPPPYE
P00113	EPPPPYEDPY
P00114	PPYEDPYWGN
P00115	EDPYWGNGDR
P00116	YWGNGDRHSD
P00117	NGDRHSDYQP
P00118	RHSDYQPLGT
P00119	DYQPLGTQDQ
P00120	PLGTQDQSLY
P00121	TQDQSLYLGL
P00122	QSLYLGLQHD
P00123	YLGLQHDGND
P00124	LQHDGNDGLP
P00125	DGNDGLPPPP
P00126	DGLPPPPYSP
P00127	PPPPYSPRDD
P00128	PYSPRDDSSQ
P00129	PRDDSSQHIY
P00130	DSSQHIYEEA
P00131	QHIYEEAGRG
P00132	YEEAGRGSMN
P00133	AGRGSMNPVC
P00134	GSMNPVCLPV
P00135	NPVCLPVIVA
P00136	CLPVIVAPYL
P00137	VIVAPYLFWL
P00138	APYLFWLAAI
P00139	LFWLAAIAAS

P00140	LAAIAASCFT
P00141	IAASCFTASV
P00142	SCFTASVSTV
P00143	TASVSTVVTA
P00144	VSTVVTATGL
P00145	VVTATGLALS
P00146	ATGLALSLLL
P00147	LALSLLLLAA
P00148	SLLLLAAVAS
P00149	LLAAVASSYA
P00150	AVASSYAAAQ
P00151	SSYAAAQRKL
P00152	AAAQRKLLTP
P00153	QRKLLTPVTV
P00154	LLTPVTVLTA
P00155	PVTVLTAVVT
P00156	VLTAVVTFFA
P00157	AVVTFFAICL
P00158	TFFAICLTWR
P00159	AICLTWRIED
P00160	LTWRIEDPPF
P00161	RIEDPPFNSL
P00162	DPPFNSLLFA
P00163	FNSLLFALLA
P00164	LLFALLAAAG
P00165	ALLAAAGGLQ
P00166	AAAGGLQGIY
P00167	GGLQGIYVLV
P00168	QGIYVLVMLV
P00169	YVLVMLVLLI
P00170	VMLVLLILAY
P00171	VLLILAYRRR
P00172	ILAYRRRWRR
P00173	YRRRWRRLTV
P00174	RWRRLTVCGG
P00175	RLTVCGGIMF

Supplementary Table 2. EBV LMP2A screening peptides. Overlapping 10-mer peptides (7 amino acid overlap) derived from the EBV LMP2A protein, strain B95-8 (UniProt ID: P13285).

MHC	Peptide	Score_EL	%Rank_EL BindLevel
HLA-A*02:01	SLEMVPMGA	0.065266	2.4900
HLA-A*02:01	GSLEMVPMGA	0.003935	10.2120
HLA-A*02:01	MGSLEMVPMGA	0.001183	16.7300
HLA-A*02:01	GSLEMVPM	0.000303	28.1110
HLA-A*02:01	MGSLEMVPM	0.000246	30.3640
HLA-A*02:01	SLEMVPMGAG	0.000183	33.6880
HLA-A*02:01	SLEMVPMG	0.000182	33.7500
HLA-A*02:01	GSLEMVPMG	0.000092	42.5000
HLA-A*02:01	LEMVPMGA	0.000059	48.6000
HLA-A*02:01	GSLEMVPMGAG	0.000033	57.2730
HLA-A*02:01	MGSLEMVP	0.00001	73.7500
HLA-A*02:01	MGSLEMVPMG	0.000008	76.6670

Supplementary Table 3. Mesothelin expressing cell lines.

Cell line	Disease	Engineered cell line	nTPM MSLN (Protein Atlas)	MSLN expression (as % of live cells)	Native line haplotype	+ HLA-A*11:01 (transduced in-house)	HLA-A*11 expression (as % of live cells)
OVCAR-3	Ovarian	No	97.1	48.2%	A*02:01:01,29:02 B*07:02:01,58:01 C*07:02:01,07	No	0.44%
					*+ A*11:01*	Yes	35.4%
DU-145	Prostate	No	14.9	35.7%	A*03:01:01,33:03 B*50:01,57:01:01 C*06:02	No	0.19%
					*+ A*11:01*	Yes	70.9%
A549 A*11:01	Lung	Yes; A*11:01 expression	3.5	57.5%	A*11:01	N/A	8.37%
Panc1	Pancreatic	No	3.2	79.1%	A*02:01,11:01 B*01,38 C*03,12	N/A	22.9%

Supplementary Table 4. EBV Panel Haplotypes.

EBV Line	Donor ID	Source Sample Vendor	HLA-A Haplotype 1	HLA-A Haplotype 2	HLA-B Haplotype 1	HLA-B Haplotype 2	HLA-C Haplotype 1	HLA-C Haplotype 2
1	D0022-EBV	San Diego Blood Bank	01:01:01:01	11:01:01:01	08:01:01:01	35:01:01:02	04:01:01:05	07:01:01:01
2	D0024-EBV	San Diego Blood Bank	01:01:01:01	01:01:01:01	08:01:01:01	27:05:02:01	01:02:01:01	07:01:01:01
3	D0023-EBV	San Diego Blood Bank	02:01:01:01	32:01:01:01	27:05:02:14	51:01:01:01	02:02:02:01	14:02:01:01
4	D0017-EBV	San Diego Blood Bank	02:01:01:01	31:01:02:01	40:01:02:01	44:03:01:01	03:04:01:01	04:01:01:01
5	D0020-EBV	San Diego Blood Bank	24:02:01:01	32:01:01:01	15:01:01:01	40:02:01:01	03:03:01:01	03:04:01:02
6	D0387-EBV	San Diego Blood Bank	02:01:01:01	30:02:01:01	07:02:01:01	27:05:02:01	02:02:02:01	07:02:01:03
7	D0018-EBV	San Diego Blood Bank	03:01:01:01	32:01:01:01	08:01:01:01	51:01:01:01	07:01:01:01	15:02:01:01
8	D0389-EBV	San Diego Blood Bank	23:01:01:01	68:01:02:01	44:03:01:01	50:01:01:01	04:01:01:01	06:02:01:02
9	D0036-EBV	San Diego Blood Bank	02:01:01:01	33:03:01:01	40:01:02:01	44:03:01:01	03:04:01:01	14:03:01:01
10	D0012-EBV	San Diego Blood Bank	02:02:01:01	24:02:01:01	08:01:01:01	15:16:01:02	07:01:01:01	14:02:01:02
11	HC07-EBV	HemaCare	03:01:01:01	24:25:00	35:01:01:02	48:01:01:01	04:01:01:01	08:01:01:01
12	HC06-EBV	HemaCare	03:01:01:01	31:01:02:01	07:02:01:01	40:02:01:01	03:04:01:02	07:02:01:03
13	SDBB008-EBV	San Diego Blood Bank	24:02:01:12	68:01:02:02	14:02:01:01	57:01:01:01	07:01:01:01	08:02:01:01
14	D0028-EBV	San Diego Blood Bank	01:01:01:01	26:01:01:01	35:03:01:01	38:01:01:01	04:01:01:01	12:03:01:01
15	SDBB007-EBV	San Diego Blood Bank	02:01:01:01	26:01:01:01	35:03:01:01	44:02:01:01	03:03:01:01	04:01:01:01
16	D0391-EBV	San Diego Blood Bank	26:01:01:01	29:02:01:01	27:05:02:01	44:03:01:01	01:02:01:01	16:01:01:01
17	D0021-EBV	San Diego Blood Bank	24:02:01:01	24:03:01:01	18:01:01:02	37:01:01:01	06:02:01:01	12:03:01:01
18	D0014-EBV	San Diego Blood Bank	01:01:01:01	11:01:01:01	18:01:01:01	55:01:01:01	03:03:01:01	05:01:01:01
19	D0032-EBV	San Diego Blood Bank	02:06:01:01	24:02:01:01	18:02:01	40:01:02:01	07:04:01:01	15:02:01:01
20	D0033-EBV	San Diego Blood Bank	03:01:01:05	32:01:01:01	15:01:01:01	47:01:01:03	03:03:01:01	06:02:01:01
21	D0053-EBV	San Diego Blood Bank	03:01:01:01	25:01:01:01	07:02:01:01	07:02:01:01	07:02:01:03	07:02:01:03
22	D0046-EBV	San Diego Blood Bank	11:01:01:01	33:03:01:01	27:06:01:01	58:01:01:01	03:02:02:01	03:04:01:18
23	DLS427-EBV	Discovery Life Sciences	02:01:01	02:01:01	44:02:01	56:01:01	01:02:01	05:01:01
24	D0041-EBV	San Diego Blood Bank	11:01:01:01	11:01:01:01	15:02:01:01	54:01:01:01	01:02:01:01	08:01:01:01
25	D0165-EBV	San Diego Blood Bank	01:01:01:01	31:01:02:01	07:02:01:01	44:02:01:01	05:01:01:02	07:02:01:03
26	AC844-EBV	AllCells	24:07:01	24:33	15:13:01	51:06:01	08:01:01	12:04:02
27	AC283-EBV	AllCells	02:01:01	26:01:01	44:02:01	52:01:01	05:01:01	12:02:02
28	AC430-EBV	AllCells	02:06:01	26:01:01	08:01:01	40:27:01	03:04:01	03:04:01
29	AC514-EBV	AllCells	02:01:01	26:01:01	44:02:01	52:01:01	05:01:01	12:02:02
30	DLS432-EBV	Discovery Life Sciences	25:01:01	29:02:01	07:02:01	44:03:01	07:02:01	16:01:01
31	BI231-EBV	BioIVT	02:01:01	68:02:01	52:01:01	57:03:01	07:01:02	12:02:02
32	BI221-EBV	BioIVT	02:01:01	02:07:01	07:02:01	46:01:01	01:02:01	07:02:01
33	SC051-EBV	Stemcell	02:01	11:01	13:01	54:01	01:02	07:02
34	BI228-EBV	BioIVT	11:01:01	24:07:01	40:01:02	40:01:02	04:82	07:02:01
35	AC376-EBV	AllCells	03:02:01	80:01:01	44:03:01	44:03:01	04:01:01	14:03:01

Supplementary Table 5. A-scan derived epitopes ranked by predicted HLA A*11:01 binding.

NetMHCpan version 4.1b query results up to ranked binding of index peptide FTYEQLDVLK (#180). Yellow fill indicates fixed A-scan motif residue. Green fill indicates overlap with index peptide residue.

Rank	Peptide	Pos 1	Pos 2	Pos 3	Pos 4	Pos 5	Pos 6	Pos 7	Pos 8	Pos 9	Pos 10	Score_EL	%Rank_EL
1	STYEPVLLAK	S	T	Y	E	P	V	L	L	A	K	0.982649	0.004
2	ATYEDQQIKK	A	T	Y	E	D	Q	Q	I	K	K	0.978947	0.005
3	ASYEPTILGK	A	S	Y	E	P	T	I	L	G	K	0.976468	0.005
4	SVYENGLSQK	S	V	Y	E	N	G	L	S	Q	K	0.968463	0.007
5	RVYEVPVETK	R	V	Y	E	V	P	V	E	T	K	0.966853	0.008
6	STYEESKVSK	S	T	Y	E	E	S	K	V	S	K	0.963745	0.008
7	SVYEPFKVRK	S	V	Y	E	P	F	K	V	R	K	0.962592	0.008
8	ATYEISQEKK	A	T	Y	E	I	S	Q	E	K	K	0.956394	0.01
9	SSYEFPPALK	S	S	Y	E	F	P	P	A	L	K	0.956068	0.01
10	KVYEATIEEK	K	V	Y	E	A	T	I	E	E	K	0.953994	0.011
11	RSYEGTLYKK	R	S	Y	E	G	T	L	Y	K	K	0.952078	0.011
12	AVYEAPQEEK	A	V	Y	E	A	P	Q	E	E	K	0.951285	0.012
13	KTYEVSLREK	K	T	Y	E	V	S	L	R	E	K	0.94674	0.014
14	ASYEIGYILK	A	S	Y	E	I	G	Y	I	L	K	0.938618	0.017
15	YTYEHDPITK	Y	T	Y	E	H	D	P	I	T	K	0.933119	0.018
16	RTYEREALKK	R	T	Y	E	R	E	A	L	K	K	0.932351	0.019
17	HTYENTLLNK	H	T	Y	E	N	T	L	L	N	K	0.925614	0.022
18	STYEKKLTIK	S	T	Y	E	K	K	L	T	I	K	0.925455	0.022
19	SSYEPDELTK	S	S	Y	E	P	D	E	L	T	K	0.919839	0.025
20	KVYEAVELLK	K	V	Y	E	A	V	E	L	L	K	0.919366	0.025
21	SSYEDKNLLK	S	S	Y	E	D	K	N	L	L	K	0.917535	0.026
22	SVYERIRLEK	S	V	Y	E	R	I	R	L	E	K	0.916227	0.027
23	VSYEDPPTAK	V	S	Y	E	D	P	P	T	A	K	0.915597	0.027
24	STYELRTALK	S	T	Y	E	L	R	T	A	L	K	0.914224	0.028
25	KTYETNLEIK	K	T	Y	E	T	N	L	E	I	K	0.910451	0.03
26	GSYEYPVAEK	G	S	Y	E	Y	P	V	A	E	K	0.906836	0.031
27	YTYEDSTVAK	Y	T	Y	E	D	S	T	V	A	K	0.901244	0.034
28	KSYEADPLKK	K	S	Y	E	A	D	P	L	K	K	0.898663	0.035
29	ASYEDFIRNK	A	S	Y	E	D	F	I	R	N	K	0.898365	0.035
30	TTYEASGPSK	T	T	Y	E	A	S	G	P	S	K	0.89704	0.035
31	QTYESMCLEK	Q	T	Y	E	S	M	C	L	E	K	0.893458	0.037
32	KSYEEIIFGK	K	S	Y	E	E	I	I	F	G	K	0.892851	0.037
33	RVYELTHNNK	R	V	Y	E	L	T	H	N	N	K	0.892071	0.037
34	TIYEPVIRLK	T	I	Y	E	P	V	I	R	L	K	0.891957	0.037
35	STYEASRDTK	S	T	Y	E	A	S	R	D	T	K	0.889863	0.038
36	ASYEVVVDEK	A	S	Y	E	V	V	V	D	E	K	0.889394	0.038
37	RVYEGFGPGK	R	V	Y	E	G	F	G	P	G	K	0.887545	0.039
38	KVYEVNVCSK	K	V	Y	E	V	N	V	C	S	K	0.886703	0.04
39	SSYEVQVRGK	S	S	Y	E	V	Q	V	R	G	K	0.88455	0.041
40	AIYERVGTYK	A	I	Y	E	R	V	G	T	Y	K	0.883844	0.041
41	VVYEFSTTKK	V	V	Y	E	F	S	T	T	K	K	0.883491	0.041
42	ITYESPQTVK	I	T	Y	E	S	P	Q	T	V	K	0.881162	0.043
43	SIYEEKLLLK	S	I	Y	E	E	K	L	L	L	K	0.880125	0.044
44	IVYEDSPLVK	I	V	Y	E	D	S	P	L	V	K	0.879075	0.044
45	ATYETKESKK	A	T	Y	E	T	K	E	S	K	K	0.875131	0.047
46	KIYEVDGVQK	K	I	Y	E	V	D	G	V	Q	K	0.873041	0.049
47	RTYELKKINK	R	T	Y	E	L	K	K	I	N	K	0.87154	0.05
48	LVYEPSTQAK	L	V	Y	E	P	S	T	Q	A	K	0.868395	0.052
49	IVYEHSQMLK	I	V	Y	E	H	S	Q	M	L	K	0.867657	0.053

50	LTYEDFPTSK	L	T	Y	E	D	F	P	T	S	K	0.867158	0.053
51	ITYESPPGLK	I	T	Y	E	S	P	P	G	L	K	0.865378	0.055
52	RSYEYLTTSK	R	S	Y	E	Y	L	T	T	S	K	0.863431	0.057
53	KTYEASCETK	K	T	Y	E	A	S	C	E	T	K	0.857674	0.061
54	KIYESLKLSK	K	I	Y	E	S	L	K	L	S	K	0.857167	0.062
55	TTYEILLKDK	T	T	Y	E	I	L	L	K	D	K	0.851591	0.065
56	AVYERTSDHK	A	V	Y	E	R	T	S	D	H	K	0.847429	0.068
57	SQYEESILTK	S	Q	Y	E	E	S	I	L	T	K	0.83702	0.073
58	YVYEHTLTGK	Y	V	Y	E	H	T	L	T	G	K	0.836376	0.073
59	KIYECNQVQK	K	I	Y	E	C	N	Q	V	Q	K	0.836287	0.073
60	KIYEEDQLEK	K	I	Y	E	E	D	Q	L	E	K	0.828584	0.076
61	KTYEEDPKSK	K	T	Y	E	E	D	P	K	S	K	0.826904	0.077
62	ATYEQMKCLK	A	T	Y	E	Q	M	K	C	L	K	0.826477	0.077
63	KIYEQEGLEK	K	I	Y	E	Q	E	G	L	E	K	0.825755	0.077
64	KIYETLIKTK	K	I	Y	E	T	L	I	K	T	K	0.824307	0.078
65	SAYELGSVRK	S	A	Y	E	L	G	S	V	R	K	0.820649	0.079
66	SSYELISTCK	S	S	Y	E	L	I	S	T	C	K	0.818579	0.08
67	KIYEYNQVEK	K	I	Y	E	Y	N	Q	V	E	K	0.815144	0.082
68	TTYEYIIKDK	T	T	Y	E	Y	I	I	K	D	K	0.814062	0.083
69	SLYESIQEYK	S	L	Y	E	S	I	Q	E	Y	K	0.81032	0.085
70	RSYEAKSTKK	R	S	Y	E	A	K	S	T	K	K	0.809363	0.085
71	AIYEDLLSGK	A	I	Y	E	D	L	L	S	G	K	0.808509	0.086
72	TAYEPVWFSK	T	A	Y	E	P	V	W	F	S	K	0.806533	0.087
73	SIYEGDNAFK	S	I	Y	E	G	D	N	A	F	K	0.802576	0.089
74	SLYEFNILQK	S	L	Y	E	F	N	I	L	Q	K	0.801985	0.089
75	GSYETSKHEK	G	S	Y	E	T	S	K	H	E	K	0.798787	0.093
76	KTYECNICEK	K	T	Y	E	C	N	I	C	E	K	0.798272	0.094
77	KAYEKLQILK	K	A	Y	E	K	L	Q	I	L	K	0.795895	0.099
78	GTYECRVSEK	G	T	Y	E	C	R	V	S	E	K	0.794246	0.101
79	GVYELTHNNK	G	V	Y	E	L	T	H	N	N	K	0.79321	0.101
80	EVYEPNPFSK	E	V	Y	E	P	N	P	F	S	K	0.790747	0.103
81	TSYEFQVKPK	T	S	Y	E	F	Q	V	K	P	K	0.78608	0.106
82	KIYEQQNYIK	K	I	Y	E	Q	Q	N	Y	I	K	0.784875	0.107
83	SIYELIALLK	S	I	Y	E	L	I	A	L	L	K	0.783195	0.108
84	SMYEPGSALK	S	M	Y	E	P	G	S	A	L	K	0.782873	0.109
85	ISYEPDSSFK	I	S	Y	E	P	D	S	S	F	K	0.782457	0.109
86	SAYEPENQSK	S	A	Y	E	P	E	N	Q	S	K	0.781913	0.109
87	TSYENSLLVK	T	S	Y	E	N	S	L	L	V	K	0.780457	0.11
88	KIYECNQVEK	K	I	Y	E	C	N	Q	V	E	K	0.778048	0.112
89	SIYEHEDIKK	S	I	Y	E	H	E	D	I	K	K	0.777137	0.113
90	EDYEVQDCLK	E	D	Y	E	V	Q	D	C	L	K	0.0014540 1	0.113
91	TTYEIEEFKK	T	T	Y	E	I	E	E	F	K	K	0.772399	0.116
92	TVYEFSMPPK	T	V	Y	E	F	S	M	P	P	K	0.771184	0.117
93	TVYEVLNPRK	T	V	Y	E	V	L	N	P	R	K	0.770726	0.117
94	KAYEKPPEKK	K	A	Y	E	K	P	P	E	K	K	0.770412	0.118
95	ALYEDPPDQK	A	L	Y	E	D	P	P	D	Q	K	0.769977	0.118
96	GSYEHWYQQK	G	S	Y	E	H	W	Y	Q	Q	K	0.766617	0.12
97	AQYEPPQEEK	A	Q	Y	E	P	P	Q	E	E	K	0.761656	0.124
98	KEYEEEERKK	K	E	Y	E	E	E	E	R	K	K	0.0014500 1	0.124
99	VVYEDTTPWK	V	V	Y	E	D	T	T	P	W	K	0.759821	0.125
100	KIYESIEEAK	K	I	Y	E	S	I	E	E	A	K	0.752109	0.129
101	SLYEIAGLNK	S	L	Y	E	I	A	G	L	N	K	0.751477	0.13
102	ASYEEYYGKK	A	S	Y	E	E	Y	Y	G	K	K	0.748091	0.132
103	SAYELPYGTK	S	A	Y	E	L	P	Y	G	T	K	0.744276	0.134
104	TQYEESILTK	T	Q	Y	E	E	S	I	L	T	K	0.741215	0.136

105	SSYEDPAGGK	S	S	Y	E	D	P	A	G	G	K	0.740663	0.136
106	ALYEQSLHIK	A	L	Y	E	Q	S	L	H	I	K	0.740656	0.136
107	KSYEHGENAK	K	S	Y	E	H	G	E	N	A	K	0.739864	0.136
108	KSYENQAETK	K	S	Y	E	N	Q	A	E	T	K	0.738134	0.137
109	AVYEDMDARK	A	V	Y	E	D	M	D	A	R	K	0.734546	0.139
110	VTYEEIQKCK	V	T	Y	E	E	I	Q	K	C	K	0.733729	0.14
111	AAYEFRVIAK	A	A	Y	E	F	R	V	I	A	K	0.732792	0.14
112	ETYEGSPVSK	E	T	Y	E	G	S	P	V	S	K	0.730748	0.142
113	FSYEGSWTQK	F	S	Y	E	G	S	W	T	Q	K	0.729355	0.142
114	NTYEQIPATK	N	T	Y	E	Q	I	P	A	T	K	0.726919	0.144
115	GAYEPRWFMK	G	A	Y	E	P	R	W	F	M	K	0.72673	0.144
116	TIYENGQSNK	T	I	Y	E	N	G	Q	S	N	K	0.72626	0.144
117	SLYENWSLSK	S	L	Y	E	N	W	S	L	S	K	0.724686	0.145
118	KSYEFKDFEK	K	S	Y	E	F	K	D	F	E	K	0.724361	0.145
119	GSYEQSGLIK	G	S	Y	E	Q	S	G	L	I	K	0.723768	0.146
120	KVYEKLFPPK	K	V	Y	E	K	L	F	P	P	K	0.719458	0.148
121	SAYEKSFPIK	S	A	Y	E	K	S	F	P	I	K	0.718831	0.148
122	SQYETGHIRK	S	Q	Y	E	T	G	H	I	R	K	0.718672	0.148
123	RTYECSQCGK	R	T	Y	E	C	S	Q	C	G	K	0.717031	0.149
124	AAYEHFETMK	A	A	Y	E	H	F	E	T	M	K	0.713216	0.152
125	ALYEILGLHK	A	L	Y	E	I	L	G	L	H	K	0.711197	0.154
126	RIYEVEQQIK	R	I	Y	E	V	E	Q	Q	I	K	0.710503	0.154
127	MVYECIPLPK	M	V	Y	E	C	I	P	L	P	K	0.709084	0.155
128	KIYECNHVEK	K	I	Y	E	C	N	H	V	E	K	0.70615	0.158
129	SIYEFLSAEK	S	I	Y	E	F	L	S	A	E	K	0.702137	0.161
130	KTYECHVCRK	K	T	Y	E	C	H	V	C	R	K	0.701845	0.161
131	KLYECPIYRK	K	L	Y	E	C	P	I	Y	R	K	0.70072	0.162
132	ITYEAAQTVK	I	T	Y	E	A	A	Q	T	V	K	0.698373	0.164
133	PGYEKVPGEK	P	G	Y	E	K	V	P	G	E	K	0.0014340 1	0.169
134	KQYEDGQWKK	K	Q	Y	E	D	G	Q	W	K	K	0.689139	0.171
135	VSYEQRQNYK	V	S	Y	E	Q	R	Q	N	Y	K	0.687384	0.172
136	VVYEDIFDAK	V	V	Y	E	D	I	F	D	A	K	0.686122	0.173
137	AAYELLHFPK	A	A	Y	E	L	L	H	F	P	K	0.685298	0.174
138	KVYEMEQDKK	K	V	Y	E	M	E	Q	D	K	K	0.682989	0.176
139	TSYEISAWAK	T	S	Y	E	I	S	A	W	A	K	0.682894	0.176
140	SSYEHYESRK	S	S	Y	E	H	Y	E	S	R	K	0.682518	0.176
141	RSYECGESSK	R	S	Y	E	C	G	E	S	S	K	0.682036	0.176
142	QIYENNPQLK	Q	I	Y	E	N	N	P	Q	L	K	0.680023	0.178
143	QTYELNETAK	Q	T	Y	E	L	N	E	T	A	K	0.679812	0.178
144	HVYERRLIEK	H	V	Y	E	R	R	L	I	E	K	0.676224	0.18
145	EDYECDFGFK	E	D	Y	E	C	D	F	G	F	K	0.0014300 1	0.18
146	QSYEFSNSKK	Q	S	Y	E	F	S	N	S	K	K	0.670455	0.185
147	HVYEHLSKPK	H	V	Y	E	H	L	S	K	P	K	0.66373	0.189
148	HSYESGTKIK	H	S	Y	E	S	G	T	K	I	K	0.654571	0.196
149	SSYEALKGKK	S	S	Y	E	A	L	K	G	K	K	0.653713	0.196
150	KSYEKMRQEK	K	S	Y	E	K	M	R	Q	E	K	0.652589	0.197
151	QSYEFSNSNK	Q	S	Y	E	F	S	N	S	N	K	0.652362	0.197
152	LHYEFLQRVK	L	H	Y	E	F	L	Q	R	V	K	0.0014240 1	0.197
153	RLYENITVVK	R	L	Y	E	N	I	T	V	V	K	0.651502	0.198
154	LVYEQVEVQK	L	V	Y	E	Q	V	E	V	Q	K	0.646407	0.203
155	SAYEKHLIIK	S	A	Y	E	K	H	L	I	I	K	0.645323	0.204
156	RGYESPTLSK	R	G	Y	E	S	P	T	L	S	K	0.643749	0.206
157	KSYECPQCGK	K	S	Y	E	C	P	Q	C	G	K	0.64317	0.207
158	TLYEQVILEK	T	L	Y	E	Q	V	I	L	E	K	0.643087	0.207
159	KIYEISNRWK	K	I	Y	E	I	S	N	R	W	K	0.642359	0.208

160	GSYEKMETVK	G	S	Y	E	K	M	E	T	V	K	0.641646	0.209
161	TSYEMVIKEK	T	S	Y	E	M	V	I	K	E	K	0.641109	0.209
162	LVYEMPIKKK	L	V	Y	E	M	P	I	K	K	K	0.638827	0.212
163	RLYEAVIDAK	R	L	Y	E	A	V	I	D	A	K	0.635658	0.216
164	KSYECPHCGK	K	S	Y	E	C	P	H	C	G	K	0.634284	0.218
165	HVYELDVQAK	H	V	Y	E	L	D	V	Q	A	K	0.633286	0.219
166	AAYEKLSEEK	A	A	Y	E	K	L	S	E	E	K	0.631086	0.222
167	LTYEVLALKK	L	T	Y	E	V	L	A	L	K	K	0.626002	0.229
168	LTYEERVGFK	L	T	Y	E	E	R	V	G	F	K	0.62186	0.234
169	SAYEWSLGIK	S	A	Y	E	W	S	L	G	I	K	0.619973	0.237
170	SLYEKAPQGK	S	L	Y	E	K	A	P	Q	G	K	0.619543	0.237
171	GSYEWGEDFK	G	S	Y	E	W	G	E	D	F	K	0.618645	0.238
172	TSYEMLIKEK	T	S	Y	E	M	L	I	K	E	K	0.618634	0.238
173	SQYERPNETK	S	Q	Y	E	R	P	N	E	T	K	0.618139	0.239
174	KMYECNPVEK	K	M	Y	E	C	N	P	V	E	K	0.615832	0.242
175	SAYEWKMPKK	S	A	Y	E	W	K	M	P	K	K	0.614541	0.244
176	ALYEDILEGK	A	L	Y	E	D	I	L	E	G	K	0.612987	0.246
177	KQYEQSLEGK	K	Q	Y	E	Q	S	L	E	G	K	0.612143	0.247
178	QIYEKIVSGK	Q	I	Y	E	K	I	V	S	G	K	0.611283	0.248
179	KVYEDWDCFK	K	V	Y	E	D	W	D	C	F	K	0.611248	0.248
180	FTYEQLDVLK	F	T	Y	E	Q	L	D	V	L	K	0.609988	0.249

Supplementary Table 6. Evaluation of potential PBMC samples for further CD8+ Treg precursor phenotypic and functional characterization. Potential samples with relatively "high" CD8+ Treg precursor frequency (≥1.83% of CD8+ cells per **Fig. 10A**).

	Sample ID	Indication	CD8+ Treg precursor (CD3+/CD8+/CD28-/CD39+CD127-) Freq. of CD8+
Cancer patients	DLS002	Lung	2.91
	DLS049	Lung	2.46
	DLS055	Melanoma	2.96
	DLS059	Lung	2.66
	DLS075	Renal	2.22
	DLS076	Lung	3.76
	DLS098	Colorectal	4.6
	DLS119	Colorectal	3.56
	DLS121	Colorectal	2.09
	DLS128	Colorectal	3.1
	DLS130	Colorectal	2.5
	DLS139	Lung	2.11
	DLS167	Colorectal	2.16
Healthy donors	SDBB019	N/A (Healthy)	2.93
	SDBB137	N/A (Healthy)	1.85
	SDBB149	N/A (Healthy)	1.83
	SDBB150	N/A (Healthy)	3.3
	SDBB152	N/A (Healthy)	2.7

Supplementary Table 7. Mass cytometry panels for evaluation of CD8+ Treg precursor subpopulation.

Metal/Channel	Panel A : Phenotype	Panel B: Functional analysis
Y-89	Live barcode	Live barcode
Cd-106	Live barcode	Live barcode
Cd-111	CD14	CD14
	CD19	CD19
Cd-114	Live barcode	Live barcode
In-115	CD57	CD57
Cd-116		IFNg
Pr-141	CD3	CD3
Nd-142	CD74(HLA-DR)	
Nd-143		Perforin
Nd-144	CD28	CD28
Nd-146	KLRG1	KLRG1
Nd-148	CD45RO	CD45RO
Nd-150	LAG3	LAG3
Eu-151	CD101	TCF1
Sm-152	CD95	CD95
Gd-155	CD278 (ICOS)	Tbet
Gd-156	TIGIT	TIGIT
Gd-157	CD183(CXCR3)	CD183(CXCR3)
Gd-158	CD27	pSTAT3
Tb-159	CD45RA	CD45RA
Gd-160	CD279(PD1)	CD279(PD1)
Dy-161	TIM-3	TIM-3
Dy-162	Ki67	FOXp3
Dy-163	CD127(IL-7Ra)	CD127(IL-7Ra)
Ho-165	CD39	CD39
Er-167	CD197(CCR7)	CD197(CCR7)
Er-168	CD8	CD8
Tm-169	CD25	CD25
Yb-171	CX3CR1	Granzyme B
Yb-172		EOMES
Yb-173	CD152(CTLA-4)	CD152(CTLA-4)
Yb-174	CD4	CD4
Bi-209	41BB(CD137)	41BB(CD137)
Ir-191/193	DNA	DNA
Pt-195	Cisplatin Live/Dead	Cisplatin Live/Dead
Pt-198	Live barcode	Live barcode

surface marker
intracellular or intranuclear marker

Supplementary Table 8. **Target cell line characteristics used in WT-1/A*02:01 TCR-T +/- CoR functional assays**. Summary antigen expression, HLA restriction, and co-stimulatory ligand expression across tumor cell lines used for in vitro characterization of A0418 WT1-targeting TCR-T cells ± co-receptor constructs. WT1 expression determined from published datasets or internal validation. HLA-A*02:01 transduction and CD70 and 4-1BBL expression were assessed by flow cytometry and are reported as the percentage of positive cells within the total population.

Parameter	Panc1	COV434	COV434 + A*02:01	K562	K562 + A*02:01	Raji A*02:01
Cancer indication	Pancreatic	Ovarian	Ovarian	Leukemia	Leukemia	Lymphoma
Reported WT-1 expression	+	+	+	+	–	–
HLA A*02:01 expression	+	–	+	–	–	+
CD70 expression (%)	4.7	0.0	1.4	0.2	0.2	86.0
4-1BBL expression (%)	0.2	0.1	21.5	11.2	25.3	6.6

Supplementary Table 9. **Target cell line characteristics used in MSLN/A*11:01 TCR-T +/- CoR functional assays**. Summary antigen expression, HLA restriction, and co-stimulatory ligand expression across tumor cell lines used for in vitro characterization of A0341 MSLN-targeting TCR-T cells ± co-receptor constructs. WT1 expression determined from published datasets or internal validation. HLA-A*11:01 transduction and CD70 and 4-1BBL expression were assessed by flow cytometry and are reported as the percentage of positive cells within the total population.

Parameter	A549 A*11:01	Panc1	DU-145	DU-145 + A*11:01	OVCAR-3	OVCAR-3 + A*11:01
Cancer indication	Lung	Pancreatic	Prostate	Prostate	Ovarian	Ovarian
Reported MSLN expression	+	+	+	+	+	+
HLA A*11:01 expression	+	+	–	+	–	+
CD70 expression (%)	0.2	25.9	32.4	45.5	0.4	0.3
4-1BBL expression (%)	0.2	0.4	0.0	0.4	0.0	0.4

Publications resulting from thesis work

- Schmidt, F., **Fields, H.F.**, et. al. In-depth analysis of human virus-specific CD8+ T cells delineates unique phenotypic signatures for T cell specificity prediction. Cell Press, 2023. 42(10):113250.

- **Fields, H.F.**, et. al. (2025). A TCR Discovery and Characterization Platform Identifies a Tumor-Reactive TCR and Accelerates Off-Target Profiling. [**Manuscript submitted for publication**].